

*Paleoseismic Investigation of Trench EOC-2,
Pajarito Fault Zone, Los Alamos National
Laboratory, New Mexico*



*Los Alamos National Laboratory is operated by the University of California
for the United States Department of Energy under contract W-7405-ENG-36.*

Cover Photo:

Trench EOC-2 looking east. A down-to-the-west fault is exposed to the left. This fault last moved sometime after 10,500 years ago.

An Affirmative Action/Equal Opportunity Employer

This report was prepared as an account of work sponsored by an agency of the United States Government. Neither The Regents of the University of California, the United States Government nor any agency thereof, nor any of their employees, makes any warranty, express or implied, or assumes any legal liability or responsibility for the accuracy, completeness, or usefulness of any information, apparatus, product, or process disclosed, or represents that its use would not infringe privately owned rights. Reference herein to any specific commercial product, process, or service by trade name, trademark, manufacturer, or otherwise, does not necessarily constitute or imply its endorsement, recommendation, or favoring by The Regents of the University of California, the United States Government, or any agency thereof. The views and opinions of authors expressed herein do not necessarily state or reflect those of The Regents of the University of California, the United States Government, or any agency thereof. Los Alamos National Laboratory strongly supports academic freedom and a researcher's right to publish; as an institution, however, the Laboratory does not endorse the viewpoint of a publication or guarantee its technical correctness.

*Paleoseismic Investigation of Trench EOC-2,
Pajarito Fault Zone, Los Alamos National
Laboratory, New Mexico*

*Steven L. Reneau
Jamie N. Gardner
Alexis Lavine
Eric V. McDonald*
Claudia Lewis
Danny Katzman
Giday WoldeGabriel
Donathan Krier
Deborah Bergfeld
Jeff Heikoop*

**Earth and Ecosystems Sciences
Desert Research Institute, Reno, NV*



TABLE OF CONTENTS

	Page
TABLE OF CONTENTS	v
LIST OF FIGURES AND PLATES	vii
LIST OF TABLES	viii
ABSTRACT	1
I. INTRODUCTION	3
II. SETTING	3
III. METHODS	5
A. Trench Siting and Excavation	5
B. Trench Cleaning and Logging	6
C. Geochronology	6
IV. RESULTS OF TRENCH INVESTIGATION	7
A. Stratigraphic Units	7
1. Early Pleistocene units	7
2. Pleistocene units of uncertain age	9
3. Late Pleistocene units	10
4. Holocene units	11
B. Structural Deformation	12
1. Main zone of faulting	12
2. Faulting between 52H and 57H	14
3. Faulting between 82H and 85H	15
4. Tilting of units	15
V. DISCUSSION	15
A. Geomorphic and Tectonic History	15
B. Paleoseismic Chronology	17
1. Trench EOC-2	17
2. Other trench investigations	18
C. Implications for Facility Siting	20
VI. CONCLUSION	21
VII. ACKNOWLEDGMENTS	21
VIII. REFERENCES	21
APPENDIX A. STRATIGRAPHIC UNIT DESCRIPTIONS	27

TABLE OF CONTENTS (continued)

	Page
APPENDIX B. RADIOCARBON DATING	32
APPENDIX C. SOIL STRATIGRAPHY AND PEDOLOGIC AGE ESTIMATES	35
A. Introduction	35
B. Methods	35
1. Quantification of soil morphology	35
2. Stratigraphic-age relationships for soils	36
3. Description of soil stratigraphy	36
C. Development of a Soil Chronofunction for Estimating Pedologic Ages	37
1. Soils used in chronofunction	37
2. Testing the precision and accuracy of the soil chronofunction	39
D. Results	41
1. Profile 69.9	41
2. Profile 55.6	44
3. Profile 37.6	48
4. Profile 67.2	49
E. Summary and Conclusions	51
F. Recommendations	51
APPENDIX D. PETROGRAPHY, GEOCHEMISTRY, AND CORRELATIONS OF TEPHRAS	53
A. Introduction	53
B. X-ray Fluorescence Analyses of Bulk Pumice	53
1. Petrographic descriptions of samples prior to high grading	53
2. Results	55
C. Electron Microprobe Analyses of Glasses from Reworked Tephra	58
1. Petrographic descriptions of samples	58
2. Results	62
APPENDIX E. BORE HOLE SAMPLES	64

LIST OF FIGURES AND PLATES

	Page
FIGURES	
1. Location Map	4
2. Geologic Map of Trench EOC-2 and Vicinity	5
3. Photograph of Trench EOC-2	6
4. Stratigraphic Column	7
5. Simplified Composite Trench Log	8
6. Photograph of Main Fault	13
C-1. Soil Chronofunction for Calculating PDI Ages	37
C-2. Comparison of Other Pajarito Plateau Soils and Soil Chronofunction	41
C-3. Schematic Stratigraphic Column for Profile 69.9	44
C-4. Schematic Stratigraphic Column for Profile 55.6	45
C-5. Schematic Stratigraphic Column for Profile 37.6	48
C-6. Schematic Stratigraphic Column for Profile 67.2	49
D-1. Zr-Nb and Zr-Rb Chemical Variation Diagrams	55
D-2. FeO-CaO Variation Diagrams	63
 PLATES	
1. Trench EOC-2 log, 0H to 25H	inside rear cover
2. Trench EOC-2 log, 25H to 50H	inside rear cover
3. Trench EOC-2 log, 50H to 75H	inside rear cover
4. Trench EOC-2 log, 75H to 95H	inside rear cover

LIST OF TABLES

	Page
B-1. Radiocarbon Analyses From Trench EOC-2	33
C-1. Summary of Soil Development Index Results for Soils Used in Developing Chronofunction . . .	38
C-2. Comparison of PDI Soil Ages with Radiometric Dates for Soils on the Pajarito Plateau	40
C-3. Summary of Soil Morphology for Trench EOC-2 Profiles	42–43
C-4. PDI Age Estimates for Soil Units in Trench EOC-2	46–47
C-5. Composite Soil Stratigraphy Used to Calculate PDI Ages for Buried Units in Trench EOC-2	50
D-1. Whole-Rock X-ray Fluorescence Analyses of Pumices From Trench EOC-2	54
D-2a. Electron Microprobe Analyses of Glasses (wt %) From Selected Tephra From Trench EOC-2:Raw Analyses	56–58
D-2b. Electron Microprobe Analyses of Glasses From Selected Tephra (wt %) From Trench EOC-2:Data Normalized on a Volatile-free Basis	59–61
E-1. Samples From Bore Holes Near Trench EOC-2	65

PALEOSEISMIC INVESTIGATION OF TRENCH EOC-2, PAJARITO FAULT ZONE, LOS ALAMOS NATIONAL LABORATORY, NEW MEXICO

by

Steven L. Reneau, Jamie N. Gardner, Alexis Lavine, Eric V. McDonald, Claudia Lewis, Danny Katzman, Giday WoldeGabriel, Donathan Krier, Deborah Bergfeld, and Jeff Heikoop

ABSTRACT

A 95-m-long, 3-m-deep trench was excavated in November 2000 at a proposed site for a new Emergency Operations Center at Los Alamos National Laboratory. The purpose of the trench was to obtain information on the location and history of movement on individual faults to satisfy Department of Energy guides and standards pertaining to evaluating potential surface rupture hazards to new facilities. In addition to having direct applications to facility siting, this work contributes to an improved understanding of the paleoseismic and geomorphic history of the area that will aid in future seismic hazard evaluations and other investigations.

The trench crossed a topographic low near the eastern base of the Pajarito fault escarpment and exposed stratigraphic units that range in age from 1.22 million years to less than 100 years, and it also exposed faults in a 33-m-wide zone that exhibit evidence for normal, strike-slip, and possibly reverse offset. Stratigraphic units include the early Pleistocene Bandelier Tuff, early Pleistocene alluvial fan deposits that pre-date incision of canyons on this part of the Pajarito Plateau, and younger Pleistocene and Holocene alluvium and colluvium that post-date drainage incision. Up to 2.5 m of Holocene alluvium and colluvium were exposed in the trench, and these deposits record the most significant period of sedimentation here in the last 50,000 to 60,000 years.

The main zone of faulting in the trench displays down-to-the-west offset and forms the eastern edge of an approximately 160-m-wide graben at the base of the east-facing Pajarito fault escarpment. Net vertical offset of about 2 to 2.5 m in the last 1.22 million years is estimated across the main fault zone in the trench, although samples from bore holes to the west indicate that the graben has a maximum structural depth of at least 8 m. The additional vertical deformation may be accommodated by offset on relatively old faults that were not exposed in the trench, by westward tectonic tilting, or by a combination of both.

The trench exposures provided evidence for a minimum of six surface rupture events in the last 1.22 million years, demonstrating the recurring nature of surface faulting at the site. The most recent event occurred sometime within the last 10,500 years and, possibly, near or after 8600 years ago. This fault zone is therefore considered active and should be avoided in the siting of new facilities. However, based on analysis of an analogous setting at Technical Area 16, the proposed site should satisfy probabilistic criteria for evaluating surface fault hazards, with the probability of significant surface rupture being less than once in 2000 years.

I. INTRODUCTION

Los Alamos National Laboratory (LANL) lies within the Española basin of the Rio Grande rift, a tectonically active area characterized by general east-west crustal extension (e.g., Kelley 1979; Manley 1979; Golombek et al. 1983; Chapin and Cather 1994; Kelson and Olig 1995). The Pajarito fault is a major bounding structure of the Española basin and has produced a prominent east-facing escarpment immediately west of LANL. Ground shaking from earthquakes on the Pajarito fault constitute the largest potential seismic hazard to LANL (Gardner and House 1987; Wong et al. 1995, 1996). Numerous smaller faults, possibly related to the Pajarito, have been identified east of the main Pajarito fault escarpment within the boundaries of LANL (e.g., Kolbe et al. 1994; Reneau et al. 1995, 1998; Krier et al. 1998; Gardner et al. 1999, 2001). These faults may present surface rupture hazards during earthquakes, and Department of Energy (DOE) guides and standards specify that the location and history of movement on individual faults should be considered in evaluating hazards to new and existing facilities (DOE 1996b, 2000).

This report documents an investigation of faulting at a proposed site for a new Emergency Operations Center (EOC) at LANL, within the Pajarito fault zone. A 95-m-long, 3-m-deep trench was excavated through the proposed site in November 2000, and field investigations were conducted in November and December 2000. The trench is referred to as trench EOC-2 because it is at the second of several sites that were initially considered for a new EOC. The focus of this investigation was to identify the location of young faults at the proposed site and to obtain information on the age of fault movement. Supplemental information on the stratigraphic and structural setting of the site was provided by drilling in support of geotechnical evaluations in February 2001. In addition to having direct applications to siting of a new EOC, this work contributes to an improved understanding of the paleoseismic and geomorphic history of LANL

that will aid in future seismic hazard evaluations and other investigations.

From the perspective of understanding the paleoseismic history of the area and potential surface rupture hazards at the proposed site, a few limitations of this study should be emphasized. The scope of this work did not include identification of all Quaternary faulting at the trench site, as older Quaternary faults could be buried at depth beneath the units exposed in the trench. In addition, because only one trench was excavated, we cannot rule out the possibility of young faults through the proposed building footprint that may trend parallel or obliquely to the trench. Additionally, this work did not allow determination of the lateral continuity of any of the identified faults, and there is some uncertainty regarding where these faults extend beyond the trench exposures. Although important age control was obtained from some key units, rigorous age estimates were not obtained for all geologic units exposed in the trench. Despite these limitations, the scope of the investigation was sufficient to identify the location of primary geologic structures oriented roughly parallel to the main Pajarito fault and to evaluate the potential for young rupture on these faults.

II. SETTING

Trench EOC-2 was located near the western boundary of LANL in Technical Area (TA) 69, adjacent to New Mexico Highway 501 (West Jemez Road) near the drainage divide between Pajarito Canyon and Twomile Canyon (Figures 1 and 2). The western end of the trench was about 80 m east of the base of the main escarpment of the Pajarito fault. The Pajarito fault has an estimated down-to-the-east offset of about 145 m in this area since 1.22 Ma (Ma = millions of years before present) based on topographic profiles (Olig et al. 1996) and an estimated offset of about 80 m based on stratigraphic sections (Gardner et al. 2001). The trench crossed the axis of a roughly north-south trending topographic low that was inferred to

overlie a structural graben bounded on the east by a down-to-the-west fault, as mapped by Rogers (1995). Analogous down-to-the-west faults have also been mapped east of the main escarpment both north and south of this site (Smith et al. 1970; Gardner and House 1987; Reneau and McDonald 1996; McCalpin 1997; Gardner et al. 1999, 2001). Trenches excavated across one of these down-to-the-west faults 1.1 to 1.2 km to the north provided evidence for Holocene surface rupture (McCalpin 1998). Based on results from another trench west of the main escarpment, McCalpin (1998, 2000) inferred an estimated age for this Holocene surface rupture of either ca. 1.5 ka (ka = thousands of years before present) or ca. 3 to 7 ka.

Surficial geologic units present near the trench site were mapped in 1996 (S. L. Reneau, unpublished) and are shown in Figure 2. Bedrock in the area consists of the early Pleistocene Tshirege Member of the Bandelier Tuff (unit Qbt; Griggs 1964; Smith et al. 1970), which comprises a series of ignimbrites erupted from the Jemez Mountains at ca. 1.22 Ma (age from Izett and Obradovich 1994 and Spell et al. 1996). The Bandelier Tuff is local-

ly overlain by early Pleistocene alluvial fan deposits that occur on mesa tops and that pre-date incision of canyons on this part of the Pajarito Plateau (unit Qoal). Inset into Qoal and Qbt are younger alluvial fans (unit Qf) that post-date initial canyon incision and that may have a wide range in age. The topographic high at the east end of the trench was mapped as "Qfo?" (inferred older post-Qoal fan; Figure 2) because the surface here is significantly lower than Qoal surfaces to the north and south, but the trench exposures show it to include both Qoal and Qfo. The topog-

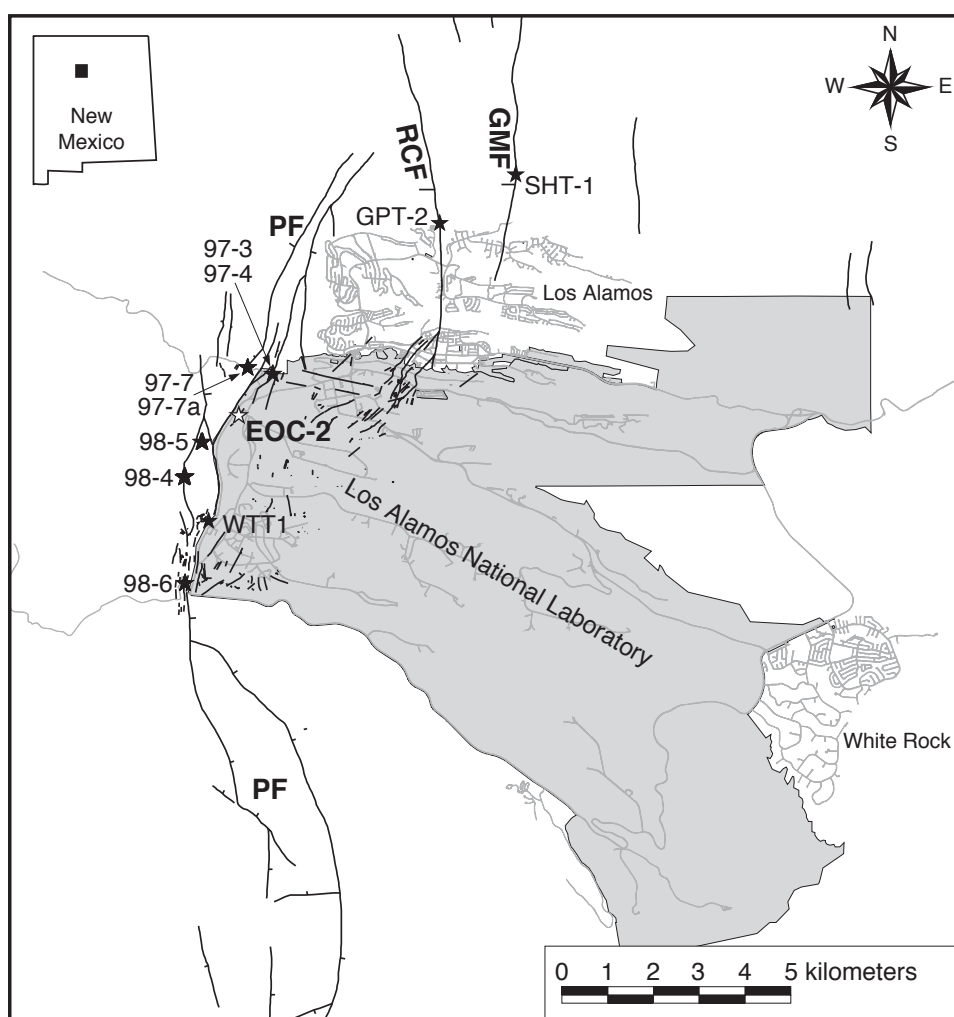


Figure 1. Map showing the location of trench EOC-2 (open star) and other paleoseismic trenches referred to in the text (filled stars). Major traces of the Pajarito fault system, shown in heavy lines, are from Gardner et al. (1999, 2001). PF = Pajarito fault; RCF = Rendija Canyon fault; GMF = Guaje Mountain fault. Paved roads are shown in light grey lines.

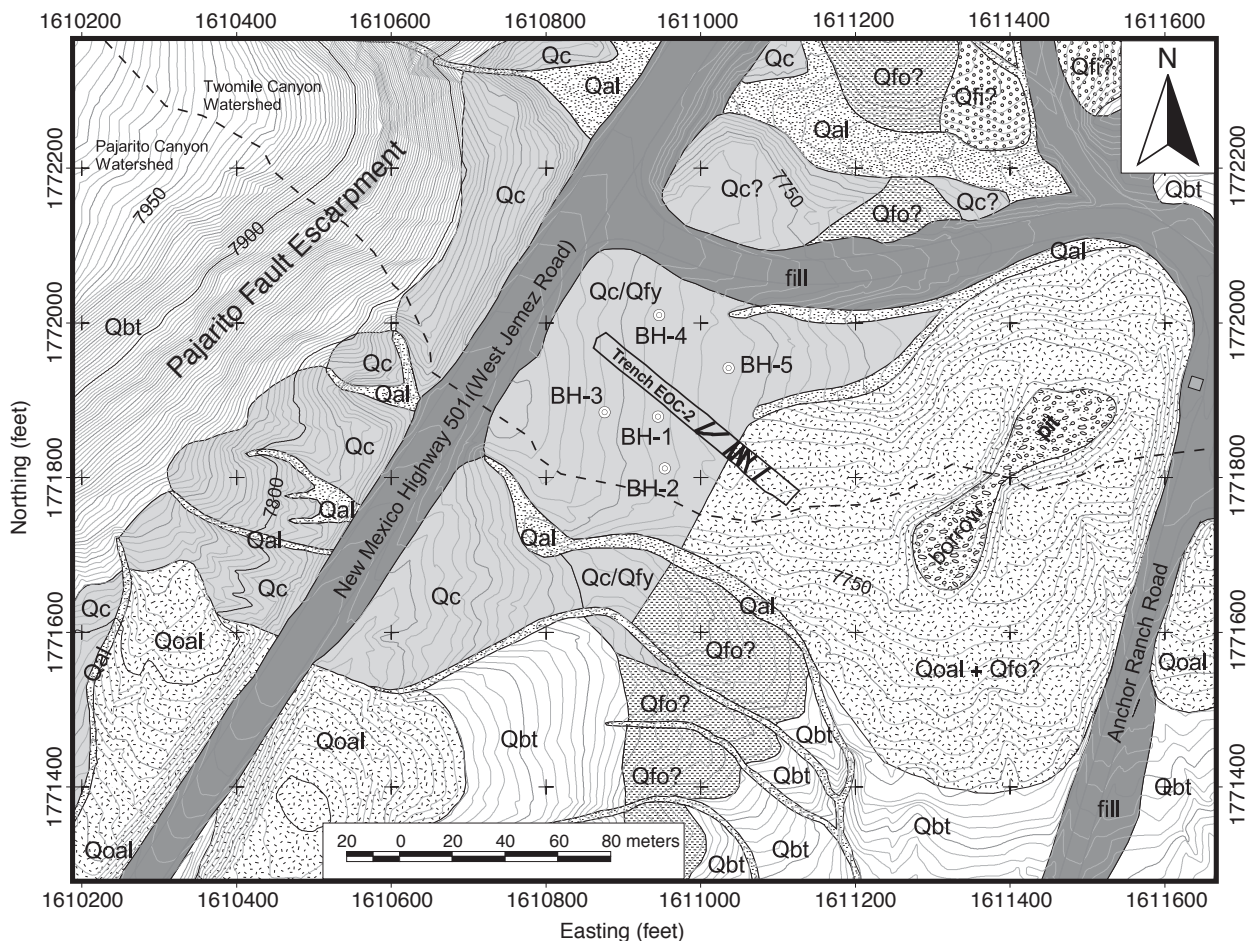


Figure 2. Map showing geologic and geographic features in the vicinity of trench EOC-2. General surficial geologic units are modified from S. Reneau (unpublished mapping, 1996). The heavy lines indicate faults exposed in the trench. BH = February 2001 bore holes; Qal = late Holocene alluvium; Qbt = Tshirege Member of Bandelier Tuff; Qc = colluvium; Qfi? = inferred intermediate age (Pleistocene) alluvial fan; Qfo? = inferred older (Pleistocene) alluvial fan; Qfy = younger (Holocene) alluvial fan; Qoal = mesa-top alluvium. Qc/Qfy indicates that Qc overlies Qfy, and Qfo?/Qoal indicates that Qfo is inferred to overlie Qoal. The topographic base, with 2-ft contours, is from the Facility for Information Management, Analysis, and Display (FIMAD). The northing and easting axes are New Mexico State Plane coordinates.

raphy in the central and western parts of the trench site slopes up to the southwest and represents the surface of a young fan (unit Qfy), derived from a small drainage off the Pajarito fault escarpment, that spans the drainage divide between Pajarito and Twomile canyons; the modern channel for this drainage is incised about 1.5 m below the fan surface and flows into Pajarito Canyon, although runoff from the trench site flows into Twomile Canyon. Colluvium (unit Qc) mantles the base of the Pajarito fault escarpment

and was also inferred to constitute the uppermost unit at the trench site (Figure 2).

III. METHODS

A. Trench Siting and Excavation

Trench EOC-2 was centered on the proposed building footprint and oriented roughly perpendicular to anticipated fault traces to optimize the probability

of intersecting faults. Trench orientation was approximately N50W. The trench was excavated with a trackhoe; about 1100 m³ of material was removed in about four days. Trench length was 95 m (310 ft), or approximately twice the length of the proposed facility (46 m, 150 ft), to allow adjustment of building location if needed. Trench EOC-2 was about 7.5 m (25 ft) wide, and the northeast and southwest sides included three walls separated by two benches to meet Occupational Safety and Health Administration (OSHA) safety standards without the use of shores (Figure 3). Trench depth was about 3 m (10 ft), intended to be deep enough to expose a sufficiently old stratigraphic section while minimizing costs and the total area disturbed in the excavation.

B. Trench Cleaning and Logging

The northeast trench walls were cleaned with hand tools to allow examination of stratigraphic and structural relations. In many places hand tools were used to dig below bench levels to resolve stratigraphic and structural uncertainties caused by the need to extrapolate between offset walls. In a few areas, the southwest walls were also cleaned to aid in structural interpretations. Color-coded nails were used to mark stratigraphic boundaries, pedologic boundaries, structures, and other key features. More than 1300 of these nails were surveyed with a total station and plotted on gridded paper at a scale of 1:20. The nails served as control points for logging features on each wall. The survey data also allow referencing of geologic features to the New Mexico State Plane coordinate system. An arbitrary datum of 0 m vertical and 0 m horizontal was established near the ground surface at the northwest corner of the trench, and locations of all features on the trench walls can be uniquely described or found on the logs relative to this datum. For example, 65H -3V indicates a location 65 m southeast of the datum and 3 m vertically below it. During logging of the trench walls, particular attention was paid to stratigraphic and structural relations near fault zones to distinguish faulted from nonfaulted units. In some units, distinc-

tive pedologic boundaries are distinguished on the trench log, but no attempt was made to systematically define all soil horizons along the length of the trench. Detailed trench logs are shown on Plates 1 to 4 (inside back cover). Concurrent with trench logging, the sedimentology and contact relations of all geologic units exposed in the trench were described (presented in Appendix A).

C. Geochronology

Several methods were used to obtain age estimates for stratigraphic units in trench EOC-2. Preliminary age estimates were made in the field using stratigraphic relations and comparison of unit characteristics with those of previously dated deposits and soils in nearby areas. Additional



Figure 3. Photograph of trench EOC-2, looking southeast.

geochronologic estimates were obtained using radiocarbon dating of charcoal samples collected from trench walls (discussed in Appendix B), soil profile descriptions and profile development index (PDI) calculations (discussed in Appendix C), and geochemical analyses of tephras as support for unit correlations (discussed in Appendix D).

IV. RESULTS OF TRENCH INVESTIGATION

A. Stratigraphic Units

Stratigraphic units exposed in trench EOC-2 range in age from early Pleistocene to late Holocene and include volcanic rocks of the Bandelier Tuff (Qbt), alluvial fan deposits (Qoal and Qf), and colluvium (Qc). The distinction between Qoal and Qf is based on lithologic and stratigraphic evidence as to whether the deposits pre-date or post-date initial incision of drainages on this part of the Pajarito Plateau. Alluvial deposits that pre-date incision are designated Qoal, and alluvial deposits that post-date incision are designated Qf. Alluvial fan and colluvial units are numbered sequentially based on inferred age relations, from oldest to youngest, although in some cases, age relations are uncertain. Inferred age relations of all units are shown schematically in Figure 4. Figure 5 is a generalized composite log showing all units present in the trench, and more detailed stratigraphic relations are shown on Plates 1 through 4.

This section presents a summary of the characteristics and ages of stratigraphic units in trench EOC-2, grouped into broad age categories and synthesizing information included in Appendices A through D. Key pedologic subdivisions are discussed for some units, although the primary focus in this discussion is on stratigraphic relations and ages. More detailed descriptions of each unit are presented in Appendix A. In this section, age estimates provided by radiocarbon analyses use calibrated (cal) ages to be consistent with age estimates derived from PDI calculations (see

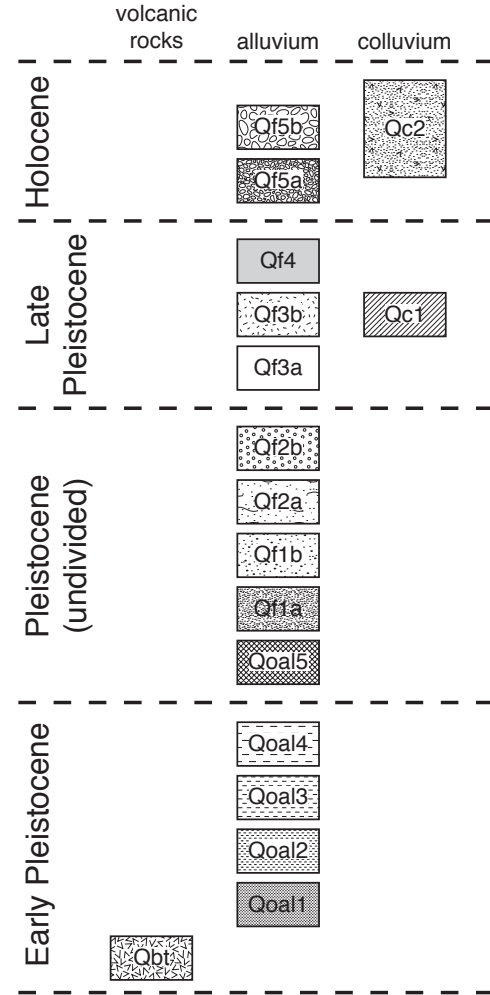


Figure 4. Stratigraphic column showing general age relations of units exposed in trench EOC-2.

Appendix B for discussion of radiocarbon analyses and Appendix C for PDI calculations). Petrographic descriptions and geochemical analyses of tephras, presented in Appendix D, provide additional age information for stratigraphic units in trench EOC-2.

1. Early Pleistocene units

A sequence of early Pleistocene units was exposed in the eastern part of trench EOC-2 (Figures 4 and 5, Plates 3 and 4). The oldest unit is an incipiently welded, pumice-rich flow unit of the Tshirege Member of the Bandelier Tuff (unit Qbt), which has been dated at ca. 1.22 Ma (Izett and

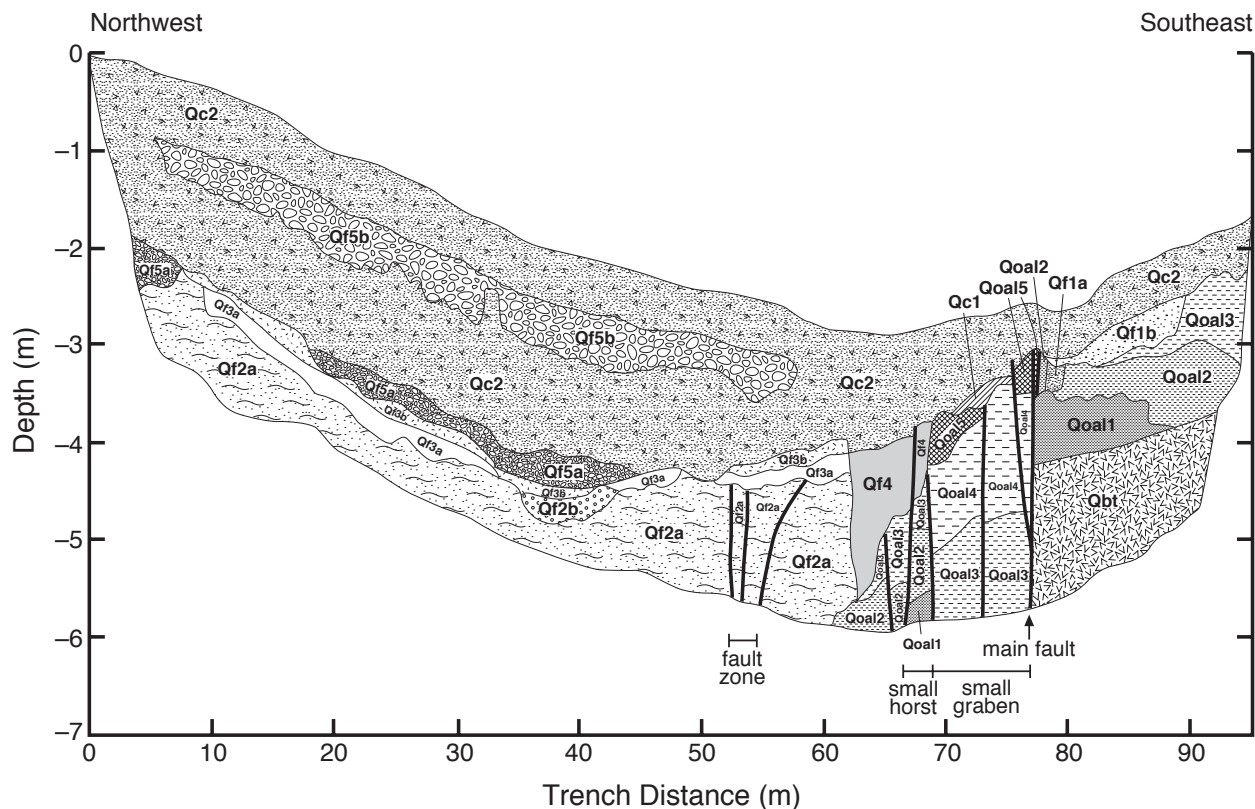


Figure 5. Simplified composite log of trench EOC-2, modified from Plates 1 to 4. The patterns corresponding to the units are shown in Figure 4. The vertical scale is exaggerated by a factor of 8x.

Obradovich 1994; Spell et al. 1996). Examination of samples from bore holes (Appendix E) suggests that this flow unit overlies tuff that is characteristic of Tshirege Member Unit 4 as exposed nearby at TA-3 (Gardner et al. 1999).

Unit Qbt is directly overlain by stratified alluvium that contains abundant crystal-rich Bandelier Tuff pumice clasts (unit Qoal1, Plate 4). These pumices are geochemically distinct from pumices in the part of Qbt exposed in the trench but are geochemically similar to Tshirege Member Unit 4 (sample EOC2/00/11-17-9; Appendix D), suggesting that they were derived from erosion of different flow units upgradient. The absence of weathering or soil development on top of Qbt and the absence of evidence for erosion at the contact suggest deposition of Qoal1 very soon after eruption of the Bandelier Tuff.

Unit Qoal2 unconformably overlies Qoal1 (Plate 4). The unit is poorly sorted and contains dacite clasts in a finer-grained matrix, which is suggestive of a debris flow deposit. The dacite clasts indicate a source in areas to the west underlain by the late Miocene-Pliocene Tschicoma Formation (Griggs 1964; Smith et al. 1970), either in the Pajarito Canyon or the Twomile Canyon drainage basins. Unit Qoal3 overlies Qoal2 and consists of well-stratified alluvium dominated by granule-to-pebble size dacite and aphyric pumice clasts, with the dacite again indicating a source in the Pajarito or Twomile drainage basins. Unit Qoal4 overlies Qoal3 and is dominated by aphyric pumice clasts that are geochemically and petrographically similar to the pumice in Qoal3 (samples EOC2/00/11-17-6, EOC2/00/11-17-7, EOC2/00/11-17-10; Appendix D). These pumice clasts also resemble pumice seen in other exposures of mesa-top alluvi-

um on the Pajarito Plateau. The presence of dacite and tuff clasts and well-developed stratification in part of Qoal4 indicates deposition by fluvial processes. The dominance of pumice suggests that Qoal4 may have been deposited relatively soon after a major eruption. Geochemical fingerprinting of pumice from Qoal3 and Qoal4 and similar pumice collected from other locations suggests that most are derived from eruptions from the Cerro del Medio dome complex in the Jemez Mountains (Appendix D; see also D. Broxton, unpublished, in Reneau and McDonald 1996, pp. 90–91). Cerro del Medio lavas have yielded an $^{40}\text{Ar}/^{39}\text{Ar}$ age estimate of ca. 1.13 Ma (Spell and Harrison 1993), and a similar $^{40}\text{Ar}/^{39}\text{Ar}$ date of ca. 1.17 Ma from stratigraphically and geochemically similar pumice collected from trench 97-3 of McCalpin (1998, Figure 13, p. 45) supports this correlation. If the correlation of the Qoal3 and Qoal4 pumice with Cerro del Medio eruptions is accurate, this suggests that units Qoal1 through Qoal4 were deposited within 100,000 years after eruption of Qbt.

2. Pleistocene units of uncertain age

Several alluvial fan units present in trench EOC-2 are inferred to be younger than Qoal4 and older than probable late Pleistocene fan units but, otherwise, have poorly-constrained ages (Figures 4 and 5).

Unit Qoal5 is a reddish, clay-rich unit with well-developed soil structure that overlies Qoal4 and is preserved on down-dropped blocks west of the most prominent fault in the trench (referred to as the “main fault”) (Plates 3 and 4). The unit records the best-developed soil in the trench, although a reliable estimate of soil age cannot be made because its top is eroded. PDI calculations indicate an age exceeding ca. 50 to 80 ka, and the composite soil-stratigraphic context indicates that the unit is older than Qf2a and has an age of at least ca. 185 to 295 ka (Appendix C). Because of its association with Qoal4, inferred to be ca. 1.1 Ma in age, Qoal5 may be much older than 185 to 295 ka.

Unit Qf1 includes two dissimilar deposits that occur east of the main fault (Plate 4). Qf1a is a rel-

atively fine-grained deposit that fills a shallow channel scoured into Qoal1 and Qoal2 and is inferred to represent a debris flow deposit. Unit Qf1b is a more extensive reddish medium-to-coarse sand deposit that unconformably overlies Qoal2, Qoal3, and Qf1a. The well-sorted nature of Qf1b contrasts with more poorly sorted fan deposits west of the fault and suggests that the unit constitutes a remnant of relatively old fluvial deposits associated with large streams, perhaps derived from Twomile or Pajarito canyons, that pre-date units Qf2a through Qf5b. Although the unit is not in contact with Qoal5, Qf1b is inferred to be younger because it is not present beneath Qoal5 west of the main fault.

Unit Qf2a is the oldest unit exposed in the western half of the trench (Plates 1, 2, and 3) and has a strong pedogenic overprint. The unit is sedimentologically complex and may include fan deposits with a wide range in age. In the eastern part of its exposure in the trench, Qf2a includes a buried soil (e.g., profile P55.6; Plate 3; Appendix C), which supports the interpretation that this unit has a complex depositional history. Qf2a is dominated by well-consolidated, clayey or silty fine or very fine sands with no visible stratification, although the local presence of fine gravel lenses demonstrates a fluvial origin for much of the unit. Coarser gravel layers also occur locally. Whitish silty lenses that are suggestive of volcanic ash were exposed in the center of the trench. A thicker whitish zone with well-developed soil structure is present above Qf2a beneath a paleotopographic low and is designated unit Qf2b. Although superficially similar to unit Qf3a (discussed below), pedologically and sedimentologically, Qf2b appears to be related to Qf2a, representing an albic soil horizon (E horizon) developed on Qf2a deposits (profile P37.6; Plate 2; Appendix C). PDI calculations provide age estimates of ca. 60 to 95 ka or greater for the upper part of Qf2a and ca. 110 to 180 ka or greater for the lower part of Qf2a in the central part of the trench (profile P55.6; Plate 3; Appendix C). In comparison, PDI calculations suggest a possible age of ca. 50 to 80 ka for the base of Qf2b farther

west (profile P37.6; Plate 2; Appendix C), overlapping with the estimated age of the El Cajete pumice (ca. 50 to 60 ka; Toyoda et al. 1995; Reneau et al. 1996a). Because of the possibility of erosion of overlying deposits, these PDI calculations provide minimum-limiting age estimates for Qf2a and Qf2b, and all of these units may be older than the El Cajete pumice. The presence of glass that has been geochemically correlated to the El Cajete pumice in the upper part of Qf2a near the western end of the trench (sample EOC2/00/11-17-2; Plate 1; Appendix D) suggests either a post-El Cajete age or, alternatively, the translocation or bioturbation of some El Cajete tephra into this unit. The latter hypothesis is preferred because the absence of any El Cajete pumice in the trench indicates extensive erosion after 50 to 60 ka, requiring a significant unconformity. Available pedologic and stratigraphic evidence indicates that the contact between Qf3a and Qf2a is the most likely candidate for this unconformity.

3. Late Pleistocene units

Several units that are inferred to be late Pleistocene in age, post-dating the ca. 50- to 60-ka El Cajete pumice, are present in trench EOC-2, including both alluvial deposits and colluvial deposits (Figures 4 and 5).

Unit Qf3a is an extensive but discontinuous whitish layer that overlies Qf2 (Plates 1, 2, and 3). In places the unit is dominated by silt and resembles a volcanic ash, but the presence of very small disseminated charcoal fragments and volcanic glass with a range in composition (samples EOC2/00/11-17-3, EOC2/00/11-17-4, EOC2/00/11-17-5; Plates 2 and 3; Appendix D) indicates the unit has a detrital origin with mixed provenance. The whitish color may also be imparted or enhanced by pedogenesis associated with an albic horizon (profile P55.6; Plate 3; Appendix C). In several parts of the trench, Qf3a has a basal gravel layer that is in unconformable contact with Qf2a, and locally, the gravels are interstratified with the silt (Plates 1, 2, and 3). These characteristics indicate that Qf3a is a thin fan deposit that was

deposited on a locally eroded surface of Qf2. The presence of biotite in Qf3a silts, along with some glass shards that are geochemically correlative with the El Cajete pumice (sample EOC2/00/11-17-4; Plate 2; Appendix D), suggests that the unit includes reworked components of the biotite-bearing El Cajete pumice, providing evidence for an age of less than ca. 50 to 60 ka. A post-El Cajete age is also consistent with the degree of soil development in this unit (profile P55.6; Appendix C). Stratigraphic relations indicate that the unit is older than Qf4 (Figure 5; Plate 3), and PDI calculations suggest it is older than ca. 43 ka (Appendix C).

Unit Qf3b is a brown layer of silt and fine sand that directly overlies Qf3a and locally overlies Qf2b (Plates 2, 3, and 4) and constitutes a buried A horizon that is apparently pedologically related to Qf2b and Qf3a (profiles P37.6 and P55.6; Plates 2 and 3; Appendix C). It is overlain by Qf5a or Qc2, and Qf3b appears to represent the surface soil in the latest Pleistocene and earliest Holocene prior to deposition of these units. In places, the original top of Qf3b may be present, although Qf5a and Qc2 are commonly in unconformable contact with Qf3b. Radiocarbon analyses of charcoal collected from Qf3b yielded ages of ca. 11.7 cal ka in the center of the trench (sample EOC2-c14; Plate 2; Appendix B), below Qf5a, and ca. 10.3 cal ka to the east (sample EOC2-c39; Plate 2; Appendix B), below Qc2. Because the dated charcoal probably represented material mixed into the unit when it constituted the surface soil, these analyses provide minimum-limiting age estimates for the Qf3b deposits and maximum-limiting age estimates for the base of the overlying units.

Unit Qf4 is dominantly a crudely stratified alluvial deposit that fills a paleochannel incised into Qf2a and Qoal (Plate 3). The unit contains common aphyric pumice derived from Qoal4. At its eastern edge, it locally includes colluvium derived from adjacent slopes. At its western edge, the unit appears to truncate Qf3a, indicating a younger age. The unit contains common clay lamellae (“Bt lamellae”), and PDI calculations suggest an age of

ca. 35 to 55 ka or more for the lower part of the deposit (profile P67.2; Appendix C). Stratigraphic relations indicate the unit is probably younger than Qf3a and thus younger than the ca. 50- to 60-ka El Cajete pumice. Qf4 underlies the present topographic low and may record a late Pleistocene channel cut-and-fill cycle associated with headward erosion of a drainage from the north. Analogous to Qf3b, the top of Qf4 may represent the latest Pleistocene and earliest Holocene ground surface prior to deposition of Qc2.

Unit Qc1 consists of thin rocky colluvial deposits west of the main fault and east of Qf4 (Plates 3 and 4). The general degree of soil development is intermediate between that in overlying Holocene colluvium (Qc2) and underlying Qoal5. The local presence of Bt lamellae suggests a similar age to Qf4, although it could possibly be older or younger than Qf4. An age estimate of ca. 8.7 cal ka was provided by a radiocarbon analysis from charcoal in Qc1 (sample EOC2-c37; Plate 3; Appendix B), but this analysis is inconsistent with the soil characteristics in this unit and field logging of a contact between Qc1 and Qc2, and the sample is inferred to represent younger charcoal bioturbated into the deposit (see Appendix B for more discussion).

4. Holocene units

Holocene units in trench EOC-2 reach a maximum of 2.5 m in combined thickness in the west-central part of the trench and include alluvial fan deposits derived from a local drainage off the Pajarito fault escarpment (units Qf5a and Qf5b) and colluvial deposits derived from both east and west (unit Qc2) (Figures 4 and 5; Plates 1, 2, 3, and 4). The topographically lowest Holocene unit, Qf5a, consists of alluvium that was deposited on top of Qf2a, Qf3a, and Qf3b in the western half of the trench. Unit Qf5a has a gravelly base and fines upwards. The unit commonly has an erosional lower contact, although it may locally be conformable on Qf3b. Unit Qf5a is overlain by a thick section of colluvium derived from the escarpment to the west, which in turn, is overlain by another gravelly alluvial deposit (Qf5b) and more colluvium. In this area,

the part of Qc2 below Qf5b contains a prominent stone line consisting of welded tuff clasts that coarsen to the west (Plates 1 and 2) and that may record a rockfall event off the escarpment. To the east, Qf5a and Qf5b pinch out, and the entire Holocene section is represented by colluvium; colluvium from the west appears to overlie colluvium from the east in this area (Plate 3). A weak Bt horizon is present in the Holocene deposits along most of the trench, suggesting that the ground surface has been relatively stable for much of the Holocene. In contrast, Qc2 thins to the east and appears to represent a young deposit with a weak soil below an eroding hillslope east of the main fault. Historic debris (barbed wire and a rusted can) was found in the uppermost part of Qc2 in two locations, within the darker surface soil (Plates 3 and 4), and suggests either that Qc2 contains some colluvium deposited in the last 100 years or that extensive historic bioturbation has occurred.

Radiocarbon analyses indicate that the base of the Holocene section is between ca. 10.7 and 11.7 cal ka in age in the center of the trench, constrained by analyses in Qf5a and Qf3b, respectively (samples EOC2-c19 and EOC2-c14; Plate 2; Appendix B). In this area, additional radiocarbon age estimates of ca. 8.6 cal ka from Qc2 (sample EOC2-c5; Plate 2; Appendix B) and ca. 5.5 cal ka from overlying Qf5b (sample EOC2-c7; Plate 2; Appendix B) document progressive aggradation through the early and middle Holocene. The ca. 8.6 cal ka date is from 15 cm below the prominent stone line, suggesting that the tuff clasts were emplaced shortly after this time. To the east, where Qc2 overlies Qf3b and the Holocene section is thinner, a radiocarbon analysis from Qf3b indicates a somewhat younger age of ca. 10.3 cal ka or less for the base of the Holocene section (sample EOC2-c39; Plate 2; Appendix B). PDI calculations indicate a somewhat older age of ca. 13.5 ka for the base of Qc2 to the east (profile P69.9; Plate 3; Appendix C), although the possible age ranges from ^{14}C (≤ 10.2 to 10.5 cal ka) and PDI (10.7 to 16.9 ka) are very close, and in combination, these methods suggest an age of ca. 10.5 ka for the base of Qc2.

B. Structural Deformation

Structural deformation in trench EOC-2 was expressed mainly as faulting in the eastern half of the trench and some minor tilting of units. Faults were exposed in three zones in the trench: a main zone, dominated by normal faulting, between 65H and 78H; a zone apparently including strike-slip faulting between 52H and 57H; and a zone with two small faults between 82H and 85H. Evidence for westward tilting in the older units in the trench also indicates broader-scale structural deformation in this area. Select faults are shown schematically in Figure 5, and all faults are shown in detail on Plates 3 and 4.

1. Main zone of faulting

The main zone of faulting between 65H and 78H includes normal faults bounding a small horst (67H to 69H) and a small graben (69H to 77H), as well as a zone of high angle reverse faults or rotated normal faults (69H to 71H).

The most prominent structural feature in trench EOC-2 is a down-to-the-west normal fault that strikes about N25E to N35E and juxtaposes Qbt, Qoa1, and Qoa2 in the eastern fault block against Qoa3, Qoa4, and Qoa5 in the western block (77H to 77.5H; Figure 6; Plate 4). This fault is vertical and fans upward from a 5- to 10-cm-wide zone of cataclastic gouge (77H, -4V to -5.6V) to a 60-cm-wide cataclastically brecciated zone of faults, fractures, and filled fissures (77H to 77.5H, -2.9V to -4V). Vertical offset across this fault is greater than 2.5 m, based on the separation between the uppermost exposure of Qoa2 and the lowermost exposure of Qoa3 across the fault. A better estimate of total offset cannot be made without drilling because the top of Qoa2 was eroded on the eastern side of the fault and the base of Qoa3 was not exposed on the western side of the fault. Uncertainties in estimating the amount of offset also result from variability in the thickness of these units. The youngest unit that is clearly displaced along this fault is Qoa5, although coarse sand that resembles Qf1b fills a 5- to 10-cm-wide

fissure in the fault zone, suggesting post-Qf1b faulting. No evidence of faulting was observed here in Qc2; however, Qc2 is relatively thin at this location and appears younger than to the west.

Evidence for younger faulting was revealed along a N25W splay of the main fault (75.5H, middle wall) that strikes into the main fault in the center of the trench. This fault juxtaposes Qoa5 on the east against Qc1 and Qc2 on the west, indicating Holocene surface rupture at this location. Predominantly strike-slip movement is suggested by the absence of Qoa5 directly west of the fault and by the absence of significant vertical displacement of Qoa4 across the fault. The uppermost extent of this fault within Qc2 was not clear, and examination of structural relations here was hindered by the occurrence of a bench at a key stratigraphic level, bioturbation, and frozen ground.

The faults discussed above not only define the eastern boundary of the graben at the base of the main Pajarito fault escarpment but also the eastern boundary of a smaller graben-within-graben exposed in trench EOC-2 (Figure 5). The small graben lies between 69H and 77H and includes numerous internal faults (Plates 3 and 4). Within the small graben, most of the faults have a down-to-the-west sense of offset, are high angle to vertical, and have strikes that vary between N5E and N70E. Most of these faults were recognized by offset of the contact between Qoa3 and Qoa4, and only a few of the faults could be traced upward through the pumice deposits of Qoa4. None of these faults had recognizable offset of overlying Qc1 or Qc2. Within the small graben, between 69.5H and 70.5H, a series of closely spaced east-dipping faults have apparent reverse offset, although these may also represent rotated normal faults. Each of these small faults exhibits a down-to-the-west sense of displacement, and the largest displacement is 18 cm on the Qoa3-Qoa4 contact. Deformation within the small graben also includes differential tilting of beds. In the eastern part of the small graben, beds within Qoa3 have an apparent west dip of 2°, whereas farther west in the

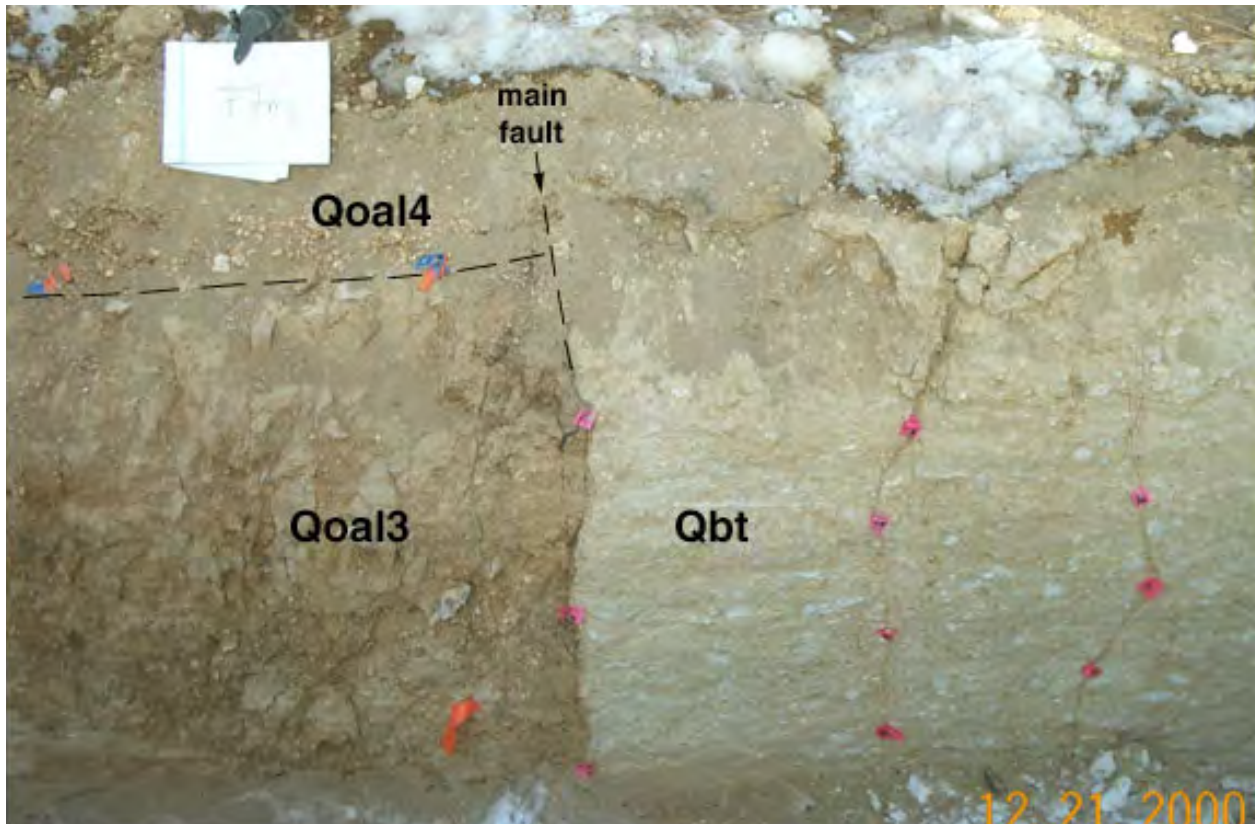


Figure 6. Photograph of main fault on the lower wall at 77H. Unit Qoal3 to the left is juxtaposed against unit Qbt to the right.

graben the dip is 7° or more westwards. In addition, two blocks at about 73H bounded by faults or fractures have east-dipping beds, contrasting with west dips in adjacent blocks to the east and west (Plate 3). Total net down-to-the-west displacement of the Qoal3-Qoal4 contact within the small graben, including both discrete faults and tilting, is estimated at 0.7 m. Local reverse faulting could result from interactions between adjacent blocks within the graben that are bounded by faults with variable strikes and dips. Alternatively, the rotation of normal faults could occur above a listric structure, and this possibility is consistent with the increase in dips within Qoal3 in the western part of this graben.

The western side of the small graben is bounded at about 69H by down-to-the east faults with measured strikes of N4E and N20E and a measured dip of 65E. These faults also form the eastern edge of

a small horst within the main zone of faulting. Vertical displacement across these faults into the small graben is estimated to be at least 1.8 m, assuming a Qoal3 thickness of at least 1.0 m here. These faults project upward to a near-vertical contact between Qf4 on the southeast and Qoal4 and Qoal5 on the northwest. Although the steepness and location of this contact suggests it may be caused by faulting, a reversal of fault movement from down-to-the-east to down-to-the-west would be required. An alternative explanation, most consistent with field evidence, is that this contact represents the erosional eastern boundary of the Qf4 paleochannel.

An estimate of the total net displacement across the small graben between 69H and 77H can be made using the contact between Qoal1 and Qoal2 as a datum, although uncertainty is imparted by differences in dip between areas east and west of the

graben and possible erosion at the base of Qoal2. East of the graben, beds have an apparent westward dip of about 2° , whereas west of the graben, beds are near horizontal. Assuming no differential erosion of the base of Qoal2 across the graben and a horizontal contact provides an estimated net down-to-the-west offset of 2.0 m. Alternatively, assuming a 2° west dip provides a slightly lower estimated net offset of 1.7 m.

Directly west of the small graben is a narrow horst bounded by a west-dipping down-to-the-west fault at about 67H (Plate 3). This fault has about 0.6 m of vertical offset of the contact between Qoal2 and Qoal3, dips about 50° W, and has measured strikes of $N45^\circ$ E and $N60^\circ$ E in the middle and lower walls, respectively. The contact between Qoal3 and Qf4 is apparently vertically offset about 16 cm along the fault, and deformation could be traced upwards as a disturbed zone through the entire thickness of Qf4. The contact between Qf4 and Qc2 is offset an estimated 7 to 8 cm along this structure, about half the offset estimated at the base of Qf4, suggesting the possibility of either multiple faulting events within Qf4 or a horizontal component of offset. However, the contact between Qf4 and Qc2 is less distinct than deeper contacts, making the estimated displacement relatively imprecise. It is possible that only one surface rupture event is recorded in Qf4 and that the displacement is entirely vertical. The fault could not be traced upwards into Qc2, suggesting that rupture may have occurred near the beginning of Qc2 deposition. However, the absence of stratification, the possibility of bioturbation, and the effects of pedogenesis in Qc2 could all make recognition of faulting within this unit difficult. It is therefore uncertain whether the most recent surface rupture event on this fault occurred early or late during deposition of Qc2.

The combined structural features in this fault zone may all result from deformation of the hanging wall (down-thrown block) of the Pajarito fault zone. The main fault exposed in trench EOC-2 has a strike that is roughly parallel to the main

escarpment of the Pajarito fault, and any along-strike or down-dip changes in the surface of the Pajarito fault would result in hanging-wall deformation such as was seen in the trench exposures. If this hypothesis is correct, then the surface rupture events recorded in trench EOC-2 were probably generated during seismic events on the Pajarito fault.

2. Faulting between 52H and 57H

The westernmost evidence of faulting in trench EOC-2 was present on the lower wall between 52H and 57H, within Qf2a (Plate 3). Because Qf2a is a complex unit with poorly resolved internal stratigraphy, the amount and net sense of offset across this fault zone cannot be determined, although major changes in stratigraphy across fault traces suggest the possibility of significant displacements.

The east end of this zone is defined by a fault that strikes $N85^\circ$ W (55–56H, lower wall, Plate 3). There is no continuity of stratigraphy across this fault, and some units to the east appear to be drag-folded into the fault plane. These relations, together with the orientation of the fault, strongly oblique to the Pajarito fault and related structures, imply the fault probably has accommodated significant horizontal (strike-slip) movement; there is no constraint on the amount of vertical displacement. This fault could be traced across the overlying bench and into the base of the middle wall at about 58.5H, where it terminated at the top of Qf2a without offsetting Qf3a. Related faults to the west, discussed below, also showed no evidence of offset of this contact.

Exposed on the lower wall between 53.5H and 55H were a series of faults with variable strikes that offset a gravel bed within Qf2a (Plate 3). Strikes of $N7^\circ$ W, $N12^\circ$ W, and E-W were measured in this fault zone. There is an apparent net down-to-the-west vertical offset of about 0.3 to 0.4 m of the base of the gravel bed within this zone, although variations in thickness of the gravel bed across fault traces also suggest horizontal compo-

nents to the displacements.

Two additional faults in Qf2a at about 52.5H and 53.5H mark the western limit of observed faulting in trench EOC-2. These faults have strikes of N73E and N68E, and there are abrupt changes in stratigraphy across them, although the sense of offset on these faults cannot be determined.

3. Faulting between 82H and 85H

Two minor east-dipping faults were present between 82H and 85H. The western fault has 5 to 8 cm of down-to-the-east displacement of the base of Qoal1 and internal layers within Qoal1 but does not offset the base of Qoal2. The eastern fault, however, does displace the base of Qoal2, in a down-to-the-west sense, by about 3 cm but does not offset the base of Qoal3. These relations indicate that at least two separate faulting events are recorded here prior to deposition of Qoal3.

4. Tilting of units

Variations in dip between units in trench EOC-2 provide evidence for tectonic tilting of this part of the Pajarito Plateau, as well as local deformation associated with faults exposed in the trench. Units Qoal1 through Qoal4 exhibit western dips in most of their exposure but, given their geomorphic setting as part of a fan derived from the Jemez Mountains, were probably originally deposited with eastern dips. In contrast, throughout the area of exposure of Qf2a between 5H and 62H along the lower wall of the trench, stratigraphic layers are relatively horizontal. These relations indicate westward tilting in at least the older units in this area, including east of the main fault in the trench, and also indicate that much or all of the tilting predated deposition of Qf2a. Because the base of Qf1b decreases in elevation to the west (Plate 4), possibly as a result of tectonic tilting, much of the tilting may also postdate Qf1b, although the base of this unit provides a less reliable structural datum than bedding within Qoal. The original bedding orientation of Qf2a is unknown, but if layers within Qf2a had an original eastern dip, some of the tilting would also postdate Qf2a.

V. DISCUSSION

A. Geomorphic and Tectonic History

The geomorphic and tectonic history of the site of trench EOC-2 can be partially reconstructed based on the results of this investigation and prior work in nearby areas.

Following deposition of the Tshirege Member of the Bandelier Tuff (unit Qbt) at ca. 1.22 Ma, this area was buried by alluvium derived from erosion of Qbt (unit Qoal1). The absence of a soil on top of Qbt or evidence for significant erosion of Qbt suggests that deposition of Qoal1 at the trench site occurred soon after deposition of Qbt. The presence of a small fault in Qoal1 at 82H that does not cut the overlying contact with Qoal2 indicates that faulting in this area also occurred relatively soon after deposition of Qbt.

Units Qoal2 and Qoal3 record the deposition of debris flows (?) and alluvium derived from areas within the Jemez Mountains that are underlain by the Tschicoma Formation, either within the Pajarito Canyon or the Twomile Canyon watersheds. Qoal2 unconformably overlies Qoal1, and an unknown amount of time elapsed between deposition of these units. Unit Qoal4 conformably overlies Qoal3 and is dominated by pumices that are inferred to have been erupted from the Cerro del Medio dome complex in the Jemez Mountains at ca. 1.13 Ma. Units Qoal2 through Qoal4 were probably part of extensive early Pleistocene alluvial fans that covered the western part of the Pajarito Plateau prior to initial canyon incision in this area; remnants of these fans are present in many areas (e.g., Reneau et al. 1995; Gardner et al. 2001).

Deposition of Qoal4 was followed by a lengthy period of soil development in at least the eastern part of the trench site, recorded by unit Qoal5. Comparison with dated soils elsewhere on the Pajarito Plateau suggests that Qoal5 represents at least 50,000 to 80,000 years of soil development,

although, because its top is eroded, the total time represented by this unit cannot be determined.

Down-to-the-west faulting juxtaposed Qoa5 and underlying units against older units across the main fault at 77H. Unit Qoa4 and at least the lower part of Qoa5 were preserved west of the fault while being eroded to the east. The erosion of these units may have been associated with general incision into the early Pleistocene alluvial fan; units Qf1a and Qf1b may represent remnants of inset fans deposited at this time. The absence of Qf1a or Qf1b above Qoa5 west of the main fault suggests that most of the faulting here occurred prior to deposition of these units; otherwise, we would expect them to be preserved at a lower elevation on the down-dropped block. However, the presence of coarse sand that was apparently derived from Qf1b within a fissure in the main fault suggests that some deformation here has also post-dated Qf1b.

At the trench site, alluvial deposits younger than Qf1b are restricted to the area west of 69H, associated with a topographic low east of the Pajarito fault escarpment. The style of deformation exposed in the trench indicates that development of this low involved both westward tilting and down-to-the-west faulting, and once formed, the low has apparently focused fluvial transport and aided deposition. The contrast in dips between Qf2a and older units indicates that most or all of the tilting pre-dated deposition of Qf2a, and much may also have post-dated Qf1b (although this is less certain). The axis of the present low is only 1.5 to 2 m lower than the topographic high east of the trench site, but local relief was at least 3 m greater prior to deposition of Qf2a and younger units. Examination of samples from bore holes (Appendix E) indicates that the top of Qbt is 5 to 8 m lower in this area than east of the main fault. This difference is significantly greater than the approximately 2 to 2.5 m of down-to-the-west deformation estimated across the main fault zone and indicates that most of the post-Qbt vertical deformation at the trench site occurred west of 69H, although the

nature and timing of deformation was not revealed in the trench exposure.

Unit Qf2a records extensive alluvial deposition, spanning an unknown length of time, in the topographic low. The lowest part of the unit exposed in the trench has an estimated age from soils of 110 to 180 ka or more, and the youngest part of the unit could be as young as ca. 50 to 60 ka. Examination of samples from bore holes (Appendix E) suggests that Qf2a may extend for another 2 m or more below the base of the trench. As exposed in the trench, Qf2a includes abundant dacite clasts in the eastern part of its exposure, suggesting a source either in the Jemez Mountains or from local reworking of older fan deposits. In the western part of its exposure, however, and in younger units, clasts are dominated by welded tuff, indicating a change in the source to drainages off the Pajarito fault escarpment that has persisted into the Holocene.

During or following deposition of Qf2a, faulting occurred between 52H and 57H, possibly including both strike-slip and normal faulting. It is not possible to determine how many faulting events are recorded in this zone, but all faulting here preceded deposition of Qf3a.

Unit Qf3a unconformably overlies Qf2a and records an unknown amount of erosion followed by relatively minor amounts of sediment deposition prior to ca. 43 ka (as estimated from soil development). Notably, the El Cajete pumice, which was erupted from the Jemez Mountains at ca. 50 to 60 ka and is present in nearby areas (e.g., Wong et al. 1995; Reneau and McDonald 1996; Gardner et al. 2001), was apparently eroded from this site between deposition of Qf2a and Qf3a. No El Cajete pumice clasts were observed in the trench exposure. However, weathered biotite crystals that may have been derived from the pumice were identified in Qf3a, and glass shards that are geochemically correlative with the pumice were found in Qf2a and Qf3a.

Unit Qf3b records a period of land surface stability

and soil development across the western half of the trench site that likely extended into the beginning of the Holocene. An exception to this general stability is recorded by unit Qf4, which has an estimated soil age of ca. 35 to 55 ka and fills a paleochannel incised into the eastern part of the topographic low. This paleochannel may have been associated with the headward erosion of a channel from the north, where an incised channel currently exists 10 m from the trench site.

A major period of sediment deposition occurred in the Holocene, including both alluvium derived from a drainage off the Pajarito fault escarpment (units Qf5a and Qf5b) and colluvium derived from both the escarpment and from the topographic high to the east (unit Qc2). Deposition of Qf5a in the center of the trench site began between ca. 10.7 and 11.7 cal ka, and deposition of Qc2 farther east began ca. 10.5 cal ka. Up to 2.5 m of deposition occurred during this period in the axis of the topographic low, constituting the most significant depositional event since at least 50 to 60 ka at the trench site. Radiocarbon analyses indicate that at least 1.5 m of deposition occurred over a 5000- to 6000-year period in the early to middle Holocene and that a maximum of 0.9 m of deposition occurred in the last 5500 years. Accompanying deposition, the axis of the topographic low migrated about 25 m eastward, from about 39H at the beginning of the Holocene to about 64H at present. This change in local topography is consistent with higher rates of sediment supply from the escarpment to the west than from the low rise to the east. It is possible that deformation within the graben contributed to the changes in topography, although the relatively small-scale nature of Holocene faulting at the trench site suggests that any structural influence was small.

The depositional record exposed in trench EOC-2 is consistent with evidence from elsewhere on the Pajarito Plateau for a period of major landscape instability in the Holocene, with sediment deposition probably triggered by accelerated rates of erosion in surrounding areas (Reneau and McDonald 1996; Reneau et al. 1996b; Reneau 2000). Notably,

the date of ca. 10.7 cal ka (ca. 9.4 ^{14}C ka) from Qf5a is virtually identical to dates from the upper part of a fan near the base of the Pajarito fault escarpment north of Water Canyon (Gardner et al. 2001), indicating contemporaneous deposition at these sites.

Holocene surface rupture was recognized at two locations in trench EOC-2, at about 67H and 76H. Holocene faulting at the western fault trace is estimated at 7 to 8 cm of net vertical offset. Holocene faulting at the eastern trace involved an unknown amount of horizontal offset and perhaps minimal vertical offset. Field evidence indicates that both faults displace the base of Qc2, which has an estimated age of ca. 10.5 cal ka or less in this part of the trench, but age control is insufficient to provide more refined age estimates or to determine if these ruptures occurred in the same event.

Indirect evidence for a possible paleoseismic event near or sometime after ca. 8.6 cal ka is provided by the prominent stone line within Qc2 in the western part of the trench. Earthquakes commonly trigger rockfalls and other mass-wasting events on steep slopes (e.g., Keefer 1984; Bull and Brandon 1998). The characteristics of the stone line are consistent with emplacement of the tuff clasts during a single rockfall event off the Pajarito fault escarpment. If this stone line records a paleoseismic event, there is insufficient evidence to determine the location or magnitude of the earthquake, and it may or may not have occurred in the Pajarito fault system. However, it is worth noting that available age constraints allow the possibility that the most recent surface rupture event discussed above and formation of the stone line were contemporaneous. This provides suggestive evidence that the most recent event at the trench site may have occurred at or since ca. 8.6 cal ka

B. Paleoseismic Chronology

1. Trench EOC-2

The exposures in trench EOC-2 provided evidence for multiple surface faulting events, which, due to the proximity of the Pajarito fault escarpment, are

likely associated with events on that fault. A minimum of six paleoseismic events are apparently recorded here, ranging in age from early Pleistocene to Holocene, and demonstrate the recurring nature of surface faulting at this site. The number of faulting events may actually be much greater than this, although data are insufficient to better refine the paleoseismic history here.

The earliest evidence for faulting is provided at 82H, where a fault within unit Qoal1 does not cut the overlying unit Qoal2, indicating an early Pleistocene event relatively soon after eruption of the Bandelier Tuff at ca. 1.22 Ma.

An additional early Pleistocene event is recorded at 85H, where a fault offsets the contact between Qoal1 and Qoal2 but does not cut the contact between Qoal2 and Qoal3. This event is inferred to have occurred prior to eruption of Cerro del Medio at ca. 1.13 Ma.

Evidence for faulting after deposition of Qoal4 but prior to development of the Qoal5 soil is present between 69H and 71H, where multiple down-to-the-west faults displace the contact between Qoal3 and Qoal4 but do not affect the base of Qoal5. This faulting event would have occurred after ca. 1.13 Ma and prior to 185 to 295 ka.

The next oldest evidence for faulting is present on the main fault at 77H, where unit Qoal5 was apparently down-dropped prior to deposition of units Qf1a and Qf1b. Because total vertical offset across this fault prior to deposition of Qf1 is estimated to be at least 2.5 m, we infer that multiple surface-rupture events here preceded deposition of Qf1b. However, because the average displacement per event is unknown, we cannot estimate the number of events that occurred here. Because the ages of Qoal5 and Qf1 are poorly constrained, we also cannot estimate the age of this faulting in more than a relative sense.

Younger Pleistocene faulting is recorded by several faults between 52H and 57H that displace layers

within unit Qf2a but do not cut the contact with overlying unit Qf3a. Because of the complexity of faulting in this zone, we infer that multiple events are probably recorded here, although we have no basis for estimating the number of events. Faulting here preceded deposition of Qf3a, with an estimated minimum age of ca. 43 ka, and post-dates deposition of the upper part of Qf2a, with an estimated age of 60 to 95 ka or greater in this part of the trench.

Evidence for Holocene faulting is present at 67H and 76H, where two faults cut the base of unit Qc2 and indicate surface rupture sometime after ca. 10.5 cal ka. The upward terminations of these faults in Qc2 were not clear. Evidence here suggests either faulting in the early Holocene when Qc2 was thin or faulting later in the Holocene with a sufficient period of time having elapsed to obscure the upper part of the faults by bioturbation and/or pedogenesis. The simplest interpretation is that both ruptures occurred during the same event, although age control is insufficient to demonstrate this or to provide a more refined age estimate on faulting. As discussed in the previous section, it is possible that the stone line in Qc2 to the west records a rockfall generated by the same paleoseismic event that produced the surface rupture in trench EOC-2, which would indicate an event near or somewhat after ca. 8.6 cal ka. However, the evidence for this is not conclusive, and this hypothesis requires testing with data from other sites.

2. Other trench investigations

One outstanding paleoseismic issue concerning the Pajarito fault system is the relation of different fault traces to each other during paleoseismic events, particularly the possibility of simultaneous rupture of the Pajarito fault and the Rendija Canyon and Guaje Mountain faults to the northeast (Wong et al. 1995; Olig et al. 1996). Data on the timing of specific paleoseismic events on each fault are required to evaluate this issue, although available data have been inconclusive and there has been no direct evidence of simultaneous rupture of the Pajarito, Rendija Canyon, and Guaje Mountain

faults. Unfortunately, data from trench EOC-2 are also insufficient to further refine the paleoseismic chronology for the Pajarito fault system, other than to confirm that Holocene faulting has occurred on multiple fault traces. Here we briefly summarize prior evidence on the timing of the most recent event (MRE) on the different faults obtained from previous paleoseismic investigations. We restrict this discussion to the MRE because age estimates for earlier faulting events are much less precise, preventing meaningful comparisons.

Evidence for the age of the MRE on the Guaje Mountain and Rendija Canyon faults has been provided by trenches excavated in Cabra Canyon and at the Guaje Pines Cemetery, respectively. At trench SHT-1 on the Guaje Mountain fault (Figure 1), the MRE was constrained between ca. 5.7 ^{14}C ka and ca. 3.8 ^{14}C ka (ca. 6.5 and 4.2 cal ka) based on radiocarbon analyses from faulted and overlying nonfaulted alluvial units (Gardner et al. 1990). In contrast, at trench GPT-2 on the Rendija Canyon fault (Figure 1), radiocarbon analyses from scarp-derived colluvium that postdated the MRE provided an age estimate ca. 7.3 ^{14}C ka (ca. 8.1 cal ka), and thermoluminescence (TL) analyses from the same unit provided an age estimate of ca. 23 ka (Wong et al. 1995; Kelson et al. 1996). These studies therefore indicate different ages for the MRE on these two faults.

Paleoseismic trenches have been excavated within the Pajarito fault zone in three separate studies prior to this investigation. In the first study, four trenches excavated in 1992 provided limited data on paleoseismic events, with the youngest recognizable deformation occurring at trench WTT1 between Cañon de Valle and Water Canyon (Figure 1) in colluvial deposits that predate the ca. 50- to 60-ka El Cajete pumice (Wong et al. 1995; Olig et al. 1996).

In the second study, a series of seven trenches was excavated in 1997 in a transect south of Los Alamos Canyon, and three of these trenches provided evidence for Holocene surface rupture (trenches 97-3, 97-4, and 97-7; McCalpin 1998). The best

constraint on the age of the MRE came from trench 97-7 and adjacent trench 97-7A (Figure 1), where radiocarbon analyses from faulted and overlying nonfaulted slopewash or colluvial deposits lead to an interpretation that the MRE occurred between ca. 1.3 and 2.3 cal ka, perhaps at ca. 1.5 cal ka (McCalpin 1998). Later, McCalpin (2000) reevaluated the available geochronologic data and proposed that the MRE occurred at ca. 3 to 7 ka, based on the interpretation that the radiocarbon analyses were all from “intrusive” material and that TL and PDI age estimates were more reliable. However, this conclusion requires that known limitations of TL (i.e., possible inheritance effects on age estimates) and PDI (i.e., possible thickness effects on age estimates) in certain settings be neglected and that the general consistency in ^{14}C analyses between two separate trenches be ignored. For these reasons, we believe that the original interpretation of McCalpin (1998) that the MRE occurred between ca. 1.3 and 2.3 ka is more reasonable.

In the third study, a series of seven trenches was excavated in 1998 across an alluvial fan and several fault traces south of Pajarito Canyon, and three of these trenches provided evidence for late Pleistocene or Holocene surface rupture (trenches 98-4, 98-5, and 98-6, Figure 1; McCalpin 1999). Age constraints on faulting were less precise here than in the 1997 trenches, and the MRE in the different 1998 trenches was roughly bracketed between ca. 2 to 3 ka and ca. 12 to 20 ka. Later, relying on recently received infrared-stimulated luminescence (IRSL) analyses, McCalpin (2000) revised the bracketing ages to ca. 8 to 10 ka and ca. 18 to 24 ka. This revision assumes that there are no significant inheritance effects in the IRSL analyses, although the analyses did suggest that such effects were present (Berger 1999, cited in McCalpin 2000). Because it is not certain that all uncertainties in the IRSL analyses are recognized, we consider it possible that the MRE in the 1998 trenches is younger than proposed by McCalpin (2000).

In summary, available data on the timing of the MRE from different paleoseismic investigations

indicate that one or more Holocene surface-rupture events have occurred on the Pajarito fault system and that different fault traces have ruptured at different times. The MRE at the site of trench EOC-2 could have been the same event as recorded at previous trenches along several faults in the Guaje Mountain, Pajarito, or Rendija Canyon fault zones, although this issue cannot be better resolved at present.

C. Implications for Facility Siting

DOE guides and standards provide two different criteria for evaluating potential surface faulting hazards to new or existing facilities that are pertinent to siting of a new EOC: the first specifying avoidance of active faults and the second involving a probabilistic assessment of potential fault rupture.

DOE Guide 420.1 states that “Siting of structures over active geologic faults . . . must be avoided” (DOE 2000), and DOE Standard 1022-94 states that “A site location that has a potential for surface-fault rupture and associated deformation from active faults should be avoided” (DOE 1996b). Faults are considered active by DOE “by the presence of surface or near-surface deformation of geologic deposits of a recurring nature within the last approximately 500,000 years or at least once in the last approximately 50,000 years” (DOE 1996b), which is adopted from the definition used by the Nuclear Regulatory Commission. By this definition, the main fault zone exposed in trench EOC-2, with movement in the Holocene, is considered active. The proposed EOC should thus be set back some distance from associated fault traces, although DOE has not provided guidance on appropriate setback criteria. Goen (2000) suggested that standards used in California (California Department of Conservation 1996) and Utah (Salt Lake City Planning Division 1989) be adopted for siting of a new EOC, specifically a minimum setback of 15 m (50 ft) from faults that have ruptured since 11 ka (the Holocene). If this setback is adopted, and if all Holocene faults present at the site were exposed in the trench, then the western

half of trench EOC-2 would be a suitable area for a new facility.

Several uncertainties concerning potential faulting at the site should be pointed out. Because only one trench was excavated, we cannot rule out the possibility of Holocene faults through the proposed building footprint that may trend parallel or obliquely to the trench, although trench siting was sufficient to locate major geologic structures oriented roughly parallel to the Pajarito fault. The location of the closest Holocene fault rupture west of the trench is also unknown. It should also be emphasized that available data are not sufficient to evaluate the possibility of recurring events since 500 ka at the site, and it is therefore uncertain if this site would meet those more stringent criteria in DOE Standard 1022-94 (DOE 1996b).

An additional uncertainty is whether the fault zone exposed between 52H and 57H has ruptured since 50 ka and whether it should thus be considered active. Available data indicate that displacement occurred before deposition of unit Qf3a, which has an estimated age of older than ca. 43 ka and younger than ca. 50 to 60 ka, and after deposition of unit Qf2a, the upper part of which has an estimated age of ca. 60 to 95 ka or greater in this part of the trench. We therefore cannot rule out the possibility of faulting between 43 and 50 ka, although, considering the available age constraints, it is more likely that faulting here preceded 50 ka.

A probabilistic approach for evaluating surface fault hazards is discussed in DOE Standard 1023-95, which states that “A probabilistic assessment . . . may be necessary if potential fault rupture may occur near a facility. If the annual probability of this ground failure mode is greater than the necessary performance goal, either the site should be avoided, mitigation measures taken, or an evaluation performed of the effects of fault offset” (DOE 1996a). A probabilistic surface-rupture assessment has not been performed for the site of the proposed new EOC, but such assessments have been performed in nearby areas at LANL (Olig et al. 1998,

2001) and allow constraining the probability of surface faulting. Following DOE guidelines (DOE 2000), the new EOC would be a Performance Category 2 (PC-2) facility, and the performance goal, or acceptable probability of seismically-induced failure, would be 5×10^{-4} , or once in 2000 years (DOE 1996c). A probabilistic assessment of potential rupture from a generic subsidiary fault in the Pajarito fault zone at TA-16, roughly analogous to the main fault zone at trench EOC-2, indicates that less than 0.1 cm of surface displacement would occur in a 2000 year period (Olig et al. 2001). Because of the structural similarity of TA-16 and the proposed EOC site, the probability of significant surface rupture should be less than 5×10^{-4} , and this site should satisfy probabilistic criteria for PC-2 facilities (Goen 2000).

VI. CONCLUSION

Trench EOC-2 exposed stratigraphic units that range in age from early Pleistocene to late Holocene and exposed faults in a 33-m-wide zone that exhibit evidence for normal, strike-slip, and possibly reverse offset. The main zone of faulting displays down-to-the-west offset and forms the eastern edge of an approximately 160-m-wide graben at the base of the east-facing Pajarito fault escarpment. Net vertical offset of the ca. 1.22 Ma Bandelier Tuff of about 2 to 2.5 m is estimated across the main fault zone in the trench, although samples from bore holes to the west indicate that the graben has a maximum structural depth of at least 8 m. The additional vertical deformation may be accommodated by offset on relatively old faults that were not exposed in the trench, by westward tectonic tilting, or by a combination of both.

The trench exposures provided evidence for a minimum of six surface rupture events that range in age from early Pleistocene to Holocene, demonstrating the recurring nature of surface faulting at the site. The most recent event occurred sometime after ca. 10.5 ka, and possibly near or after ca. 8.6 ka, although a more refined age estimate is not

possible. Following DOE guides and standards, this fault zone is considered active and should be avoided in the siting of new facilities. However, based on analysis of an analogous setting at TA-16, the proposed EOC site should satisfy probabilistic criteria for evaluating surface-fault hazards, with the probability of significant surface rupture being less than once in 2000 years.

VII. ACKNOWLEDGMENTS

This work was supported by the LANL Seismic Hazards Program and by planning efforts for a new Emergency Operations Center, as part of Cerro Grande fire-recovery activities. We thank Larry Goen, Keith Orr, and George Vantien for their support in these projects; Calvin Martin for access to bore hole samples; Clyde Vigil for surveying support; Anthony Garcia for drafting support; Robert Brady and Larry Goen for helpful review comments; and Roger Eckhardt for editing and compositing.

VIII. REFERENCES

- AMEC. 2001. Geotechnical engineering study, Emergency Operations Center, Los Alamos National Laboratory, Los Alamos, New Mexico. Unpublished report. Albuquerque, NM: AMEC Earth and Environmental, Inc.
- Berger, G. W. 1999. Optical dating of sediments from Pajarito fault trenches at Los Alamos, New Mexico. Unpublished report. Reno, NV: Desert Research Institute.
- Bull, W. B., and Brandon, M. T. 1998. Lichen dating of earthquake-generated regional rockfall events, Southern Alps, New Zealand. *Geological Society of America Bulletin* 9110: 60–84.
- California Department of Conservation. 1996. Earthquake Fault Zoning. In *Geology, Mines, and Mining, Public Resources Code, Division 2*

- (Alquist-Priolo Earthquake Fault Zoning Act), Chapter 7.5. Sacramento, CA: State of California, Division of Mines and Geology.
- Chapin, C. E., and Cather, S. M. 1994. Tectonic setting of the axial basins of the northern and central Rio Grande rift. In *Basins of the Rio Grande Rift: Structure, Stratigraphy, and Tectonic Setting*, Keller, G. R., and Cather, S. M., editors. *Geological Society of America Special Paper 29*, pp. 5–25.
- DOE (Department of Energy). 1996a. Natural phenomena hazards assessment criteria. DOE-STD-1023-95, Change Notice #1, January 1996. Washington, D.C.: U.S. Department of Energy.
- DOE. 1996b. Natural phenomena hazards characterization criteria. DOE-STD-1022-94, Change Notice #1, January 1996. Washington, D.C.: U.S. Department of Energy.
- DOE. 1996c. Natural phenomena hazards design and evaluation criteria. DOE-STD-1020-94, Change Notice #1, January 1996. Washington, D.C.: U.S. Department of Energy.
- DOE. 2000. Guide for the mitigation of natural phenomena hazards for DOE nuclear facilities and nonnuclear facilities. DOE G 420.1-2. Washington, D.C.: U.S. Department of Energy.
- Gardner, J. N., Goff, F., Garcia, S., and Hagan, R. C. 1986. Stratigraphic relations and lithologic variations in the Jemez volcanic field, New Mexico. *Journal of Geophysical Research* 91: 1763–1778.
- Gardner, J. N., and House, L. 1987. Seismic hazard investigations at Los Alamos National Laboratory, 1984–1985. Los Alamos National Laboratory report LA-11072-MS, 76 pp.
- Gardner, J. N., Baldrige, W. S., Gribble, R., Manley, K., Tanaka, K., Geissman, J. W., Gonzalez, M., and Baron, G. 1990. Results from Seismic Hazards Trench #1 (SHT-1), Los Alamos Seismic Hazards Investigations. Los Alamos National Laboratory memorandum EES1-SH90-19.
- Gardner, J. N., Lavine, A., WoldeGabriel, G., Krier, D., Vaniman, D., Caporuscio, F., Lewis, C., Reneau, P., Kluk, E., and Snow, M. J. 1999. Structural geology of the northwestern portion of Los Alamos National Laboratory, Rio Grande rift, New Mexico: Implications for seismic surface rupture potential from TA-3 to TA-55. Los Alamos National Laboratory report LA-13589-MS, 112 pp.
- Gardner, J. N., Reneau, S. L., Lewis, C. J., Lavine, A., Krier, D., WoldeGabriel, G., and Guthrie, G. 2001. Geology of the Pajarito fault zone in the vicinity of S-Site (TA-16), southwestern corner of Los Alamos National Laboratory, Rio Grande rift, New Mexico. Los Alamos National Laboratory report LA-13831-MS, 86 pp.
- Goen, L. 2000. Proposed EOC siting near West Jemez Road at TA-58. Los Alamos National Laboratory memorandum ESA-EA:00-250 to Keith Orr, December 13, 2000.
- Golombek, M. P., McGill, G. E., and Brown, L. 1983. Tectonic and geologic evolution of the Española basin of the Rio Grande rift: Structure, rate of extension, and relation to the state of stress in the western U.S. *Tectonophysics* 94: 483–507.
- Griggs, R. L. 1964. Geology and groundwater resources of the Los Alamos area, New Mexico. U.S. Geological Survey Water-Supply Paper 1735, 107 pp.
- Harden, J. W. 1982. A quantitative index of soil development from field descriptions: Examples from a soil chronosequence in central California. *Geoderma* 28: 1–28.
- Harden, J. W. 1990. Soil development of stable landforms and implications for landscape studies. In *Soils and Landscape Evolution*, Knuepfer, P. L. K., and McFadden, L. D., editors.

Geomorphology 3: 391–398.

Harden, J. W., and Taylor, E. M. 1983. A quantitative comparison of soil development in four climatic regimes. *Quaternary Research* 20: 342–359.

Harden, J. W., Taylor, E. M., Hill, C., Mark, R. L., McFadden, L. D., Reheis, M. C., Sowers, J. M., and Wells, S. G. 1991. Rates of soil development from four soil chronosequences in the southern Great Basin. *Quaternary Research* 35: 383–399.

Heiken, G., Goff, F., Stix, J., Tamanyu, S., Shafiqullah, M., Garcia, S., and Hagan, R. 1986. Intracaldera volcanic activity, Toledo caldera and embayment, Jemez Mountains, New Mexico. *Journal of Geophysical Research* 91: 1799–1815.

Izett, G. A., and Obradovich, J. D. 1994. $^{40}\text{Ar}/^{39}\text{Ar}$ age constraints for the Jaramillo Normal Subchron and the Matuyama-Brunhes geomagnetic boundary. *Journal of Geophysical Research* 99: 2925–2934.

Keefer, D. K. 1984. Landslides caused by earthquakes. *Geological Society of America Bulletin* 95: 406–421.

Kelley, V. C. 1979. Tectonics, middle Rio Grande rift, New Mexico. In *Rio Grande Rift: Tectonics and Magmatism*, Riecker, R. E., editor, pp. 57–70. Washington, D.C.: American Geophysical Union.

Kelson, K. I., and Olig, S. S. 1995. Estimated rates of Quaternary crustal extension in the Rio Grande rift, northern New Mexico. In *Geology of the Santa Fe Region, New Mexico: New Mexico Geological Society Forty-Sixth Annual Field Conference Guidebook*, Bauer, P. W., Kues, B. S., Dunbar, N. W., Karlstrom, K. E., and Harrison, B., editors, pp. 9–12.

Kelson, K. I., Hemphill-Haley, M. A., Olig, S. S., Simpson, G. D., Gardner, J. N., Reneau, S. L., Kolbe, T. R., Forman, S. L., and Wong, I. G. 1996. Late Pleistocene and possibly Holocene displace-

ment along the Rendija Canyon fault, Los Alamos County, New Mexico. In *The Jemez Mountains Region: New Mexico Geological Society Forty-Seventh Annual Field Conference Guidebook*, Goff, F., Kues, B. S., Rogers, M. A., McFadden, L. D., and Gardner, J. N., editors, pp. 153–160.

Kolbe, T., Sawyer, J., Gorton, A., Olig, S., Simpson, D., Fenton, C., Reneau, S., Carney, J., Bott, J., and Wong, I. 1994. Evaluation of the potential for surface faulting at the proposed Mixed Waste Disposal Facility, TA-67. Unpublished report, 3 volumes. Oakland, CA: Woodward-Clyde Federal Services.

Krier, D., Caporuscio, F., Gardner, J. N., and Lavine, A. 1998. Stratigraphy and geologic structure at the Chemical and Metallurgy (CMR) building, Technical Area 3, Los Alamos National Laboratory. Los Alamos National Laboratory report LA-13522-MS, 32 pp.

Manley, K. 1979. Stratigraphy and structure of the Española basin, Rio Grande rift, New Mexico. In *Rio Grande Rift: Tectonics and Magmatism*, Riecker, R. E., editor, pp. 71–86. Washington, D.C.: American Geophysical Union.

McCalpin, J. P. 1997. Geomorphology and structure of the Pajarito fault west of Los Alamos National Laboratory, New Mexico. Unpublished report. Estes Park, CO: GEO-HAZ Consulting, Inc.

McCalpin, J. P. 1998. Late Quaternary faulting on the Pajarito fault, west of Los Alamos National Laboratory, north-central New Mexico: Results from the seven-trench transect excavated in summer of 1997. Unpublished report. Estes Park, CO: GEO-HAZ Consulting, Inc.

McCalpin, J. P. 1999. Late Quaternary faulting on the Pajarito fault, west of Los Alamos National Laboratory, north-central New Mexico: Results from seven trenches excavated in summer of 1998. Unpublished report. Estes Park, CO: GEO-HAZ Consulting, Inc.

- McCalpin, J. P. 2000. Late Quaternary faulting on the Pajarito fault, west of Los Alamos National Laboratory, north-central New Mexico: Summary chronology of Quaternary faulting events. Unpublished report. Estes Park, CO: GEO-HAZ Consulting, Inc.
- McDonald, E. 1999. LANL seismic hazard trench investigations: Soil stratigraphy and pedologic age estimates for late Quaternary faulting on the Pajarito fault, west of Los Alamos National Laboratory: Results from 1997 and 1998 trench excavations. Unpublished report. Reno, NV: Desert Research Institute.
- McDonald, E. V., Reneau, S. L., and Gardner, J. N. 1996. Soil-forming processes on the Pajarito Plateau: Investigation of a soil chronosequence in Rendija Canyon. In *The Jemez Mountains Region: New Mexico Geological Society Forty-Seventh Annual Field Conference Guidebook*, Goff, F., Kues, B. S., Rogers, M. A., McFadden, L. D., and Gardner, J. N., editors, pp. 367–374.
- Olig, S. S., Kelson, K. I., Gardner, J. N., Reneau, S. L., and Hemphill-Haley, M. 1996. The earthquake potential of the Pajarito fault system. In *The Jemez Mountains Region: New Mexico Geological Society Forty-Seventh Annual Field Conference Guidebook*, Goff, F., Kues, B. S., Rogers, M. A., McFadden, L. D., and Gardner, J. N., editors, pp. 143–151.
- Olig, S., Youngs, R., and Wong, I. 1998. Probabilistic seismic hazard analysis for surface fault displacement at TA-3, Los Alamos National Laboratory. Unpublished report. Oakland, CA: Woodward-Clyde Federal Services.
- Olig, S., Youngs, R., and Wong, I. 2001. Probabilistic seismic hazard analysis for surface fault displacement at TA-16, Los Alamos National Laboratory. Unpublished report. Oakland, CA: URS Corporation.
- Phillips, W. M., McDonald, E. V., Reneau, S. L., and Poths, J. 1998. Dating soils and alluvium with cosmogenic ^{21}Ne depth profiles: Case studies from the Pajarito Plateau, New Mexico, USA. *Earth and Planetary Science Letters* 160: 209–223.
- Reneau, S. L. 2000. Stream incision and terrace development in Frijoles Canyon, Bandelier National Monument, New Mexico, and the influence of lithology and climate. *Geomorphology* 32: 171–193.
- Reneau, S. L., and McDonald, E. V. 1996. Landscape history and processes on the Pajarito Plateau, northern New Mexico: Rocky Mountain Cell, Friends of the Pleistocene, Field Trip Guidebook. Los Alamos National Laboratory report LA-UR-96-3035, 195 pp.
- Reneau, S. L., Kolbe, T., Simpson, D., Carney, J. S., Gardner, J. N., Olig, S. S., and Vaniman, D. T. 1995. Surficial materials and structure at Pajarito Mesa. In “Geological site characterization for the proposed mixed waste disposal facility,” Los Alamos National Laboratory, Reneau, S. L., and Raymond, R., Jr., editors. Los Alamos National Laboratory report LA-13089-MS, pp. 31–69.
- Reneau, S. L., Gardner, J. N., and Forman, S. L. 1996a. New evidence for the age of the youngest eruptions in the Valles caldera, New Mexico. *Geology* 24: 7–10.
- Reneau, S. L., McDonald, E. V., Gardner, J. N., Kolbe, T. R., Carney, J. S., Watt, P. M., and Longmire, P. A. 1996b. Erosion and deposition on the Pajarito Plateau, New Mexico, and implications for geomorphic responses to late Quaternary climatic changes. In *The Jemez Mountains Region: New Mexico Geological Society Forty-Seventh Annual Field Conference Guidebook*, Goff, F., Kues, B. S., Rogers, M. A., McFadden, L. D., and Gardner, J. N., editors, pp. 391–397.
- Reneau, S. L., Broxton, D. E., Carney, J. S., and LaDelfe, C. 1998. Structure of the Tshirege

- Member of the Bandelier Tuff at Mesita del Buey, Technical Area 54, Los Alamos National Laboratory. Los Alamos National Laboratory report LA-13538-MS, 16 pp.
- Rogers, M. A. 1995. *Geologic Map of the Los Alamos National Laboratory Reservation*. Santa Fe, NM: New Mexico Environment Department.
- Salt Lake County Planning Division. 1989. Salt Lake County Zoning Ordinance Chapter 19.75. Salt Lake City: UT: Salt Lake County Planning Division.
- Smith, R. L., Bailey, R. A., and Ross, C. S. 1970. Geologic map of the Jemez Mountains, New Mexico. U.S. Geological Survey Miscellaneous Geologic Investigations Map I-571.
- Soil Survey Staff. 1981. Examination and description of soils in the field. In *Soil Survey Manual (USDA-ARS)*. Washington, D.C.: U.S. Government Printing Office.
- Spell, T. L. 1987. Geochemistry of the Valle Grande Member ring fracture rhyolites, Valles caldera, New Mexico. M.S. thesis, 212 pp. Socorro, NM: New Mexico Institute of Mining and Technology.
- Spell, T. L., and Harrison, T. M. 1993. $^{40}\text{Ar}/^{39}\text{Ar}$ geochronology of post-Valles caldera rhyolites, Jemez volcanic field, New Mexico. *Journal of Geophysical Research* 98: 8031–8051.
- Spell, T. L., McDougall, I., and Doulgeris, A. P. 1996. Cerro Toledo Rhyolite, Jemez volcanic field, New Mexico: $^{40}\text{Ar}/^{39}\text{Ar}$ geochronology of eruptions between two caldera-forming events. *Geological Society of America Bulletin* 108: 1549–1566.
- Stuiver, M., Reimer, P. J., Bard, E., Beck, J. W., Burr, G. S., Hughen, K. A., Kromer, B., McCormac, G., van der Plicht, J., and Spurk, M. 1998. INTCAL98 radiocarbon age calibration, 24,000-0 cal BP. *Radiocarbon* 40: 1041–1083.
- Switzer, P. S., Harden, J. W., and Mark, R. K. 1988. A statistical method for estimating rates of soil development and ages of geologic deposits: A design for soil-chronosequence studies. *Mathematical Geology* 20: 49–61.
- Talma, A. S., and Vogel, J. C. 1993. A simplified approach to calibrating ^{14}C dates. *Radiocarbon* 35: 317–322.
- Taylor, E. M. 1988. Instructions for the soil development index template-Lotus 1-2-3. U.S. Geological Survey Open-File Report 233A.
- Toyoda, S., Goff, F., Ikeda, S., and Ikeya, M. 1995. ESR dating of quartz phenocrysts in the El Cajete and Battleship Rock members of the Valles Rhyolite, Valles caldera, New Mexico. *Journal of Volcanology and Geothermal Research* 67: 29–40.
- Wolff, J. A., and Gardner, J. N. 1995. Is the Valles caldera entering a new cycle of activity? *Geology* 23: 411–414.
- Wolff, J. A., Gardner, J. N., and Reneau, S. L. 1996. Field characteristics of the El Cajete pumice deposit and associated southwestern moat rhyolites of the Valles caldera. In *The Jemez Mountains Region: New Mexico Geological Society Forty-Seventh Annual Field Conference Guidebook*, Goff, F., Kues, B. S., Rogers, M. A., McFadden, L. D., and Gardner, J. N., editors, pp. 311–316.
- Wong, I., Kelson, K., Olig, S., Kolbe, T., Hemphill-Haley, M., Bott, J., Green, R., Kanakari, H., Sawyer, J., Silva, W., Stark, C., Haraden, C., Fenton, C., Unruh, J., Gardner, J., Reneau, S., and House, L. 1995. Seismic hazards evaluation of the Los Alamos National Laboratory. Unpublished report, 3 volumes. Oakland, CA: Woodward-Clyde Federal Services.
- Wong, I., Kelson, K., Olig, S., Bott, J., Green, R., Kolbe, T., Hemphill-Haley, M., Gardner, J.,

Reneau, S., and Silva, W. 1996. Earthquake potential and ground shaking hazard at the Los Alamos National Laboratory, New Mexico. In *The Jemez Mountains Region: New Mexico Geological Society Forty-Seventh Annual Field Conference Guidebook*, Goff, F., Kues, B. S., Rogers, M. A., McFadden, L. D., and Gardner, J. N., editors, pp. 135–142.

APPENDIX A. STRATIGRAPHIC UNIT DESCRIPTIONS

Unit Qbt

Bandelier Tuff (Tshirege Member). This unit is an incipiently welded pumice-rich ash-flow tuff, consisting of approximately 60% pumice lapilli in a matrix of ash with a small fraction of phenocrysts, with no apparent stratification. The pumice is glassy, grayish-white in color, and contains 5 to 10% phenocrysts up to 2 to 3 mm in diameter. The mean pumice diameter is < 0.5 cm, with a maximum long dimension of 20 cm. The unit has discontinuous orange-brown Bt lamellae and mottling; approximately 15 to 20% of the outcrop is white in color. The unit contains < 5% accidental lithic fragments, with a maximum long dimension of 2.5 cm. The lower contact is not exposed. Maximum exposed thickness is 1.5 m.

Unit Qoal1

Early Pleistocene Alluvium. This unit is well-bedded alluvium that consists mostly of coarse-grained sand and pumice clasts. The pumice has a maximum diameter of 5 cm and is crystal-rich, derived from Qbt. The matrix has abundant coarse sand-sized quartz crystals. The unit contains scattered clasts of dacite and welded tuff up to 9 cm in length. Unit Qoal1 has a fairly planar lower contact with Qbt and an erosional upper contact. Maximum observed thickness is 0.8 m.

Unit Qoal2

Early Pleistocene Debris Flow (?) Deposit. This unit is poorly sorted and has matrix-supported cobble-sized clasts. The matrix consists predominantly of coarse- to very coarse-grained sand with minor silt. Clasts are angular to subrounded and consist of dacite and pumice. Clast size generally ranges from 5 to 15 cm in maximum dimension. Cobble-sized dacite clasts become more abundant upward within the unit. Reddish clay is disseminated throughout the sandy matrix in the lower part of the unit and is also present as 1- to 2-mm-thick coat-

ings on larger clasts. Included within this unit is a continuous fine-grained upper layer that is 15 to 20 cm thick, consisting of a silty very fine- to fine-grained sand matrix surrounding subrounded dacite clasts up to 5 cm in maximum dimension. Unit Qoal2 has an erosional lower contact with Qoal1 and a planar to undulatory upper contact with Qoal3. Maximum thickness of the unit is 0.9 m.

Unit Qoal3

Early Pleistocene Alluvium. This unit is well-bedded, moderately well-sorted alluvium that has abundant dacite and aphyric pumice clasts. It generally consists of fining-upwards depositional sequences that are < 10 cm thick, with many being 2 to 4 cm thick. The bases of most sequences are moderately sorted sandy gravel. Typical clast size is 2 to 6 mm, and some clasts are up to 10 cm in long dimension. Dark-red clay coatings are present on grains in the gravel layers. The upper part of the depositional sequences consist of moderately well-sorted medium- to fine-grained sand, with fewer clay coatings. Individual sequences are lenticular and persist laterally for one to several meters. The unit is somewhat lithified, especially the fine sandy intervals. Unit Qoal3 has a planar to undulatory lower contact with Qoal2 that, at least in part, reflects scour into Qoal2, with up to 15 cm of local relief. Unit Qoal3 has a generally planar upper contact with Qoal4, although the westernmost exposure of this unit appears to be erosionally truncated by Qoal4. Maximum observed thickness is 1.0 m.

Unit Qoal4

Early Pleistocene Pumice. The lower part of this unit is ~50 cm thick and is dominated by very coarse, faintly bedded aphyric pumice. Mean pumice size is ~4 cm in maximum dimension. The pumice is largely fresh glass with some clay lamellae, and the glass is mostly frothy and white, with some brown alteration on vesicle walls. The lower

part of the unit contains ~10% weathered subangular dacite clasts, with a mean size of ~1.5 cm in long dimension and a maximum length of ~6 cm, a few large tuff clasts up to ~13 cm in long dimension, and some small clasts of obsidian. Upsection, the overlying 50 cm is finer grained and contains many fining-upwards, moderately well-sorted alluvial sequences. The bases of each of these sequences contain well-sorted, rounded pumice with mean sizes of ~0.5 to 1.5 cm in long dimension. The upper parts of these sequences are fine- to coarse-grained sand, and the finer layers are well lithified. Bedding is discontinuous, traceable laterally up to ~0.5 m. Dacite and obsidian clasts are less common than in the lower half of the unit, constituting ~5% of the upper half of the unit. All pumice and lithic clasts throughout the unit have dark-red clay coatings. Unit Qoal4 has a generally sharp, planar lower contact with Qoal3 and an irregular upper contact with Qoal5. Maximum observed thickness is 1.3 m.

Unit Qoal5

Strong Bt Soil Horizon. This unit is a massive, dark-red, clay-rich soil horizon that has a well-developed blocky soil structure developed above Qoal4. It contains 5% gravel-sized clasts of dacite and obsidian, with a mean clast size of ~1 cm in long dimension and some clasts up to 10 cm long. The unit contains about 5% weathered, orange pumice derived from Qoal4 and is extensively bioturbated. Unit Qoal5 has a gradational, irregular lower contact with Qoal4. The top of Qoal5 is eroded, and Qoal5 is unconformably overlain by Qc1 and Qc2. Maximum thickness is 0.6 m.

Unit Qf1a

Pleistocene Debris Flow (?) Deposit. This unit is poorly sorted, has abundant matrix-supported cobbles, and fills a 1.8-m-wide channel. The matrix is slightly silty fine- to very coarse-grained sand. Clasts are predominantly dacite, with some tuff. The unit includes a 30-cm by 15-cm clast of Qoal3 and possesses moderately strong B-horizon devel-

opment. Unit Qf1a unconformably overlies Qoal1 and Qoal2 and has a roughly planar upper contact with Qf1b. Maximum thickness is 0.3 m.

Unit Qf1b

Pleistocene Alluvium. This unit has moderately well-sorted, locally stratified, largely medium- to coarse-grained sand with gravel lenses. The unit is dominantly quartz and feldspar sand with some glass fragments, including glass fibers. The gravel is largely composed of dacite and pumice clasts, with sparse tuff clasts. Most dacite clasts are subangular to subrounded, with some rounded. Maximum clast dimension is ~10 cm. The base is locally well-stratified sand and gravel, with local channel forms. Unit Qf1b is unconsolidated, which distinguishes it from underlying Qoal3, and is commonly reddish. The unit appears moderately well bioturbated. It has a sharp and undulatory erosional lower contact, locally including channels cut into Qoal2 and Qoal3, and a sharp to gradational upper contact with Qc2 that is commonly bioturbated. Maximum thickness is 0.5 m.

Unit Qf2a

Pleistocene Alluvium. The unit consists of highly variable alluvial deposits with a strong pedogenic overprint. It is possibly colluvial in part, especially at the west end of the trench. The most prominent texture is massive clayey or silty fine- or very fine-grained sand with locally scattered granules or pebbles, but the unit locally contains distinct gravel lenses. Clasts within the gravel lenses are typically granule to pebble size and include abundant dacite and pumice clasts to the east and tuff clasts to the west, suggesting two different provenances and perhaps different ages. Locally, the unit contains lenses of whitish silt up to 10 cm thick that resemble volcanic ash. In the eastern part of the unit, a reddish clay-rich interval overlies a light-colored sandy interval, representing a Bt soil horizon overlying a buried albic soil horizon. The lower contact is not exposed. Unit Qf2a has a gradational upper contact with Qf2b or Qf3a in some areas that

apparently reflects post-depositional soil development; elsewhere, Qf2a has an erosional upper contact beneath Qf3a, Qf5a, or Qc2. Maximum exposed thickness is 1.5 m.

Unit Qf2b

Albic Horizon in Pleistocene Alluvium. This unit consists of whitish silty very fine sand, with lenses of heavily altered granules and pebbles of tuff (?). The unit contains strong soil structure with clay coatings on ped faces and characteristics of an albic (E) horizon. Unit Qf2b occurs above Qf2a for a distance of 8 m beneath a paleotopographic low. There is extensive weathering of clasts in Qf2b and underlying Qf2a, and local gleying suggests prolonged periods of saturation in this unit. Unit Qf2b has a gradational lower contact with Qf2a and a gradational upper contact with Qf3b that apparently reflects post-depositional soil development. Maximum thickness is 0.3 m.

Unit Qf3a

Whitish Late Pleistocene (?) Alluvium. The dominant composition of this unit is whitish silt and very fine-grained sand with some quartz and feldspar crystals. The unit is locally mottled light orange and is locally tan in color and lacks the strong soil structure of Qf2b. In several areas, the unit has a basal gravel layer up to 10 cm thick, and it locally contains gravel lenses above the base. The gravel layers are composed of moderately well-sorted subangular to subrounded highly weathered tuff clasts, dominantly pebble size, in a fine- to medium-grained sand matrix. Maximum clast length is 3 cm. The unit fines upwards in several areas. In some areas, the unit consists of poorly sorted very fine sand with granules and pebbles, suggesting bioturbation. The unit contains disseminated very small (mm-size) charcoal fragments. Locally, it possesses albic (E) horizon characteristics. Unit Qf3a has a lower contact that is relatively planar and gradational where silt overlies Qf2a, which possibly reflects post-depositional soil development, and a lower contact that is sharp and

erosional where gravel overlies Qf2a, including several distinct channels scoured into Qf2a. Unit Qf3a locally overlies Qf2b with apparent erosional contact. Unit Qf3a has a gradational upper contact where overlain by Qf3b except where eroded by younger units. Maximum thickness is 0.4 m.

Unit Qf3b

Late Pleistocene Soil. This unit is dominantly brown silt and very fine sand with characteristics of a buried A horizon. It contains scattered gravel where it overlies gravelly parts of Qf3a and is clayey where it overlies Qf2b. Locally, it contains abundant small charcoal fragments. Unit Qf3b has a lower contact that is a gradational soil horizon boundary with Qf3a or Qf2b. Unit Qf3b has an upper contact with Qf5a or Qc2 that is commonly erosional, although the top of the soil may be locally preserved. Maximum thickness is 0.3 m.

Unit Qf4

Late Pleistocene (?) Alluvium. This unit consists of crudely stratified alluvium, dominated by silty very fine-grained sand or sandy silt with scattered pebbles and cobbles. It contains discontinuous interstratified lenses of fine- to medium-grained sand and sandy pebble lenses. The gravel is dominantly large pebble to small cobble in size, including dacite, pumice, and scattered obsidian, with maximum lengths of 3 to 4 cm. Some gravel lenses are predominantly composed of aphyric pumice from Qoal4. Bt lamellae up to 3 cm thick are common and are typically located within pebble lenses. Lamellae are relatively continuous but wavy. The unit fills a 6-m-wide paleochannel, bounded by Qf2a to the west and Qoal3, Qoal4, and Qoal5 to the east. The paleochannel appears to truncate Qf3a and Qf3b, although unit boundaries are not well defined in this area. The upper part of the unit at the eastern limit of exposure is colluvial and contains a large clast of Qoal5. Unit Qf4 has an erosional lower contact and an upper contact with Qc2 that is generally sharp but locally bioturbated. Maximum thickness is 1.6 m.

Unit Qf5a

Lower Holocene Alluvium. This unit consists of moderately well-sorted gravel with a very coarse-grained sand matrix overlain by very fine-grained sand and silt with scattered gravel. It consists of a fining-upwards sequence. The gravel is dominantly pebble size and composed of subangular tuff clasts, with a maximum clast size of ~3 cm. The unit is locally bioturbated, and the upper contact with Qc2 is also bioturbated. Unit Qf5a has a lower contact that is generally erosional into Qf3b, Qf3a, or Qf2a, but Qf5a may also overlie the original upper surface of Qf3b. Maximum thickness is 0.5 m.

Unit Qf5b

Upper Holocene Alluvium. This unit consists of well-stratified, moderately well-sorted gravel and very coarse-grained sand overlain by fine-grained sand and silt with scattered gravel. The unit consists of a fining-upwards sequence in two lenses within Qc2. The gravel is dominantly pebble size and composed of subangular tuff clasts, with a maximum clast size of ~7 cm. The unit contains abundant Bt lamellae, and the base of the lamellae roughly approximates the lower contact of the unit. The unit is locally bioturbated, and the upper contact with Qc2 is also bioturbated. Unit Qf5b has a lower contact that is locally erosional into Qc2, but Qf5b locally overlies a buried soil within Qc2. Maximum thickness is 0.5 m.

Unit Qc1

Late Pleistocene (?) Colluvium. This unit consists of poorly sorted fine- to medium-grained sand with scattered matrix-supported gravel. The gravel ranges from granule to cobble size and includes dacite clasts up to 10 cm in length and highly weathered pumice up to 2 cm in length. The eastern part of the unit has a clayey matrix surrounding fine-grained sand lenses and may include clasts of Qoal5; the cobbles here lack clay coatings. The western part of the unit has moderate to well-

developed Bt lamellae, 3 cm thick, that are similar to lamellae in Qf4 but are possibly better developed. Unit Qc1 has an irregular lower contact with Qoal4 and Qoal5 and an irregular upper contact with Qc2. Maximum thickness is 0.35 m.

Unit Qc2

Holocene Colluvium. This unit is a poorly sorted, nonstratified deposit with matrix-supported clasts. The characteristics of the matrix and the gravel vary greatly from west to east and vertically within the unit. The matrix is most commonly silt to fine-grained sand, coarsest to the west where it contains abundant coarse-grained sand and finest in the central part of the trench where it is dominated by silt and very fine-grained sand. The gravel is dominated by angular to subangular welded tuff clasts to the west and by subangular to subrounded dacite clasts to the east. The lower part of the unit in the western part of the trench, below Qf5b, contains a discontinuous stone line that coarsens to the west, with tuff clasts up to 30 cm in length. The gravel content in the lower part of the unit decreases from ~50% at the western end of the trench to < 5% to the east, beneath the present topographic low. Dacite clasts are up to 25 cm in length in the eastern part of the trench and appear to be most abundant near the present ground surface, suggesting a gravel lag. Dacite clasts decrease in abundance and size from east to west. The unit has a darkened A horizon developed along the full length of the trench that varies in thickness from 0.1 to 0.4 m, with abundant evidence of bioturbation and an irregular lower boundary. The A horizon includes historic debris (barbed wire and a rusted can) at two locations, at depths of 5 and 20 cm. Below the A horizon, the unit includes abundant animal burrows (krotovinas) and root holes filled with material from the A horizon. A weak Bt horizon, including Bt lamellae to the west, is present within the unit along most of the trench, except in the far eastern parts where the unit is thinnest. A buried A horizon was recognized at one location directly beneath

Qf5b but could not be traced east of the Qf5b lens. Unit Qc2 has a lower contact that is locally distinct and locally irregular and bioturbated. Maximum unit thickness is 2.1 m between Qf5b lenses in the western trench, and minimum thickness is 0.35 m at the east end of the trench.

APPENDIX B. RADIOCARBON DATING

Forty samples were collected from trench EOC-2 for possible radiocarbon (^{14}C) dating, and a subset of 10 of these samples was selected for analysis. These samples consisted of one or more discrete charcoal fragments that were hand-picked from the trench walls. Areas with discolored soil (suggesting the possibility of roots burned in place) or disrupted soil (such as that due to animal burrows or the decay of large roots) were avoided. However, the absence of distinct stratigraphy within many sampled units suggests some degree of mixing, and the possibility of bioturbation of younger charcoal into older deposits cannot be ruled out. In addition, the possibility of the recycling of older charcoal exists, potentially providing ages older than the sampled deposits. Where possible, multiple samples were collected from single units or single stratigraphic sections to provide internal checks on the analyses.

Before submission to the analytical laboratory, each sample was air-dried, examined under a binocular microscope, and cleaned to remove dirt and roots. All samples were analyzed by the accelerator mass spectrometry (AMS) method and were processed by Beta Analytic, Inc., of Miami, Florida. Sample pretreatment by Beta Analytic included a standard hot acid (HCl) treatment to remove carbonates from the samples, followed by an alkali (NaOH) treatment to remove secondary organic acids, a second HCl treatment, and conversion to graphite (which constituted the actual accelerator target).

One of the submitted samples could not be dated because it was too small. A second sample could not be dated because the material did not yield CO_2 following combustion, indicating that the sample did not consist of charcoal. Analytical results and other information on the remaining eight samples are presented in Table B-1. The ^{14}C dates were converted to calibrated (cal) ages (Table B-1) to correct for the effects of fluctuations in the $^{14}\text{C}/^{12}\text{C}$ ratio in the atmosphere and to allow direct compar-

ison of the ^{14}C analyses with age estimates obtained by other methods. Calibration was performed by Beta Analytic, following the process of Talma and Vogel (1993) and using the calibration data set of Stuiver et al. (1998).

The ^{14}C dates are stratigraphically consistent and are also consistent with general expectations of unit ages with two exceptions. Sample EOC2-c37, collected from unit Qc1, was expected to be Pleistocene in age based on the apparent greater degree of soil development at the sample site than in units Qc2, Qf5a, and Qf5b, for which inferred Holocene ages were supported by the ^{14}C analyses. Because Qc1 was faulted and the age of this unit has important paleoseismic implications, the possibility that Qc1 was incorrectly interpreted to be Pleistocene in the field was considered. Two hypotheses that could explain the presence of higher clay content in this unit than in Holocene units elsewhere in the trench are 1) that clay was locally recycled from unit Qoal5 upslope to the east and 2) that clay content was elevated associated with a compressed Holocene Bt horizon in this area of thin colluvium. However, field relations are inconsistent with these two hypotheses. Specifically, a contact was logged between the more clay-rich Qc1 and typical Qc2 only 1 m west of the sample site, indicating an observable difference in clay content over a short distance. If either hypothesis was correct, then higher clay content would be expected to persist farther to the west because of the same processes of recycling of clay from the east and/or compression of a Holocene Bt horizon. In addition, the sample site was originally logged as Qoal5, emphasizing the significantly higher clay content than Qc2, and only later subdivided in the field into a unit intermediate in characteristics between Qoal5 and Qc2. Therefore, it is inferred that this analysis is unreliable due to the mixing of Holocene charcoal into an older deposit or contamination of the sample with younger carbon. This sample was collected at a relatively shallow depth below the base of Qc2, and the unexpectedly

Table B-1. Radiocarbon Analyses From Trench EOC-2

Field Number	Laboratory Number	¹⁴ C Date (yr BP)*	Calibrated Age (cal yr BP)†	δ ¹³ C (‰)	Unit	Depth (m)	Trench Location (m)	Notes
EOC2-c5	Beta-151202	7880 ± 40	8630 [8580–8960]	–23.4	Qc2	1.8	33.3H –3.5V	Disseminated small charcoal fragments between Qf5a and Qf5b, 15 cm below stone line.
EOC2-c7	Beta-151203	4750 ± 60	5480–5570 [5320–5600]	–23.1	Qf5b	0.9	30.4H –2.5V	Disseminated small charcoal fragments in fine-grained interbed within gravels, 8 cm above base of Qf5b.
EOC2-c14	Beta-151204	10,100 ± 70	11,650 [11,290–12,290]	–24.4	Qf3b	2.5	35.0H –4.3V	Disseminated small charcoal fragments near top of buried soil above Qf2b, 5 cm below base of Qf5a.
EOC2-c19	Beta-151205	9420 ± 60	10,660 [10,510–11,030]	–25.6	Qf5a	2.2	39.1H –4.2V	Disseminated small charcoal fragments in fine-grained fan facies, immediately above basal Qf5a gravels.
EOC2-c32	Beta-151206	5260 ± 60	6000 [5910–6190]	–21.5	Qc2	0.8	67.1H –3.6V	Large charcoal fragments 28 cm above base of Qc2; date represents a stratigraphic reversal in relation to EOC2-c38 and is inferred to be too young due to introduction of charcoal into deposit.
EOC2-c37	Beta-151208	7930 ± 40	8740 [8610–8990]	–23.9	Qc1	0.9	71.5H –3.5V	Disseminated small charcoal fragments 8 cm below base of Qc2; date younger than expected from soil-stratigraphic context and is inferred to be too young due to bioturbation of charcoal into deposit.
EOC2-c38	Beta-151209	6530 ± 60	7430 [7320–7560]	–23.0	Qc2	0.6	66.9H –3.4V	Disseminated small charcoal fragments in lower part of Qc2.
EOC2-c39	Beta-151210	9210 ± 40	10,280–10,380 [10,240–10,500]	–24.9	Qf3b	1.4	58.6H –4.1V	Single small charcoal fragment in buried soil 5 cm above Qf3a.

*Radiocarbon dates corrected for δ¹³C by Beta Analytic, Inc.; dates presented as years before present (yr BP), which by convention, is relative to 1950 AD; ± indicates one standard deviation (1σ) uncertainty in analyses.

†Calibrated by Beta Analytic, Inc., based on Talma and Vogel (1993) and Stuiver et al. (1998); age range given for samples with multiple intercepts of calibration curve; possible age range using 2σ uncertainty shown in brackets.

young date of ca. 7.9 ¹⁴C ka (ca. 8.7 cal ka) may be due to the introduction of charcoal into the deposit by bioturbation during deposition of Qc2. Based on the stratigraphic context and the results of other ¹⁴C analyses, it is possible that this date approximates the age of the base of Qc2 at this location, although PDI calculations suggest an older age of ca. 11 to 17 ka for the base of Qc2 at a nearby soil profile (P69.9, Appendix C). The ca. 7.9 ¹⁴C ka analysis from Qc1 is virtually identical to the analysis of sample EOC2-c5 in unit Qc2 (Table B-1), and this coincidence may be due to both samples recording the same fire.

The other exception is a reversal of ages between samples EOC2-c38 (0.6 m depth, ca. 6.5 ¹⁴C ka) and EOC2-c32 (0.8 m depth, ca. 5.3 ¹⁴C ka). Field observations indicated that sample EOC2-c32 was possibly suspect because it consisted of a cluster of relatively large charcoal fragments in an area without other visible charcoal, although no soil discoloration or textural variations were observed that would clearly associate this sample with burned roots or krotovinas. Sample EOC2-c32 also seems relatively young compared to analyses from the Holocene section farther west in the trench, whereas the analysis from sample EOC2-c38 seems more reasonable. Because of these reasons, we consider that the analysis from sample EOC2-c32 should be rejected and that the analysis from sample EOC2-c38 should be retained.

APPENDIX C. SOIL STRATIGRAPHY AND PEDOLOGIC AGE ESTIMATES

A. Introduction

Soil profiles were described at four locations in trench EOC-2 to provide additional age control for key geologic units. The basic premise of using soils to provide age estimates is that soils develop in a systematic and progressive pattern over time. The rate and trends of soil formation can be determined by examining a sequence of soils on well-dated surfaces. Multiple soils developed on dated surfaces in the vicinity of LANL have been used to calculate a soil chronofunction, which is a simple linear equation that relates the degree of soil development to soil age. The soil chronofunction developed specifically for application to soils around LANL (McDonald et al. 1996; Reneau and McDonald 1996, modified in McDonald 1999) has been previously used to estimate ages of surface and buried soils exposed in paleoseismic trenches in the Pajarito fault zone (McCalpin 1998, 1999). Application of this soil chronofunction to surface and buried soils provides reasonable age estimates for soil stratigraphy and related structural and geomorphic features exposed in trenches. Because it has not been previously presented outside of the unpublished report of McDonald (1999), the development of this revised soil chronofunction is documented in this appendix.

B. Methods

Soil morphology was described according to the standard methods and nomenclature of the Soil Survey Staff (1981). The locations of the described soil profiles were chosen to include key soil-stratigraphic units in the trench. Soil profiles are identified relative to their horizontal location (i.e., P37.6 is a soil profile described at 37.6H). Descriptions reflect soil morphology exposed within approximately 0.5 m on either side of this horizontal position.

1. Quantification of soil morphology

Soil morphology was quantified using the Soil

Development Index (SDI) procedures of Harden (1982), Harden and Taylor (1983), and Taylor (1988). Calculation of SDI values is based on a conversion of soil properties (i.e., color, structure) into numerical data to enable a quantitative comparison of the degree of soil development. Points are assigned to each property based on the difference between the described soil property and the parent material. Points for each property are normalized to a percentage scale of maximum property development based on comparison of each property to a published or conceptual maximum value of development for each particular property. Maximum soil property values from Taylor (1988) were used to normalize soil property values in this study. Normalized property values are summed for each horizon and averaged yielding a Horizon Development Index (HDI) value that provides an estimate of overall horizon development relative to a conceptual idea of maximum possible horizon development. HDI values are multiplied by horizon thickness and summed for each profile yielding a Profile Development Index (PDI) value for that profile. PDI values provide a means of comparing soils within a given area and can be used to develop a soil chronofunction. In turn, the chronofunction can be inverted to provide soil age estimates based on calculated PDI values.

PDI values for described soils in trench EOC-2 were calculated using morphologic properties of rubification (soil redness), texture, structure, dry and moist consistence, and argillans (clay skins). An important consideration in applying the SDI is determining the soil parent material values. Parent material values for each profile were adjusted to reflect vertical changes in texture, consistence, and color of the inferred parent material that correspond to vertical stratification associated with colluvial deposition. For the buried soils in this study, the weakly to nonaltered colluvium common to the surface of many sites in the Pajarito fault zone was used as a starting point for assessing parent material (discussed in more detail below).

2. Stratigraphic-age relationships for soils

PDI values were calculated to the base of each described soil (including both buried and surface soils), with the summed PDI of the entire overlying soil column (if more than one soil was present) used to calculate an approximate soil age. The PDI-based soil age estimate therefore reflects the total time required to develop the overlying soil stratigraphy (i.e., the overlying stack of buried and surface soils) down to a specific depth (the base of each buried soil). In other words, the PDI age estimates reflect the time that the overlying strata have been exposed to soil-forming processes. These age estimates assume that there is no missing soil between the surface and the base of each soil, although this is not realistic for all profiles because some soils are either partially truncated by erosion or completely missing from within any stratigraphic section. Further, in cases where deposits have been exposed by erosion of overlying material (after initial post-deposition burial), the time of soil formation will reflect the time of exposure to soil-forming processes, not the age of the deposit. The degree of soil formation reflects the time interval that any surface or deposit has been exposed to soil-forming processes, which will generally occur whenever the deposit is within approximately 1 to 2 m of the ground surface. In many cases involving the deposits exposed in trenches at LANL, this interval will be equivalent to the age of the deposit. In other cases, however, in which erosion has exposed previously buried deposits, the degree of soil formation is a result of pre-burial exposure (if any) to soil-forming processes and the length of time after post-burial exposure. In cases in which erosion has resulted in missing strata (identified based on stratigraphic, sedimentologic, or soil information), PDI-based age estimates should be considered minimum ages.

3. Description of soil stratigraphy

Vertically stacked sequences of multiple buried soils were exposed in trench EOC-2 (designated by the suffix 'b' at the end of each horizon designation). Buried soils are former surface soils that have been buried by subsequent periods of collu-

vial or alluvial deposition. In most cases, the top of each buried soil is recognized by an increase in B-horizon properties, especially an increase (relative to the overlying horizon) in argillans (clay skins or vertically translocated clay), rubification (soil redness), and the strength of soil structure. In other words, the top of each buried soil is often recognized as the top of the strongest B horizon of each buried soil. When soils form at the land surface, B horizons normally lie below the surface and are usually overlain by some combination of A, E, and transitional horizons (e.g., AB, BA, or EB). In many cases, these former surface horizons are preserved within the base of the overlying soil, and subsequent soil-forming processes have altered the original morphology of these soils. In these cases, the base of the overlying soil is pedogenetically "welded" to the underlying soil. Horizons of the buried soil can be pedologically transformed because soil-forming processes, such as oxidation and the translocation and accumulation of clay, extend through the new layer of soil and into the top of the underlying soil. The resulting morphology of these welded or overlapping soil horizons (i.e., horizons that are now part of both soils) can appear more like B horizons rather than the original A and B horizons. A lack of recognizable A, E, or related transitional horizons may also be due to truncation of soils prior to burial. Truncation of a soil is often recognized by sharp contacts with the overlying deposit and/or abrupt changes in sediment texture. However, some of the soils described in trench EOC-2 are in geomorphic settings that are more conducive to deposition than erosion, promoting preservation of buried soils.

Most of the soils exposed in trench EOC-2 contain a similar range of genetic horizons. The horizons at the top of the soil profile, A horizons, usually contain slightly higher concentrations of disseminated organic matter that impart a slightly darker coloration (i.e., lower soil chroma and value). Transitional horizons, BA and AB horizons, have dominant properties that are similar to both A and underlying B horizons. Weakly developed B horizons, Bw horizons, have either redder soil color

(i.e., higher value and chroma) due to the accumulation of iron (oxy)hydroxides relative to the parent material and/or development of soil structure. Horizons that are 1) usually better developed than Bw horizons and 2) have noticeable accumulation of translocated clay (argillans) are designated as Bt horizons. In these soils, argillans are commonly developed as coatings on pedfaces and clasts and lining pores. The E horizon is usually very light colored (chroma < 2) due to the lack of appreciable accumulation of either organic matter or iron (oxy)hydroxides on mineral particles. Skeletans (bleached quartz or feldspar grains) are common along pedfaces in E horizons. Horizons that are poorly altered to unaltered are C horizons and may represent the properties of the original soil parent material, although these were not present in trench EOC-2. Transitional horizons that have dominant properties similar to both B and C horizons are designated as BC or CB horizons. Former E horizons that have had B-horizon properties overprinted on them from subsequent soil formation related to burial are EB horizons.

C. Development of a Soil Chronofunction for Estimating Pedologic Ages

Soil ages can be estimated based on a systematic increase in soil-profile morphology using simple linear regression analysis of logarithmic relationships between PDI values and soil ages (Figure C-1; Table C-1). Several different methods of linear statistical analysis have been employed for evaluating rates of soil development based on SDI values and to account for poor age control of studied soil surfaces (Switzer et al. 1988; Harden 1990; Harden et al. 1991). For soils on the Pajarito Plateau, simple linear regression was used to develop a soil chronofunction to provide age estimates for nondated surfaces based on time-related

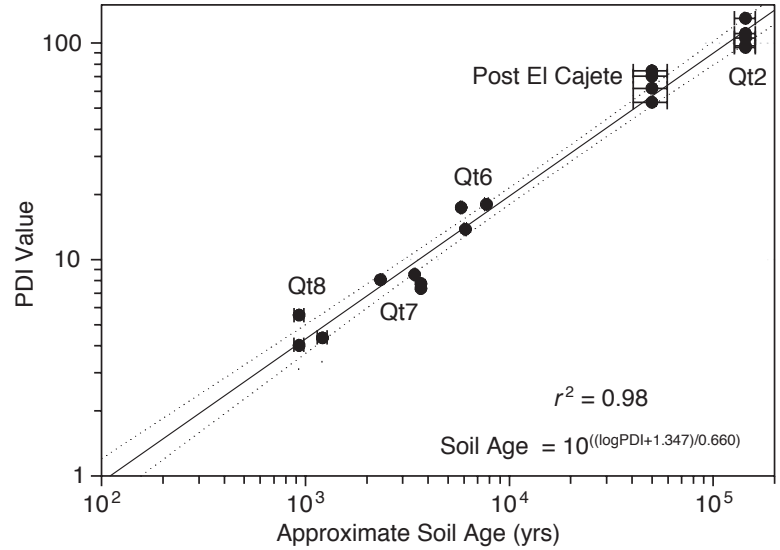


Figure C-1. Soil chronofunction for calculating PDI ages. The bars represent $\pm 1\sigma$ error range. Filled circles represent soils listed in Table C-1.

increases in PDI values (McDonald et al. 1996; Reneau and McDonald 1996; McDonald 1999). Justification for the straightforward application of linear regression is the fact that the chronosequence used in this study is extremely well dated in that each soil used is directly dated as opposed to being based on correlative ages (e.g., soil age estimates based on correlation to dated soils or deposits in other areas).

1. Soils used in chronofunction

PDI values from twenty soils were used to develop the soil chronofunction for the Pajarito Plateau used in this study and in previous seismic hazard investigations at LANL (McDonald 1999; Table C-1; Figure C-1). These included soils formed on the Qt8, Qt7, Qt6, and Qt2 terraces in Rendija Canyon and soils formed in colluvium overlying the El Cajete pumice near the northwest corner of LANL (adjacent to NM 501, in TA-16) (McDonald et al. 1996; Reneau and McDonald 1996; Phillips et al. 1998). Between three and five soils are included from each surface (Table C-1).

Soils used in the chronofunction are those with the best combination of reliable age control and low

Table C-1. Summary of Soil Development Index Results for Soils Used in Developing Chronofunction

Geomorphic Surface	Soil Field Number	PDI	Average PDI	¹⁴ C Age* or ²¹ Ne Profile Age† (years)	Dating Method
Qt8	RCT8-1	4.01	4.6 ± 0.8	930 ± 55	¹⁴ C
	RCT8-3	5.54		930 ± 45	¹⁴ C
	RCT8-5	4.35		1205 ± 40	¹⁴ C
Qt7	RCT7-1	8.52	7.9 ± 0.5	3430 ± 70	¹⁴ C
	RCT7-4	8.07		2330 ± 85	¹⁴ C
	RCT7-7	7.74		3680 ± 50	¹⁴ C
	RCT7-8	7.35		3670 ± 50	¹⁴ C
Qt6	RCT6-1	18	16.4 ± 2.3	7710 ± 75	¹⁴ C
	RCT6-2	13.8		6080 ± 70	¹⁴ C
	RCT6-3	17.38		5800 ± 50	¹⁴ C
Post EC‡	WJR-5	74.28	64.9 ± 9.4	50000 ± 9500	¹⁴ C and ²¹ Ne
	WJR-9	53.26		50000 ± 9500	¹⁴ C and ²¹ Ne
	WJR-10	70.33		50000 ± 9500	¹⁴ C and ²¹ Ne
	WJR-11	61.76		50000 ± 9500	¹⁴ C and ²¹ Ne
Qt2	RCT2-1	95.49	107.7 ± 14.0	144000 ± 17000	²¹ Ne
	RCT2-2	130.14		144000 ± 17000	²¹ Ne
	RCT2-3	110.55		144000 ± 17000	²¹ Ne
	RCT2-4	105.62		144000 ± 17000	²¹ Ne
	RCT2-5	96.93		144000 ± 17000	²¹ Ne

*Calibrated ¹⁴C ages, with 1σ uncertainty.

†Age for the Qt2 terrace and supporting age for the post-El Cajete soil from Phillips et al. (1998).

‡Soil formed in colluvium and loess overlying the ca. 50- to 60-ka El Cajete pumice.

variation in soil profiles due to factors such as erosion. Soils formed on the Qt8, Qt7, and Qt6 terraces are directly dated by radiocarbon analyses on charcoal from underlying sediments (Table C-1). The soils formed in a layer of colluvium overlying the El Cajete pumice were originally thought to represent soil formation that has occurred since ca. 50 to 60 ka (McDonald et al. 1996; Reneau and McDonald 1996). A more recent radiocarbon date of 40.5 ± 1.2 ¹⁴C ka and a cosmogenic ²¹Ne depth profile through this soil that yielded an exposure age of 44 ± 11 ka (Phillips et al. 1998) suggest that

this soil could be as young as about 40 ka, indicating a possible soil age range of 40 to 60 ka. Therefore, an estimated age of 50 ka was used in the chronofunction for soils formed in the post-El Cajete colluvium at this site. An age of 144 ± 17 ka was estimated for a Qt2 terrace soil using a cosmogenic ²¹Ne depth profile (Phillips et al. 1998), and this dated terrace was used in the soil chronofunction. Because dating soil surfaces using ²¹Ne is considered an experimental technique, some may question use of these dates as part of the soil chronofunction. The use of these dates can be jus-

tified in two ways, however. First, the quality of the ^{21}Ne depth profile indicates that this may be a reasonable date for this soil. Specifically, the ^{21}Ne results exhibited a near-uniform, exponentially decreasing profile pattern consistent with expected trends for a soil-depth function. A near-uniform depth profile indicates that there was not excessive soil mixing due to bioturbation and that the resulting ^{21}Ne depth profile provides a reasonable numerical age for the Qt2 surface. Second, a ^{21}Ne age range of 144 ± 17 ka for the Qt2 soil overlaps and agrees with the PDI age of 124 ± 24 ka for the Qt2 soils based on a soil chronofunction developed using only dated Qt8, Qt7, Qt6, and post-El Cajete soils (i.e., the same chronofunction but without inclusion of the Qt2 soils). Therefore, the PDI and ^{21}Ne age estimates show reasonable agreement, further justifying the use of the ^{21}Ne -dated soils in the chronofunction. Inclusion of the Qt2 soils provides a better foundation for use of the chronofunction in estimating the age of older soils. Excluding the Qt2 soil data would favor younger soils (i.e., Holocene soils). Previous versions of the chronofunction developed from Rendija Canyon soils (McDonald et al. 1996; Reneau and McDonald 1996) included PDI values from soils developed in the colluvial cap that overlies the Qt4 and Qt2 soils. These colluvial soils were excluded from this data set because it is not clear when soil formation started.

2. Testing the precision and accuracy of the soil chronofunction

The soil chronofunction discussed above for the Pajarito Plateau can be used to calculate approximate ages for other soils if environmental conditions are generally similar (i.e., parent material, climate, vegetation, and topography). The soils exposed in trench EOC-2 have formed under similar environmental conditions as those used to construct this chronofunction. The one major exception is that the trench soils formed primarily in colluvium and locally derived alluvium; in contrast, most of the chronofunction soils formed primarily in alluvium along a larger stream, although the post-El Cajete soil and the upper part of the Qt2

soils also formed in colluvium. Color and texture could conceivably be influenced by colluviation, especially if the colluvium is derived from the erosion of older, well-developed soils just upslope and without significant winnowing of clay and fine silt by surface runoff. Not accounting for the reworking of older soils may result in inflation of PDI values, although it can be argued that the magnitude of inflated PDI values would be minimal. This result is because the PDI values are based on an averaging of all soil changes and will tend to lessen potential impacts of inherited contributions to soil properties that are excluded in the index parent material values. Examination of soils formed in colluvium and/or alluvium at other areas on the Pajarito Plateau that are downslope of older, well-developed soils, indicate that little, if any, of the character of the eroded soils is preserved within the colluvium (Reneau and McDonald 1996). Basically, soil properties used in PDI calculations (e.g., structure, argillans) will represent soil formation following colluviation because these properties will not survive colluvial processes. In the present study, parent material values were set to realistically represent possible variations in the parent material due to colluviation. Poorly weathered material within the surface soil at previous trenches in the Pajarito fault zone was used as a starting point for parent material values.

Given this variation in parent material and the general uncertainties in the application of a soil chronofunction for providing age estimates, it is desirable to have some means of determining the accuracy and precision of age estimates generated by a soil chronofunction. Confidence intervals for PDI age estimates were calculated based on linear relationships between PDI values and best age estimates for chronosequence soils. At a 95% confidence level, variation in age estimates is ± 0.07 of the log of the estimated soil age. This represents an estimated error of -16% and $+19\%$ of the age calculated using the soil chronofunction. A means to test this confidence level is available given the abundance of relatively well-dated soils on the Pajarito Plateau. Soil ages based on the soil

chronofunction average within $\pm 18\%$ of the “true” soil age for soils dated radiometrically (using ^{14}C and ^{21}Ne) and formed in both colluvium and alluvium ($n = 23$ soils; McDonald, unpublished data; Reneau and McDonald 1996; Table C-2; Figure C-2). In other words, testing PDI-based age estimates with ages for dated soils (soils not used in the

chronofunction) indicates that the PDI-based ages are within approximately 18% of the dated soil age. This result agrees well with the confidence-interval estimates above suggesting that the soil ages for buried soils in the trenches are likely to be within 20% of the actual soil age (except where trench soils have been truncated or stripped by erosion).

Table C-2. Comparison of PDI Soil Ages with Radiometric Dates for Soils on the Pajarito Plateau

Parent Material*	Soil	PDI	PDI Age (yrs)	Radiometric Age (yrs)	Dating Method [†]	% Error
C	SC-1	50.15	37630	55000	EC	0.26
A	SC-2	6.32	1679	1400	^{14}C	0.22
C	FC-1A	59.51	48644	55000	EC	0.03
A	AC-1	6.77	1859	1240	^{14}C	0.53
A	WJR-8	19.75	9288	10470	^{14}C	0.06
C	FRR-1	13.00	4958	9500	^{14}C	0.46
C	FRR-1	67.06	58199	55000	EC	0.16
C	EG&G	11.21	3968	3970	^{14}C	0.04
C	EG&G	16.75	7251	8050	^{14}C	0.05
						0.20 ± 0.19
C/A	RCT4-1	76.03	70275	89000 [‡]	^{21}Ne	0.13
C/A	RCT4-2	71.44	64003	89000	^{21}Ne	0.21
C/A	RCT4-3	78.63	73919	89000	^{21}Ne	0.09
C/A	RCT4-4	78.86	74238	89000	^{21}Ne	0.08
C/A	RCT4-5	79.88	75685	89000	^{21}Ne	0.06
						0.17 ± 0.11
C	RCT4-1H	22.07	10972	10540	^{14}C	0.10
C	RCT4-2H	24.21	12605	10540	^{14}C	0.27
C	RCT4-3H	14.55	5870	10540	^{14}C	0.42
C	RCT4-4H	19.48	9094	10540	^{14}C	0.09
C	RCT4-5H	21.19	10323	10540	^{14}C	0.04
C	RCT2-1H	16.92	7362	10540	^{14}C	0.27
C	RCT2-2H	16.35	6990	10540	^{14}C	0.30
C	RCT2-4H	20.17	9584	10540	^{14}C	0.04
C	RCT2-5H	17.05	7444	10540	^{14}C	0.26
						0.20 ± 0.13
						All 0.18 ± 0.15

*Soils formed in colluvium (C); in alluvium (A); and in colluvium over alluvium (C/A).

[†]Dating control: radiocarbon (^{14}C); El Cajete pumice (EC); and cosmogenic neon-21 (^{21}Ne). Soil data from McDonald, unpublished; Reneau and McDonald (1996). Radiocarbon dates from Reneau, unpublished; Reneau and McDonald (1996).

[‡]Cosmogenic ^{21}Ne age for the Qt4 deposit from Phillips et al. (1998).

#Average calibrated age for colluvium overlying Qt4 and Qt2 soils.

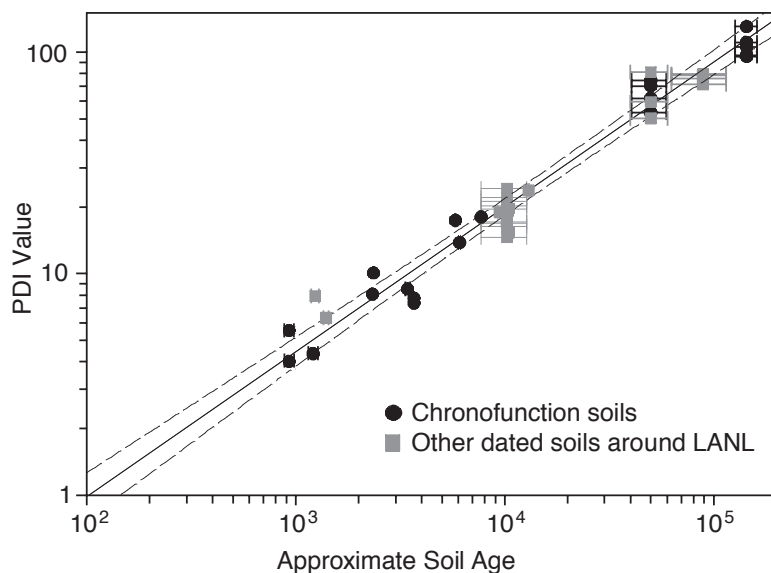


Figure C-2. Soil chronofunction as compared with dated soils on the Pajarito Plateau. Soils used in the chronofunction are shown as filled circles, and other dated soils, listed in Table C-2, are shown as grey squares.

Soil PDI age estimates cited in this report include upper and lower age estimates based on the analysis discussed above. The upper and lower age estimates reflect ± 0.07 of the log of the estimated soil age, which is at the 95% confidence level.

D. Results

The following section provides a general overview of the soil stratigraphy described in trench EOC-2. Profiles were described at four trench locations (37.6H, 55.6H, 67.2H, and 69.9H) and were chosen to characterize key stratigraphic intervals. Schematic diagrams showing representative morphology for each profile are shown in Figures C-3 through C-6, a summary of soil morphology is presented in Table C-3, and a summary of PDI results and correlation of soils to designated trench units are shown in Tables C-4 and C-5. Profile 69.9H is discussed first because it is the only profile extending to the surface, and profile 55.6H is discussed second because it is the longest described profile. Profiles 37.6H and 67.2H are both shorter and are discussed last. Profile depths shown in Figures C-

4 through C-6 and Table C-3 are relative depths because profiles were not extended to the surface (with the exception of P69.9). Soil horizon designations used in this report reflect interpretation of soil features and processes based on Pajarito Plateau-wide studies of soils and soil-forming processes by McDonald et al. (1996) and Reneau and McDonald (1996).

Two sets of PDI soil age estimates are shown in Table C-4: the minimum estimated age (PDI age estimate) and the estimated “true” age of the soil (composite PDI age estimate). The minimum estimated age indicates the approximate time required to form the soil features associated with the described soil profile. These are,

in most cases, especially for buried soils, minimum-limiting ages and do not reflect the age of the soil or the deposit because the entire overlying stratigraphic sequence of soils is not accounted for. More accurate age estimates based on a soil PDI requires that all overlying soil be included in the calculation of the PDI values. Composite PDI age estimates are based on a composite stratigraphic column of overlapping soil and stratigraphic units (excluding any stratigraphic overlap among soil units). It should be noted that these may also be minimum ages in cases where erosion has removed soil units.

1. Profile 69.9

Soil characteristics for two soils were described at 69.9H to a profile depth of 200 cm (Figure C-3, Table C-3). The profile description begins at the surface.

Surface Soil. The surface soil at P69.9 is 95 cm thick, is weakly to moderately developed, and coincides with unit Qc2. The top of the soil contains a well-developed A horizon with abundant

continued on page 44

Table C-3. Summary of Soil Morphology for Trench EOC-2 Profiles

Horizon	Lower Depth (cm)*	Gravel (%)	Dry Color (Matrix)	Moist Color (Matrix)	Texture [†]	Structure [‡]	Consistence: Dry [#]
Profile 37.6							
BAb1	23	5–15	10YR 5/3	10YR 3/3	sil	1 c+m sbk: 2-1 f sbk	h
CB1b1	40	40–60	10YR 7/3	10YR 3/4	l	sg	sh
AB1b2	45	2–5	10YR 7/2	10YR 3/3	sil	3 m pr	h
AB2b2	51	2–5	10YR 7/2	10YR 3/3	sicl-sil	3 m pr: 2 f+m abk	h
EBtb2	80	5–10	10YR 8/2	10YR 5/2	sicl-sil	1 m pr: 2-1 m+c abk	h-vh
Bt1b2	96	5–10	10YR 7/2	10YR 5/2	sicl-sil	2-1 m+c sbk	h
Bt2b2	113	10–20	7.5YR 7/4	7.5YR 5/4	l	2 m+c sbk	h-sh
Profile 55.6							
ABb1	9	5–10	10YR 6/3	10YR 3/4	sil-sic	2-1 c sbk: 2 m+f sbk	h-sh
Bw1b1	38	5–15	10YR 5/3	10YR 3/4	sic	1 m pr: 1-2 m+f sbk	sh-so
Bw2b1	63	5–15	10YR 7/3	10YR 4/4	sil	1 m pr: 1-2 c+m sbk	sh
AB1b2	74	0–5	10YR 6/3	10YR 5/4	sil	1 m+c sbk: 2-1 f sbk	sh
AB2b2	81	0–5	10YR 7/3	10YR 5/3	sil	2-1 m+f sbk	sh-h
Etb2	92	0–5	10YR 8/2	10YR 5/3	sil	3-2 c+m pr	h-sh
Bt1b2	105	5–10	7.5YR 7/4	7.5YR 5/4	sicl	2 m+f pr: 2 m+f abk	h-vh
Bt2b2	126	50–70	7.5YR 6.5/4	7.5YR 4/4	sicl	1-2 m+c pl: 2 m+f abk/sbk	h-vh
EBtb3	151	5–15	7.5YR 7/3	7.5YR 4/4	sil	1-2 c+m pr: 2-1 c+m abk	h-vh
Bt1b3	178	10–20	7.5YR 5/5	7.5YR 4/4	sicl	1 c+m pr: 1-2 c+m abk/sbk	h
Bt2b3	214	10–20	7.5YR 6/4	7.5YR 4/4	sicl-sil	1 c+m pr: 1-2 c+m abk/sbk	h-vh
Profile 67.2							
Bt2	16	10–15	8.75YR 7/3	8.75YR 4/4	sil	1 c pr: 1-2 m sbk	sh
Bt1b1	48	30–50	10YR 7/3	10YR 4/4	l	2 f pr: 1-2 m+f sbk (Bt); sg (CB)	sh-h
Bt2b1	74	45–65	10YR 7/3	10YR 4/4	l	m (CB); 1 m sbk (Bt)	sh-h
Bt3b1	105	30–45	7.5YR 7/4	7.5YR 4/4	sil	1 c sbk	h
Profile 69.9							
A1	10	10–20	10YR 5/2	10YR 3/2	sil	1-2 m sbk: 2-3 m crb	so-sh
A2	31	10–20	10YR 5/2	10YR 3/2	sil	1 m pr: 2-1 c+m sbk	so-sh
BA	49	10–20	10YR 6/3	10YR 3/3	sil	1 m pr: 2 m+c sbk	so-sh
Bt1	79	10–20	10YR 6/4	10YR 4/4	sil	1-2 c+m pr: 2-1 c+m sbk	h
Bt2	95	15–25	8.75YR 7/4	7.5YR 4/4	sil	1 c pr: 1 c+m sbk	h
Bt1b1	116	5–10	6.25YR 5/6	6.25YR 4/4	sicl	3-2 c+m pr: 2 m+f abk	h
Bt2b1	143	5–10	7.5YR 5/6	6.25YR 4/4	sicl	2 c+m pr: 2 m+f sbk	h
Bt3b1	168	20–35	7.5YR 6/6	6.25YR 4/4	sil	1 c pr: 1-2 m sbk	h
Bt4b1	200	40–60	7.5YR 6/6	6.25YR 4/6	sil-l	1 c+m sbk	h-sh

*Depth from top of profile where described, not from top of trench (except for P69.9)

[†]Texture: l = loam, sil = silt loam, sicl = silty clay loam, sic = silty clay

[‡]Structure: Grade: 1 = weak, 2 = moderate; 3 = strong; Size: c = coarse, m = medium, f = fine;

Type: sbk = subangular blocky, abk = angular blocky, pr = prismatic, pl = platy, sg = single grain, crb = crumbly;

Other: a colon (e.g., pr: abk) = parting to, a slash (e.g., abk/sbk) = consists of both

[#]Consistence: Dry: so = soft, sh = slightly hard, h = hard, vh = very hard

[§]Consistence: Moist: vfr = very friable, fr = friable, fi = firm

[¥]Consistence: Wet: Stickiness: vss = very slightly sticky, ss = slightly sticky, s = sticky, vs = very sticky;

Plasticity: vps = very slightly plastic, ps = slightly plastic, p = plastic

Table C-3 Continued

Consistence:		Argillans [^]	Lower	Other	Notes
Moist ^s	Wet ^y		Horizon	Cutans [^]	
			Boundary		
Profile 37.6					
fr-vfr	ss, ps	2 f po	cs-cw		fecal pellets, bioturbation
vfr	vs-ss, vps		aw-as		
fi-fr	ss, ps	2 f po	as	3 f pr skel: 3 d irg PI skel	
fi-fr	ss-s, p	2 f co:pf	as-aw	5 f prfc	
fr-fi	ss-s, p	5 f-p po	cs-cw	4 p-d irg skel	vertical clay lined fractures
fr	ss, p	5 p po	a-cw	5 p prfc	
vfr-fr	vss, vps-ps	2 f-p po			bioturbated, mixed tuff/pumice
Profile 55.6					
vfr	s-ss, ps		cs		bioturbation
vfr	ss, ps		cs		bioturbation
vfr	ss, p-ps		cs		
vfr	ss, ps		cs		abundant bioturbation
vfr	ss, ps		as		abundant bioturbation
fr	ss, ps	5 d po: 4 f co:pf	as-aw	4 d-p irg skel: 5 p pr:pf skel	
fi-fr	ss-s, p	5 p po: 4 f co:pf	cs-gs	4 f prfc	argillans along pr:pf contain organic matter
fr-fi	ss, p	5 p-d co: 3 d-p br	cs-cw		
fr	ss, ps-p	5 f-d po: 3 f-d co:pf	cs	4 p-d irg skel	
fr-fi	ss, p	5 d po: 4 f-d co:pf	gs-cs	2-3 d-f skel	
fr	ss-s, p-ps	5 p-d co:pf: 5 d po		1-2 f skel	
Profile 67.2					
vfr	ss, ps	2 f co:pf	as-aw		
fr-vfr	vps	4 d-f pr:pf: 3 f co	cs		truncated top
vfr-fr	ss, vps	3 d br	gs		
vfr	ss, ps	2 f-d br			
Profile 69.9					
vfr	ss, ps		cs		land surface/top of trench; abund. bioturb.
vfr	ss, ps		cs		abundant bioturbation
vfr	ss, ps		cs		bioturbation
fr-fi	ss, ps	2 f-d co:pf + po	cs		
fr	ss, ps-p	3 d-f pr:pf	aw-cw		
fr	ss, p	5 p pr:pf, 5 d bk:pf	cs		top of Qoal; truncated top of soil
fr	ss-s, p	5 p pr:pf, 4 d bk:pf	cs		pumice gravel
fr	ss, ps	4 f-d pf: 4 d po	cs		
fr	ss, ps-vps	2 d br			stratified gravel/pumice

[^]Argillans and Other Cutans:

Abundance: 1 = very few (< 5%), 2 = few (2–25%), 3 = common (25–50%), 4 = many (50–75%), 5 = nearly continuous (75+%);

Thickness/Distinctness: f = thin (faint), d = moderately thick (distinct), p = thick (prominent);

Location/Type: po = along pores, co = coating gravel or ped faces, br = bridging grains, pf = along ped faces,

co:pf = coatings along ped faces, pr:pf = along prismatic ped faces, bk:pf = along blocky ped faces, PI = ped interior,

prfc = pressure faces, irg = irregular shape

Type: skel = skeletal

P69.9

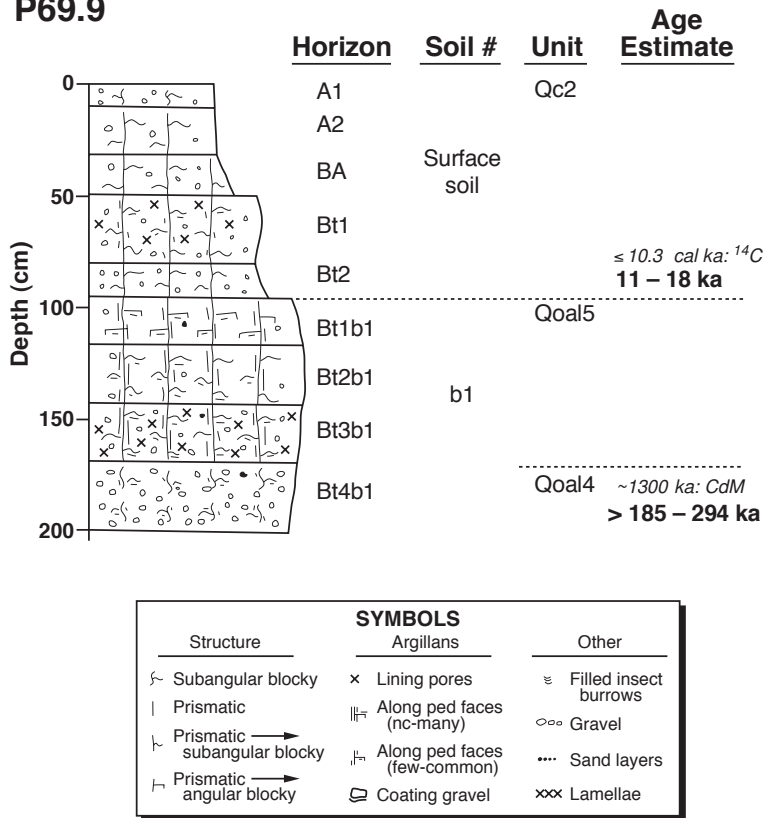


Figure C-3. Schematic stratigraphic column for Profile 69.9. The PDI age estimates are in bold; radiocarbon and pumice age estimates are in italics. CdM is pumice with an inferred Cerro del Medio source.

continued from page 41

features of bioturbation and accumulation of organic matter. The soil B horizon is a weakly developed Bt horizon with few argillans along prismatic pedfaces and lining pores. Dry soil color ranges from 10YR 5/2 to 10YR 6/4. Soil structure is predominantly prismatic parting to subangular blocky. A PDI age of ca. 11 to 17 ka was estimated for this soil (Table C-4). The degree of soil development is similar to soils found elsewhere on the Pajarito Plateau that have formed in Holocene age materials; therefore, an age closer to 11 ka is considered more likely. A radiocarbon analysis from the unit beneath Qc2 11 m west (sample EOC2-c39, Table B-1) suggests that the base of the surface soil is somewhat less than 10.3 cal ka, also suggesting that the PDI may have slightly overestimated the age of the soil at

this location.

Buried soil b1. The first buried soil at P69.9 is at least 105 cm thick and is strongly developed. This soil coincides with unit Qoal5 and the upper part of Qoal4. This soil is denoted by the presence of a strongly developed Bt horizon that has considerably better development of argillans and a redder hue than the overlying surface soil. The top of the soil has been truncated by erosion and is unconformably overlain by Qc2. Dry soil color ranges from 6.25YR 5/6 to 7.5YR 6/6. Soil structure consists of prismatic structure parting to angular and subangular blocky structure. Argillan development is strong and ranges from nearly continuous to few coatings and bridges along pedfaces (best along prismatic pedfaces) and lining pores. A PDI age of ca. 51 to 81 ka was estimated for this soil (Table C-4); however, this is a minimum age because of the overlying unconformable contact. The composite PDI age indicates that soil b1 has an age of at least 185 to 294 ka. Unit

Qoal4 is dominated by pumice that is inferred to be associated with early Pleistocene eruptions from Cerro del Medio (ca. 1.13 Ma; Spell and Harrison 1993), suggesting that soil b1 may be considerably older. The overall strength of B-horizon development and composite stratigraphic relations also indicate that Qoal5 is older than the ca. 50- to 60-ka El Cajete pumice.

2. Profile 55.6

Soil characteristics for two buried soils were described at 55.6H to a profile depth of 214 cm (Figure C-4; Table C-3). The top of the described profile lies about 90 cm below the surface.

Buried soil b1. The first buried soil at P55.6 is 63 cm thick and is weakly to moderately developed.

This soil coincides with unit Qc2. The top of the soil profile was not described but most likely coincides with the surface soil described at P69.9. The ABb1 horizon at P55.6 probably coincides with the BA horizon at P69.9. The ABb1 is denoted by a noticeable accumulation of disseminated organic matter and abundance of evidence of bioturbation. The soil B horizon is a strongly developed Bw horizon with prismatic structure that parts to subangular blocky structure. Dry soil color ranges from 10YR 5/3 to 7/3. A PDI age of 5.3 to 8.4 ka was estimated for this soil (Table C-4); however, this is a minimum age because of the time required for formation of soil in the overlying sediment of Qc2 and Qf5b. A radiocarbon analysis from the overlying alluvial unit Qf5b yielded a date of ca. 5.5 cal ka (sample EOC2-c7, Table B-1), suggesting an age of ca. 10.6 to 13.9 ka or more for the base of soil b1. This age is slightly older than a radiocarbon analysis of ca. 10.3 cal ka from the unit beneath Qc2 that is 3 m east (sample EOC2-c39, Table B-1) but is within the estimated age range of ca. 10.7 to 11.7 cal ka for the base of the Holocene section 17 to 21 m farther west (samples EOC2-c14 and EOC-c19, Table B-1). By comparison, PDI ages for a complete soil profile in Qc2 (surface soil at P69.9) yield an age of ca. 11 to 17 ka. Together, the PDI and ¹⁴C methods suggest an age of ca. 10 to 11 ka for the base of soil b1 at P55.6.

Buried soil b2. The second buried soil at P55.6 is moderately developed and is 63 cm thick. This soil coincides with units Qf3b and Qf3a and the top of Qf2a. The top of the soil is denoted by the presence of two AB horizons (AB1b2 and AB2b2) that are noticeably bioturbated. The soil contains a well-developed albic E horizon that has a distinct white color (10YR 8/2), strong prismatic structure,

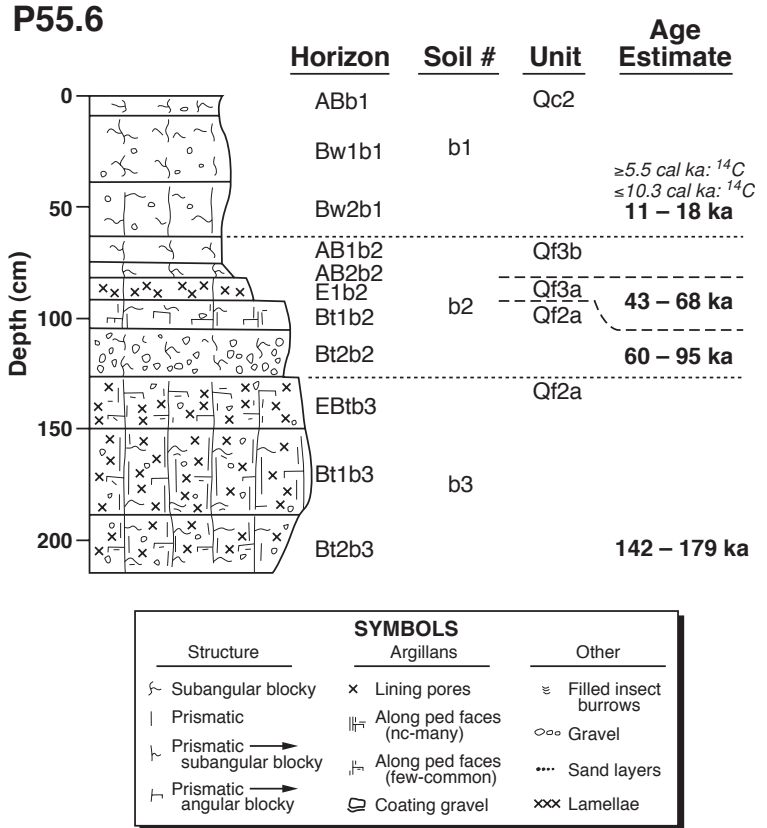


Figure C-4. Schematic stratigraphic column for Profile 55.6. The PDI age estimates are in bold; radiocarbon age estimates are in italics.

and a pronounced development of skeletal along pedfaces and within ped interiors. The soil Bt horizon is well developed with prismatic structure that parts to angular and subangular blocky structure and with argillans ranging from nearly continuous to common as coatings on pedfaces and clasts and lining pores. The Bt2b2 horizon formed in a layer that has considerably more fine gravel than the overlying soil, and stratigraphic relations elsewhere in the trench suggest that the parent material for this horizon unconformably underlies the Etb2 horizon, although there is no pedogenic evidence here for an unconformity and an additional buried soil. Dry color for the b2 soil ranges from 7.5YR 7/4 to 10YR 8/2. A PDI age of 21 to 33 ka was estimated for this soil (Table C-4). This PDI age range is probably a minimum because Qf3b and Qf3a thicken to the east, and the PDI age calcula-

Table C-4. PDI Age Estimates for Soil Units in Trench EOC-2

Horizon	Lower Horizon Depth from Profile Top (cm)	Upper Horizon Depth from Trench Top (cm)	Unit	HDI	PDI	PDI Age* Estimate (ka)	Upper PDI Age* Estimate (ka)	Lower PDI Age* Estimate (ka)	Composite PDI Upper Age† Estimate (ka)	Composite PDI Lower Age† Estimate (ka)
Profile 37.6										
BAb1	23	210	Qf5a	4.51						
CB1b1	40	233	Qf5a	1.01	5.5	1.4	1.7	1.1	17 [‡]	11
AB1b2	45	250	Qf3b	1.69						
AB2b2	51	255	Qf3b	2.37						
EBtb2	80	261	Qf2b	13.85	23.4	12.8	6.1	10.2	81	51
Bt1b2	96	290	Qf2a	5.31						
Bt2b2	113	306	Qf2a	3.67	32.4	21.1	26.6	16.8	98	62
Profile 55.6										
ABb1	9	90	Qc2	2.11						
Bw1b1	38	99	Qc2	7.60						
Bw2b1	63	128	Qc2	5.60	15.3	6.7	8.4	5.3	17 [‡]	11
AB1b2	74	153	Qf3b	2.06						
AB2b2	81	164	Qf3b	1.82						
Etb2	92	171	Qf3a	3.63	22.8	12.3	15.5	9.8	68	43
Bt1b2	105	182	Qf2a	6.45						
Bt2b2	126	195	Qf2a	8.31	37.6	26.5	33.3	21.0	95	600
EBtb3	151	216	Qf2a	10.15						
Bt1b3	178	241	Qf2a	11.64						
Bt2b3	214	268	Qf2a	15.79	75.2	76.9	96.9	61.1	179	113
Profile 67.2										
Bt2	16	90	Qc2	4.08	10.2	3.6	4.5	2.8	17 [‡]	11
Bt1b1	48	106	Qf4	25.93						
Bt2b1	74	138	Qf4	4.40						
Bt3b1	105	164	Qf4	7.96	42.4	31.9	40.1	25.3	55	35
Profile 69.9										
A1	10	0	Qc2	1.73						
A2	31	10	Qc2	3.78						
BA	49	31	Qc2	3.38						
Bt1	79	49	Qc2	10.23						
Bt2	95	79	Qc2	5.08	24.2	13.5	16.9	10.7	17	11
Bt1b1	116	95	Qoal5	11.05						
Bt2b1	143	116	Qoal5	13.30						
Bt3b1	168	143	Qoal5	9.97						
Bt4b1	200	168	Qoal4	8.30	66.8	64.2	80.9	51.0	>294	>185

*Represents minimum-limiting age for soil unit and does not account for all younger stratigraphic units.

†PDI estimate of soil age based on composite stratigraphic section and assumes no erosional loss (i.e., time) between soils.

‡PDI age estimate from surface soil at P69.9.

Table C-4 Continued

Age Estimate Using ¹⁴ C and Stratigraphic Context (cal ka)	Notes
Profile 37.6	
~10.66	
>10.66 <11.65	Base of Holocene gravel
> 11.65	Radiocarbon; minimum-limiting age for deposit
> 11.65	
> 50–60	Inferred age > El Cajete pumice based on stratigraphy
> 50–60	
> 50–60	
Profile 55.6	
>= ~5.5	Immediately beneath dated alluvial unit
> ~5.5	
< ~10.3	
> ~10.3	Radiocarbon; minimum-limiting age for deposit
> ~10.3	
< 50–60	Contains biotite grains, inferred to be derived from EC
> 50–60	Logged as stratigraphic break; inferred > El Cajete pumice based on stratigraphy
> 50–60	
> 50–60	
> 50–60	
> 50–60	>100 ka estimate from soils and stratigraphy
Profile 67.2	
< ~10.3	Inferred age for base of Holocene colluvium in eastern trench
< 50–60	Inferred to be younger than EC based on soils and stratigraphy
< 50–60	
< 50–60	
Profile 69.9	
< ~10.3	
< ~10.3	
< ~10.3	
< ~10.3	
< ~10.3	Inferred age for base of Holocene colluvium in eastern trench
> 100	Older than Qf2a, with age estimate of >100 ka
> 100	
> 100	
1160–1210	Early Pleistocene pumice bed, inferred Cerro del Medio source

tions for soil formed in these thicker units, therefore, would most likely result in a slightly older PDI age estimate. In addition, stratigraphic relations indicate that it is older than soil b1 at P67.2 (discussed below). The PDI age of soil b2 based on the composite stratigraphic column is ca. 60 to 95 ka. Geochemical and mineralogic evidence (Appendix D) suggest that the Etb2 horizon locally contains reworked components of the El Cajete pumice, indicating that the upper part of soil b2 is likely to be less than ca. 50 to 60 ka. A PDI composite age estimated for the base of the Etb2 horizon yields an age of ca. 43 to 68 ka (Table C-4). In combination, these lines of evidence suggest that the upper parts of soil b2 (units Qf3a and Qf3b) are slightly younger than the ca. 50- to 60-ka El Cajete pumice and that the lower parts of soil b2 (unit Qf2a) are somewhat older than the pumice.

Buried soil b3. The third buried soil at P55.6 is strongly developed and is 88 cm thick. This soil coincides with the lower part of unit Qf2a. The top of the soil is denoted by the presence of an albic EB horizon (EBtb3) and a

noticeable increase in the development of structure and argillans relative to the overlying soil. A pronounced development of skeletans along pedfaces and within ped interiors occurs in the EBtb3 horizon producing a distinct very pale-brown coloration (7.5YR 7/3). Skeletans also occur along prismatic pedfaces in the underlying Bt horizons. Prismatic soil structure parts to angular and subangular blocky structure. Argillans range from nearly continuous to common as coatings on pedfaces and lining pores. Dry color ranges from 7.5YR 7/3 to 7.5YR 5/5. A PDI age of ca. 61 to 97 ka was estimated for this soil (Table C-4). As discussed for soil b2, this is probably a minimum age, and a PDI composite age estimated for the base of the b3 soil is ca. 113 to 179 ka.

3. Profile 37.6

Soil characteristics for two buried soils were described at 37.6 H to a profile depth of 113 cm (Figure C-5; Table C-3). The top of the described profile lies about 210 cm below the surface.

Buried soil b1. The first buried soil at P37.6 is 40 cm thick and is weakly developed. This soil coincides with unit Qf5a. The top of the soil is denoted by a noticeable increase in disseminated organic matter and signs of bioturbation compared to the overlying soil. Dry soil color ranges from 10YR 7/3 to 5/3. Soil structure ranges from subangular blocky to single grain. A PDI age of 1.1 to 1.7 ka was estimated for this soil (Table C-4); however, this is a minimum age because of the time required for formation of soil in the overlying sediment of Qc2 and Qf5. Because stratigraphic relations suggest that the base of Qf5a is roughly correlative to the base of Qc2 farther east in the trench, the PDI composite age is assumed to be the same as obtained for P69.9, or ca.

11 to 17 ka. Radiocarbon analyses from surrounding sediments provide an age estimate of between ca. 10.7 and ca. 11.7 cal ka for the base of Qf5a in this part of the trench (samples EOC2-c14 and EOC2-c19, Table B-1), which overlaps with the younger range of the PDI estimate.

Buried soil b2. The second buried soil at P37.6 is well developed and is 73 cm thick. This soil coincides with units Qf3b, Qf2b, and Qf2a. The top of the soil is denoted by the presence of two AB horizons (AB1b2 and AB2b2) that contain abundant charcoal fragments and a grayish-black coloration suggesting the accumulation of organic matter. Dry color for soil b2 ranges from 7.5YR 7/4 to 10YR 8/2. Prismatic soil structure parts to moderate and angular and subangular blocky structure in most horizons. Argillan development is moderate and ranges from nearly continuous coatings along pedfaces to few lining pores. A pronounced development of skeletans along pedfaces and within ped interiors occurs in the EBtb3 horizon producing a distinct light grey coloration (10YR 8/2). The

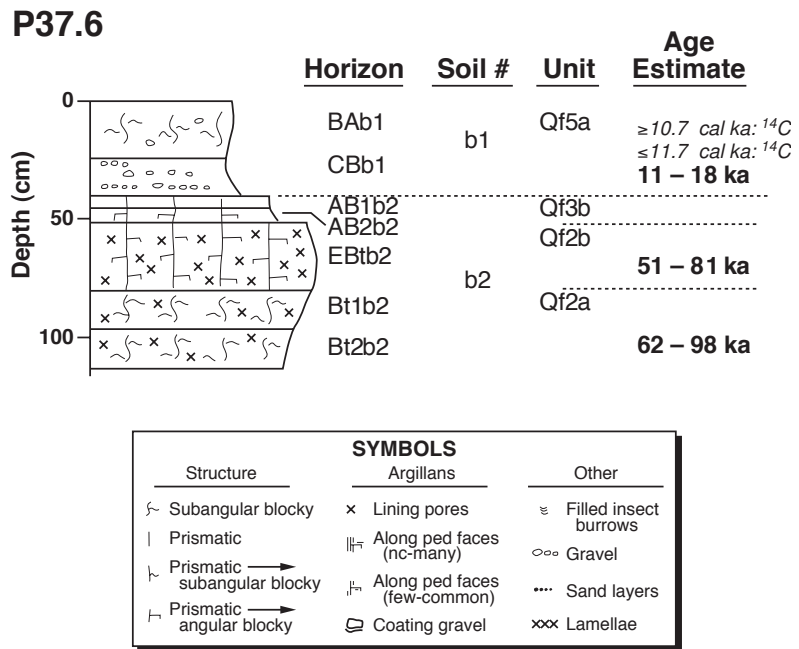


Figure C-5. Schematic stratigraphic column for Profile 37.6. The PDI age estimates are in bold; radiocarbon age estimates are in italics.

presence of the two AB horizons suggests that the top of this soil is largely intact. A PDI age of ca. 17 to 27 ka was estimated for this soil (Table C-4); however, this is a minimum age because of the time required for formation of soil in the overlying sediment of Qc2 and Qf5. A PDI composite age estimated for the base of the b2 soil yields an age of ca. 62 to 98 ka (Table C-4), or somewhat older than the ca. 50- to 60-ka El Cajete pumice. A PDI composite age estimated for the base of the EBtb2 horizon is ca. 51 to 81 ka, or possibly overlapping in age with the El Cajete pumice.

4. Profile 67.2

Soil characteristics for two buried soils were described at 67.2H to a profile depth of 105 cm (Figure C-6; Table C-3). The top of the described profile lies about 90 cm below the surface.

Surface Soil. The first soil at P67.2 is 16 cm thick and is weakly to moderately developed. This soil coincides with unit Qc2. The top of the soil profile was not described and most likely coincides with

the surface soil described nearby at P69.9. The Bt2 horizon at P67.2 probably coincides with the Bt2 horizon at P69.9. A PDI age of 2.8 to 4.5 ka was estimated for this soil (Table C-4); however, this is a minimum age because of the incomplete description of the surface soil. By comparison, the PDI age estimate for a complete soil formation in Qc2 at P69.9 is ca. 11 to 17 ka. A radiocarbon analysis from the unit beneath Qc2 9 m west (sample EOC2-c39, Table B-1) suggests that the base of the surface soil is somewhat less than 10.3 cal ka.

Buried soil b1. The first buried soil at P67.2 is at least 89 cm thick and is moderately developed and coincides with the top of unit Qf4. This soil is denoted by the presence of a weakly to moderately developed Bt horizon that has considerably better development of argillans than the overlying surface soil. The soil has formed in crudely stratified alluvium. The top of the soil has been truncated by erosion and is unconformably overlain by the surface soil. Dry soil color ranges from 7.5YR 7/4 to 10YR 7/3. Soil structure consists predominantly of subangular blocky structure.

Argillan development is predominantly represented by the pronounced development of lamellae. Lamellae are about 1 to 5 cm thick and consist of argillans bridging and coating coarse sand and gravel. A PDI age of 25 to 40 ka was estimated for this soil (Table C-4); however, this is a minimum age because of the time required for formation of soil in the overlying colluvium of Qc2. A PDI composite age estimated for the base of the b1 soil is ca. 35 to 55 ka, although the actual age may be somewhat older because of the evidence for erosion at the top of soil b2. Stratigraphic relations indicate that the b1 soil at P67.2 is somewhat older than the b2 soil at P55.6, which has a PDI composite age estimate of ca. 43 to 68 ka and an

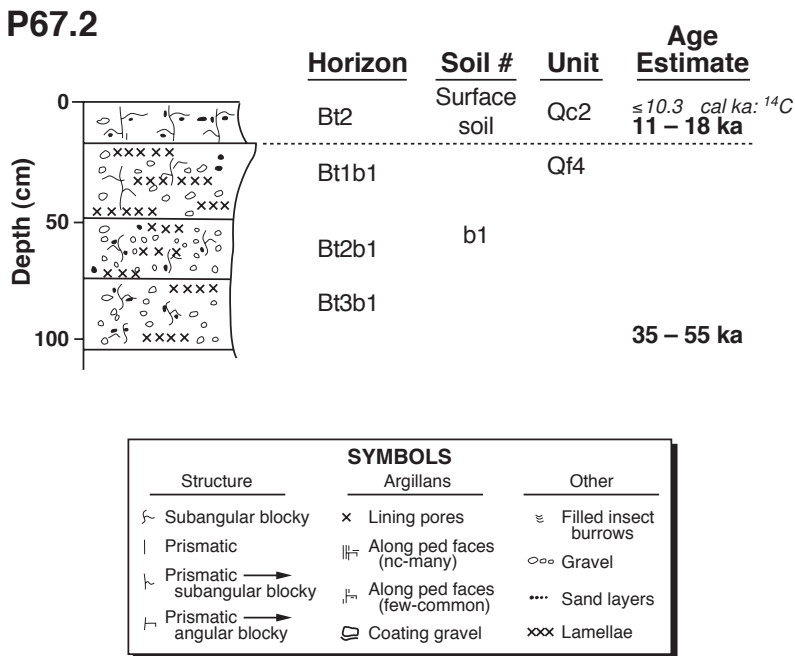


Figure C-6. Schematic stratigraphic column for Profile 67.2. The PDI age estimates are in bold; radiocarbon age estimates are in italics.

Table C-5. Composite Soil Stratigraphy Used to Calculate PDI Ages for Buried Units in Trench EOC-2

Horizon	Horizon Thickness (cm)	Cumulative Depth (cm)	Unit	HDI	Cumulative PDI	Inferred PDI Age (ka)	Inferred PDI Upper Age (ka)	Inferred PDI Lower Age (ka)
Cumulative Section								
Profile 69.9								
A1	10	10	Qc2	1.73				
A2	21	31	Qc2	3.78				
BA	18	49	Qc2	3.38				
Bt1	30	79	Qc2	10.23				
Bt2	16	95	Qc2	5.08	24.2	13	17	11
Profile 37.6								
BAb1	23	118	Qf5a	4.51				
CB1b1	17	135	Qf5a	1.01	29.7	13	17	11
Profile 67.2								
Bt1b1	32	127	Qf4	9.93				
Bt2b1	26	153	Qf4	4.40				
Bt3b1	31	184	Qf4	7.96	52.0	44	55	35
Profile 55.6								
AB1b2	5	279	Qf3b	2.06				
AB2b2	6	285	Qf3b	1.82				
Etb2	11	357	Qf3a	3.63	59.5	54	68	43
Bt1b2	13	370	Qf2a	6.45				
Bt2b2	21	391	Qf2a	8.31	74.3	76	95	60
EBtb3	25	416	Qf2a	10.15				
Bt1b3	27	443	Qf2a	11.64				
Bt2b3	36	479	Qf2a	15.79	111.9	142	179	113
Profile 69.9								
Bt1b1	21	500	Qoal5	11.05				
Bt2b1	27	527	Qoal5	13.30				
Bt3b1	25	552	Qoal5	9.97				
Bt4b1	32	584	Qoal4	8.30	154.5	233	294	185
Cumulative Section to Upper Part of Unit Qf2a								
Profile 69.9								
A1	10	10	Qc2	1.73				
A2	21	31	Qc2	3.78				
BA	18	49	Qc2	3.38				
Bt1	30	79	Qc2	10.23				
Bt2	16	95	Qc2	5.08	24.2	13	17	11
Profile 37.6								
BAb1	23	118	Qf5a	4.51				
CB1b1	17	135	Qf5a	1.01	29.7	13	17	11
Profile 67.2								
Bt1b1	32	167	Qf4	9.93				
Bt2b1	26	193	Qf4	4.40				
Bt3b1	31	224	Qf4	7.96	52.0	44	55	35
Profile 37.6								
AE1b2	5	229	Qf3b	1.69				
AE2b2	6	235	Qf3b	2.37				
EBtb2	39	274	Qf2b	13.85	69.9	69	87	55
Bt1b2	16	290	Qf2a	5.31				
Bt2b2	17	307	Qf2a	3.67	78.9	83	104	66

inferred age of younger than the ca. 50- to 60-ka El Cajete pumice. Available evidence therefore suggests that Qf4 and soil b2 at P67.2 are in the younger part of the ca. 35- to 55-ka PDI composite age range and only slightly older than Qf3a and soil b1 at P55.6.

E. Summary and Conclusions

Ages for surface and buried soil stratigraphic units in trench EOC-2 were determined using a commonly applied soil-development index that has been locally calibrated for use around LANL. Soil ages are derived from the simple linear relationship between the soil chronofunction and PDI values calculated for surface and buried soils described at the trench.

Soil-based ages are generally consistent with strata dated by radiocarbon analyses (Appendix B) and by the stratigraphic relation to units containing reworked components of the ca. 50- to 60-ka El Cajete pumice. An overall consistency between soil ages and radiometric dates indicates that the use of a soil development index provides stratigraphically reasonable age estimates that enhance the interpretation of the geomorphic and paleoseismic history at the trench site. Further, the degree of soil development provides relative age information that can be used to support geochronologic and other geologic information. Given that there are several key assumptions involved in the application of PDI values for dating soil strata, the soil age estimates reported here may not be as robust as standard and well-tested radiometric techniques and should be used with caution. In addition, PDI soil age estimates reflect the time interval that strata have been exposed to soil-forming processes, which in some cases may not be the same as the actual age of the deposit.

F. Recommendations

The application of soil stratigraphy and soil-based PDI ages will remain a principal means of dating Quaternary geologic events around LANL.

Additional effort is warranted to improve and test the application of a soil-development index for determining the ages of key geologic strata. Confidence in PDI age estimates would be enhanced by further assessment using two key approaches:

Soil parent material. An important component of generating PDI ages is determining the original characteristics of the soil parent material. Further assessment of the morphology of colluvium that commonly serves as the parent material for most of the soils associated with fault-related features would increase confidence in PDI ages. Field descriptions of the morphology of late Holocene (i.e., < 1 to 3 ka) or historic colluvium would enhance estimates of the original morphology for soils described in this (and future) trench locations.

Local testing of PDI ages for multiple buried soils. Direct comparison of PDI ages for a sequence of multiple soils with datable strata would provide a means to directly test the accuracy of PDI age techniques used in this report. A sequence of multiple buried soils, currently exposed in a deep borrow pit adjacent to NM 501 at TA-16 (Reneau and McDonald 1996, p. 90), provides a unique opportunity to directly evaluate soil ages. The exposed section at this site consists of an approximately 10- to 14-m sequence of buried soils and colluvium and probably represents one of the most complete records of soils and colluvial and alluvial deposition along the main Pajarito fault escarpment. Methods used to describe soils and calculate PDI ages in previous trench studies could be used to develop PDI age estimates for soils exposed in the borrow pit. These PDI ages could be directly compared with stratum dated using the position of interstratified pumice layers (several of known age or possibly datable) and the development of magnetostratigraphy. Additional independent dating of strata may also be possible through TL or IRSL dating. Evaluation of the source of any age discrepancies between PDI ages and dated strata could be used to adjust or modify the PDI age-based approach. Results of such an investigation

would directly increase the confidence in PDI age estimates for use in seismic hazard assessments.

Development of a soil-stratigraphic column at TA-16, which is possibly a complete soil stratigraphic section, could also be used to evaluate problems with recognition of possible unconformities in past and future trench excavations. Recognition of unconformities was a problem frequently encountered during previous trench excavations (McCalpin 1998, 1999; McDonald 1999). Accurate determination of the presence of an unconformity is often critical for correct interpretation of trench stratigraphy and ages of related events. Soil-stratigraphic correlations between the key soils at the TA-16 site and soils exposed in trenches could be used to determine if stratigraphic unconformities are present in trench exposures. For example, juxtaposition of soils in a trench that are not stratigraphically in sequence at the TA-16 site could indicate the position of a stratigraphic unconformity within the exposed trench strata. Further, stratigraphic information from the TA-16 site would enhance evaluation of possible long-term fault activity along the Pajarito fault escarpment.

APPENDIX D. PETROGRAPHY, GEOCHEMISTRY, AND CORRELATIONS OF TEPHRAS

A. Introduction

Samples of tephtras and tephtra-bearing deposits were collected from a number of stratigraphic units exposed in trench EOC-2. Petrographic and geochemical studies of these tephtras may allow their correlation to dated volcanic sources, thus providing additional time-stratigraphic constraints for units from the trench. The likely source region for most or all of the tephtras in trench EOC-2 is the Jemez volcanic field, which exhibits a 13 million year record of geologically continuous volcanism (Gardner et al. 1986). Notably, the volcanic field hosts the Valles-Toledo caldera complex whose eastern rim is just 5 km west of the trench site. The Valles-Toledo caldera complex formed during two major sequences of eruption of the Bandelier Tuff at about 1.61 Ma (the Otowi Member) and 1.22 Ma (the Tshirege Member) (ages from Izett and Obradovich 1994). Smaller volume, intracaldera eruptions followed each major Bandelier Tuff sequence, producing the Cerro Toledo Rhyolite (roughly 1.6 to 1.23 Ma; Heiken et al. 1986; Spell et al. 1996) and the Valles Rhyolite (about 1.13 Ma to about 50 to 60 ka; Spell and Harrison 1993; Toyoda et al. 1995; Reneau et al. 1996a). Thus, volcanoclastic deposits on the Pajarito Plateau, on the flanks of the Jemez Mountains, will likely contain tephtras that can ultimately be correlated to their sources in the volcanic field.

Samples from trench EOC-2 were washed with deionized water in an ultrasonic bath. Floatable organic particles and suspended fines were decanted and the remaining sample was dried in an oven at about 100°C. Samples of alluvial deposits were sieved and the medium to coarse-sand size fraction or the silt to very fine-sand size fraction were used for further analysis. Some samples were prepared as thin-section grain mounts for petrographic and electron microprobe analyses. Pumice was selectively picked (high graded) from some samples and crushed, fused, and analyzed for major and selected trace elements by x-ray fluorescence (XRF) (see

Gardner et al. 1999, 2001, for analytical methods and parameters). XRF results are presented in Table D-1 and electron microprobe analyses of glass are tabulated in Table D-2.

B. X-ray Fluorescence Analyses of Bulk Pumice

1. Petrographic descriptions of samples prior to high grading

EOC2/00/11-17-6: unit Qoal3; 65.6H, -5.0V. This sample is from stratified pumice- and dacite-rich alluvium. The thin section is composed of moderately rounded, coarse sand-sized grains and is about 80% pumice fragments and about 20% lithic fragments. The lithic population is dominated by vitrophyric to hyalopilitic dacite clasts, which contain sparse phenocrysts of plagioclase, hornblende, clinopyroxene, and trace sanidine (?). Lithic clasts exhibit a variety of degrees of oxidation and range from fresh groundmass glass to groundmass of devitrification products of cryptofelsite and rare spherulites; flow banding is locally preserved. The lithic population also includes trace, apparently aphyric fragments of perlite. The pumice population is dominated by mostly aphyric clasts with fairly equant, mildly deformed vesicles; however, trace elongate, tubular vesicles mark a few clasts. The glass in most pumice fragments is fresh but shows incipient alteration to clay. Rare, fragmental pieces of feldspar, mostly plagioclase with even rarer sanidine, occur as phenocrysts in some pumice clasts.

EOC2/00/11-17-7: unit Qoal4; 71.8H, -4.1V. This sample is from a reworked, bedded pumice deposit. The thin section was made from a single, large pumice fragment. The pumice is aphyric with mostly fresh glass, exhibiting incipient clay alteration. Vesicles are equant to mildly stretched.

EOC2/00/11-17-8: unit Qbt; 81.1H, -4.6V. This sample is from pumices, hand-picked from the pumice flow. The thin section was made from about ten pebble-sized fragments of subrounded to

Table D-1. Whole-Rock X-ray Fluorescence Analyses of Pumices From Trench EOC-2

Oxides (wt %)											
Sample	SiO ₂	TiO ₂	Al ₂ O ₃	Fe ₂ O ₃	MnO	MgO	CaO	Na ₂ O	K ₂ O	P ₂ O ₅	Total
EOC2/00_11_17_6	72.27	0.14	12.70	1.63	0.05	0.17	0.34	3.45	4.65	0.00	95.40
EOC2/00_11_17_7	71.41	0.12	13.15	1.64	0.05	0.21	0.40	2.87	5.00	0.01	94.87
EOC2/00_11_17_8	75.33	0.15	11.40	1.98	0.07	0.13	0.35	3.06	4.54	0.02	97.02
EOC2/00_11_17_8a	75.15	0.12	11.74	1.58	0.05	0.00	0.32	3.34	4.90	0.00	97.20
EOC2/00_11_17_9	68.73	0.29	13.86	3.30	0.14	0.42	0.64	2.99	4.50	0.03	94.90
EOC2/00_11_17_10	73.22	0.10	12.10	1.26	0.05	0.00	0.31	3.55	4.84	0.00	95.42

Trace Elements (ppm)							
Sample	Zn	Rb	Sr	Y	Zr	Nb	Ba
EOC2/00_11_17_6	48.39	158.08	12.76	32.16	152.80	55.10	94.16
EOC2/00_11_17_7	60.69	150.80	10.58	63.92	162.31	46.20	61.15
EOC2/00_11_17_8	73.16	120.54	12.51	62.25	265.65	69.92	94.70
EOC2/00_11_17_8a	62.02	102.59	17.90	36.26	248.57	55.94	91.09
EOC2/00_11_17_9	87.33	99.38	57.16	47.13	338.33	48.88	287.21
EOC2/00_11_17_10	54.22	152.23	0.00	42.18	161.40	45.68	56.86

subangular pumices. The pumices are sparsely phyrlic with large (2 mm) crystal fragments of quartz and sanidine; some crystal fragments exhibit relict bipyramidal forms in quartz and euhedral forms of sanidine. One pumice fragment contains a crystal clot of plagioclase, rimmed with another feldspar, and brownish hornblende. A different pumice contains a clinopyroxene fragment with pale-green pleochroism. Vesicle textures are dominated by mildly deformed, stretched forms, although one pumice contains nondeformed, equant vesicles. Glasses are quite fresh, but clay lines some vesicles, and there are trace amounts of incipient alteration of glass to clay.

EOC2/00/11-17-9: unit Qoal1; 84.2H, -3.6V. This sample is from pumice-rich alluvium. The thin section was made from medium- to coarse-sand-sized grains. Clasts are 95% subrounded pumice fragments and about 5% subangular crystal fragments. One fragment of nonwelded tuff was observed. Pumices have dominantly deformed, stretched vesicles, but a few tubular, elongate forms were noted.

Most pumice possesses a moderate degree of clay alteration after glass. Pumices are sparsely phyrlic with rounded, large (2 mm) quartz and potassium feldspar crystal fragments and crystal clots; however, a few relict bipyramidal forms of quartz do occur. The crystal clots are large (> 2 mm), dominated by potassium feldspar with pronounced zoning, exhibit hypidiomorphic-granular textures, and contain trace plagioclase and pale-green clinopyroxene. Sand-sized crystal fragments in the sample are clearly derived from the phenocrysts and crystal clots of the pumices.

EOC2/00/11-17-10: unit Qoal3; 95.0H (projected; sample was collected from east wall of trench), -2.7V. This sample is from stratified pumice- and dacite-rich alluvium. The thin section is identical to sample EOC2/00/11-17-6 except for the following: fine- to coarse-sand-sized clasts; fragments of perlitic glass constitute up to 1% and contain very sparse feldspar phenocrysts; one crystal clot, 1.5 mm in diameter, similar to those described in sample EOC2/00/11-17-9, was observed.

2. Results

XRF analyses of five tephra samples from trench EOC-2 are tabulated in Table D-1; one sample, EOC2/00/11-17-8, was split (EOC2/00/11-17-8A) and both splits were analyzed. Figure D-1 shows chemical variations for selected analytes for these samples compared to whole-rock data for the upper part of the Tshirege Member of the Bandelier Tuff (Gardner et al. 1999) and the post-caldera domes of the Valle Grande Member of the Valles Rhyolite (Spell 1987). Precise stratigraphic correlations for the Bandelier Tuff cannot be made reliably by direct comparison of whole-rock XRF data of tuff to XRF data of selected individual pumices. However, it is clear from the XRF data that samples EOC/00/11-17-8 and -8A are Bandelier Tuff; furthermore, the petrography of these samples, described above, is fairly characteristic of the Bandelier Tuff (Gardner et al. 1999, 2001). EOC2/00-11-17-9 is tephra high graded from alluvial deposits and shows geochemistry typical of Unit 4 (of Gardner et al. 2001) of the Tshirege Member. Additionally, the sample contains crystal clots, described above, that are characteristic of Unit 4.

Pumices from samples EOC2/00/11-17-6, -7, and -10 all exhibit similar geochemistry. Stratigraphically, the units from which these samples came all overlie the Bandelier Tuff. Comparing the chemistry of these samples to the chemistry of the post-Valles caldera domes (Spell 1987) shows that they are most like samples from the Cerro del Medio dome complex (Figure D-1), which have yielded an $^{40}\text{Ar}/^{39}\text{Ar}$ age estimate of 1.133 ± 0.011 Ma (Spell and Harrison 1993; note that Izett and Obradovich (1994) have also reported ages of ca. 1.10 to 1.21 for Cerro del Medio eruptions, but these analyses are considered less reliable than those of Spell and Harrison 1993). Although chemical comparisons of pumices, derived from reworked fallout deposits, with whole-rock chemistry of dome lavas do not form the most robust basis for correlation, petrography lends additional credence to our correlation of these tephras to the Cerro del Medio dome complex. These tephras from trench EOC-2 are largely

continued on page 58

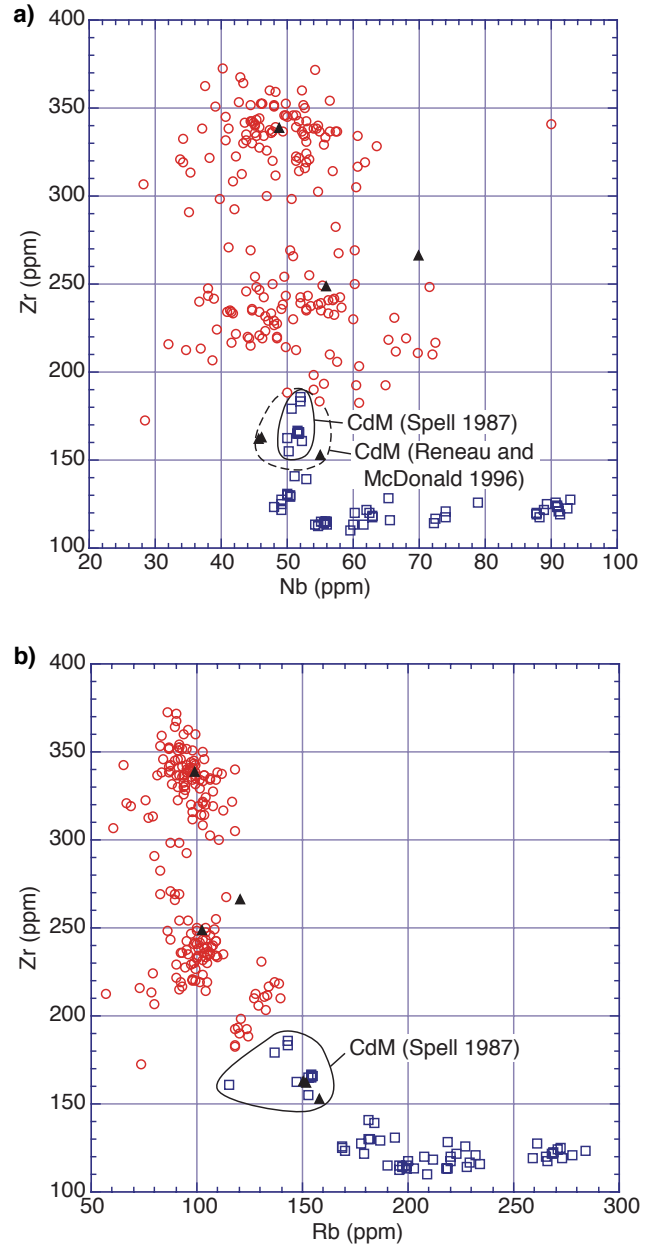


Figure D-1. Chemical variation diagrams of whole-rock XRF data for the upper Tshirege Member of the Bandelier Tuff (circles; data from Gardner et al. 1999), Valle Grande Member of the Valles Rhyolite (boxes; data from Spell 1987), and pumices from trench EOC-2 (solid triangles). Shown are a) variation of Zr versus Nb with correlation fields for Cerro del Medio (CdM) from Spell (1987) (solid line) and Reneau and McDonald (1996) (dashed line) and b) variation of Zr versus Rb with the correlation field for Cerro del Medio (CdM) from Spell (1987).

**Table D-2a. Electron Microprobe Analyses of Glasses (wt %)
From Selected Tephra From Trench EOC-2: Raw Analyses**

Sample	SiO ₂	TiO ₂	Al ₂ O ₃	FeO	MnO	MgO	CaO	Na ₂ O	K ₂ O	P ₂ O ₅	BaO	Total
EDC2_00-11-17-2	72.38	0.09	12.17	0.82	0.00	0.14	0.76	3.59	4.42	0.00	0.00	94.37
EDC2_00-11-17-2	74.54	0.10	11.92	0.70	0.01	0.09	0.55	3.17	4.52	0.00	0.11	95.72
EDC2_00-11-17-2	74.68	0.12	11.78	0.72	0.08	0.02	0.37	3.65	4.51	0.01	0.12	96.05
EDC2_00-11-17-2	73.34	0.19	12.16	0.82	0.05	0.14	0.77	3.60	4.26	0.04	0.14	95.51
EDC2_00-11-17-2	72.49	0.29	12.29	0.86	0.02	0.16	0.87	3.49	4.29	0.01	0.03	94.78
EDC2_00-11-17-2	71.57	0.19	11.90	0.84	0.05	0.15	0.79	3.31	3.81	0.03	0.12	92.75
EDC2_00-11-17-2	71.80	0.24	12.42	0.92	0.06	0.16	0.89	3.37	4.12	0.01	0.00	93.99
EDC2_00-11-17-2	74.26	0.14	11.49	1.27	0.07	0.00	0.16	3.10	5.04	0.00	0.00	95.53
EDC2_00-11-17-2	73.93	0.14	11.79	1.25	0.08	0.00	0.16	3.67	4.70	0.00	0.00	95.72
EDC2_00-11-17-2	74.08	0.00	11.54	1.37	0.08	0.00	0.03	3.90	4.66	0.04	0.17	95.87
EDC2_00-11-17-2	75.42	0.08	12.10	0.72	0.03	0.08	0.64	3.28	4.45	0.04	0.09	96.93
EDC2_00-11-17-2	70.94	0.25	12.53	1.06	0.06	0.19	1.11	3.58	4.12	0.03	0.05	93.91
EDC2_00-11-17-2	73.66	0.03	11.53	1.45	0.09	0.00	0.18	4.03	4.27	0.02	0.00	95.24
EDC2_00-11-17-2	73.94	0.02	11.64	1.18	0.04	0.00	0.30	3.67	4.48	0.00	0.09	95.35
EDC2_00-11-17-2	71.76	0.11	11.14	1.25	0.06	0.02	0.29	3.66	4.50	0.03	0.00	92.81
EDC2_00-11-17-2	73.44	0.19	12.37	0.84	0.02	0.16	0.85	3.70	4.40	0.02	0.00	96.00
EDC2/00-11-17-3	72.85	0.00	11.46	1.20	0.04	0.01	0.11	3.08	5.63	0.01	0.00	94.39
EDC2/00-11-17-3	73.78	0.07	11.51	1.44	0.06	0.00	0.27	4.33	4.07	0.04	0.00	95.57
EDC2/00-11-17-3	73.92	0.04	11.80	1.16	0.07	0.02	0.26	4.39	4.08	0.00	0.06	95.81
EDC2/00-11-17-3	73.39	0.09	11.60	1.38	0.06	0.00	0.27	4.05	4.15	0.00	0.00	94.99
EDC2/00-11-17-3	70.23	0.11	11.88	0.88	0.06	0.02	0.37	3.76	4.25	0.02	0.11	91.68
EDC2/00-11-17-3	72.13	0.07	11.73	0.96	0.07	0.04	0.34	3.85	4.18	0.00	0.25	93.62
EDC2/00-11-17-3	73.50	0.10	11.60	0.95	0.07	0.02	0.35	3.89	4.25	0.00	0.00	94.72
EDC2/00-11-17-3	73.56	0.05	11.66	0.75	0.03	0.02	0.36	3.55	4.25	0.00	0.00	94.22
EDC2/00-11-17-3	72.75	0.06	11.88	0.81	0.11	0.03	0.35	3.84	4.35	0.00	0.11	94.27
EDC2/00-11-17-3	72.63	0.12	12.01	0.80	0.06	0.05	0.36	4.11	4.24	0.00	0.00	94.36
EDC2/00-11-17-3	74.16	0.05	11.56	1.41	0.10	0.00	0.27	4.13	4.06	0.00	0.04	95.78
EDC2/00-11-17-3	71.89	0.13	11.70	0.98	0.02	0.03	0.24	3.51	4.85	0.01	0.00	93.34
EDC2/00-11-17-3	73.68	0.07	11.56	1.40	0.07	0.00	0.24	3.59	4.83	0.00	0.01	95.45
EDC2/00-11-17-3	71.83	0.10	11.41	1.38	0.10	0.00	0.12	4.06	4.21	0.01	0.00	93.22
EDC2/00-11-17-3	74.23	0.13	11.49	1.50	0.09	0.00	0.09	4.31	4.41	0.00	0.14	96.37
EDC2/00-11-17-3	74.16	0.05	11.77	1.25	0.10	0.00	0.32	4.06	4.61	0.00	0.04	96.37
EOC2_00_11_17_4	67.62	0.11	10.61	0.70	0.04	0.01	0.32	3.40	3.99	0.00	0.05	86.84
EOC2_00_11_17_4	73.05	0.10	12.06	0.82	0.08	0.03	0.39	3.81	4.53	0.00	0.00	94.89
EOC2_00_11_17_4	74.76	0.05	11.57	1.30	0.09	0.00	0.16	4.12	4.27	0.00	0.00	96.32
EOC2_00_11_17_4	73.30	0.11	11.88	0.83	0.08	0.02	0.33	4.09	4.34	0.01	0.00	94.99
EOC2_00_11_17_4	69.51	0.05	11.55	0.82	0.07	0.01	0.33	3.83	4.20	0.01	0.00	90.38
EOC2_00_11_17_4	73.71	0.16	11.57	0.82	0.05	0.04	0.33	3.73	4.11	0.00	0.04	94.55
EOC2_00_11_17_4	73.63	0.07	11.92	0.89	0.03	0.03	0.36	3.90	4.43	0.00	0.03	95.30

**Table D-2a Continued. Electron Microprobe Analyses of Glasses (wt %)
From Selected Tephra From Trench EOC-2: Raw Analyses**

Sample	SiO ₂	TiO ₂	Al ₂ O ₃	FeO	MnO	MgO	CaO	Na ₂ O	K ₂ O	P ₂ O ₅	BaO	Total
EOC2_00_11_17_4	71.75	0.14	11.78	0.84	0.03	0.02	0.36	3.95	4.20	0.02	0.12	93.22
EOC2_00_11_17_4	72.95	0.11	12.07	0.75	0.08	0.02	0.32	4.07	4.59	0.02	0.00	94.98
EOC2_00_11_17_4	74.72	0.04	11.70	1.14	0.00	0.00	0.27	3.92	4.61	0.00	0.07	96.47
EOC2_00_11_17_4	73.83	0.02	11.97	0.91	0.05	0.02	0.38	4.05	4.57	0.05	0.00	95.85
EOC2_00_11_17_4	74.11	0.09	11.71	0.91	0.05	0.04	0.32	3.93	4.22	0.02	0.00	95.40
EOC2_00_11_17_4	73.32	0.00	11.56	0.90	0.05	0.01	0.33	3.51	4.58	0.00	0.00	94.26
EOC2_00_11_17_4	73.54	0.06	11.96	0.84	0.06	0.11	0.70	3.39	4.40	0.05	0.12	95.22
EOC2_00_11_17_4	71.77	0.13	11.91	0.86	0.04	0.03	0.34	3.78	4.24	0.01	0.16	93.27
EOC2_00_11_17_4	75.17	0.13	11.91	0.59	0.06	0.04	0.52	3.46	4.55	0.02	0.15	96.61
EOC2_00_11_17_4	72.86	0.13	12.13	0.80	0.03	0.05	0.35	3.92	4.40	0.01	0.00	94.69
EOC2_00_11_17_4	72.78	0.14	11.73	0.85	0.03	0.01	0.36	3.85	3.94	0.02	0.00	93.70
EOC2_00_11_17_4	72.65	0.15	11.90	0.82	0.07	0.02	0.35	3.76	4.35	0.00	0.11	94.18
EOC2_00_11_17_4	72.56	0.23	11.97	0.81	0.05	0.03	0.35	3.91	4.39	0.02	0.06	94.37
EOC2_00_11_17_4	73.35	0.19	11.96	0.88	0.07	0.03	0.33	3.87	4.32	0.00	0.00	95.00
EOC2_00_11_17_4	73.39	0.15	12.00	0.82	0.04	0.02	0.34	3.92	4.60	0.02	0.00	95.30
EDC2/00-11-17-5	73.76	0.24	11.63	1.33	0.02	0.02	0.41	3.22	5.32	0.02	0.00	95.97
EDC2/00-11-17-5	74.62	0.16	11.52	1.18	0.06	0.02	0.12	3.37	5.10	0.01	0.11	96.27
EDC2/00-11-17-5	75.12	0.09	11.71	1.31	0.11	0.00	0.17	4.16	4.29	0.01	0.04	97.02
EDC2/00-11-17-5	74.42	0.04	11.59	1.31	0.07	0.00	0.05	4.18	4.50	0.03	0.00	96.20
EDC2/00-11-17-5	75.97	0.01	11.83	0.91	0.09	0.01	0.35	4.04	4.21	0.00	0.08	97.49
EDC2/00-11-17-5	74.29	0.14	11.70	1.18	0.01	0.04	0.33	3.71	4.75	0.00	0.15	96.28
EDC2/00-11-17-5	74.89	0.02	11.66	1.42	0.06	0.00	0.09	4.20	4.31	0.00	0.12	96.78
EDC2/00-11-17-5	72.42	0.04	11.79	0.88	0.04	0.02	0.36	4.06	4.09	0.00	0.12	93.83
EDC2/00-11-17-5	73.32	0.07	11.58	1.18	0.02	0.01	0.29	3.83	4.29	0.00	0.06	94.66
EDC2/00-11-17-5	68.96	0.04	10.65	1.30	0.07	0.01	0.21	3.98	4.03	0.06	0.00	89.29
EOC2/00_11_17_6	73.56	0.09	11.66	0.88	0.03	0.02	0.33	3.91	4.30	0.03	0.00	94.81
EOC2/00_11_17_6	73.61	0.11	11.65	0.94	0.04	0.01	0.33	3.74	4.25	0.00	0.00	94.66
EOC2/00_11_17_6	74.36	0.15	11.82	0.80	0.04	0.01	0.35	3.68	4.71	0.07	0.09	96.06
EOC2/00_11_17_6	74.32	0.10	11.78	0.96	0.02	0.02	0.35	4.03	4.32	0.01	0.03	95.93
EOC2/00_11_17_6	73.82	0.09	11.68	0.93	0.09	0.02	0.35	3.86	4.23	0.02	0.00	95.08
EOC2/00_11_17_6	74.69	0.11	11.61	0.94	0.01	0.01	0.35	3.84	4.25	0.00	0.08	95.89
EOC2/00_11_17_6	74.92	0.11	11.04	0.90	0.02	0.02	0.28	3.34	4.67	0.00	0.05	95.33
EOC2/00_11_17_6	74.76	0.05	11.62	0.93	0.04	0.01	0.35	4.04	4.13	0.00	0.14	96.06
EOC2/00_11_17_6	74.06	0.07	11.63	0.95	0.04	0.03	0.37	3.82	4.26	0.00	0.27	95.50
EOC2/00_11_17_6	73.92	0.09	11.77	0.86	0.02	0.03	0.34	3.87	4.27	0.08	0.01	95.25
EOC2/00_11_17_6	73.93	0.09	11.58	0.81	0.04	0.02	0.37	3.86	4.14	0.01	0.25	95.09
EOC2/00_11_17_6	73.85	0.04	11.70	0.88	0.08	0.02	0.37	3.89	4.14	0.00	0.00	94.96
EOC2/00_11_17_6	73.71	0.12	11.66	0.96	0.06	0.02	0.35	3.80	4.28	0.05	0.25	95.24
EOC2/00_11_17_6	74.16	0.02	11.69	0.87	0.04	0.02	0.35	3.96	4.32	0.00	0.11	95.53

**Table D-2a Continued. Electron Microprobe Analyses of Glasses (wt %)
From Selected Tephros From Trench EOC-2: Raw Analyses**

Sample	SiO ₂	TiO ₂	Al ₂ O ₃	FeO	MnO	MgO	CaO	Na ₂ O	K ₂ O	P ₂ O ₅	BaO	Total
EOC2/00_11_17_6	74.42	0.00	11.62	0.91	0.09	0.01	0.32	3.82	4.16	0.00	0.14	95.49
ta49_00_11_21_00	74.91	0.06	11.86	0.52	0.03	0.05	0.55	2.92	4.98	0.02	0.00	95.89
ta49_00_11_21_00	72.18	0.25	12.67	0.97	0.03	0.18	0.90	3.57	4.33	0.01	0.00	95.10
ta49_00_11_21_00	73.21	0.17	12.74	1.06	0.03	0.22	0.98	3.70	4.32	0.00	0.15	96.58
ta49_00_11_21_00	73.61	0.05	11.75	0.66	0.04	0.07	0.56	3.34	4.42	0.04	0.00	94.55
ta49_00_11_21_00	73.59	0.09	11.94	0.62	0.04	0.07	0.58	3.36	4.52	0.01	0.24	95.07
ta49_00_11_21_00	73.26	0.30	12.68	0.81	0.09	0.13	0.72	3.49	4.57	0.00	0.09	96.12
ta49_00_11_21_00	74.84	0.17	11.84	0.65	0.01	0.02	0.49	3.57	4.50	0.00	0.00	96.09
ta49_00_11_21_00	74.76	0.12	11.95	0.71	0.05	0.03	0.51	3.44	4.63	0.03	0.06	96.30
ta49_00_11_21_00	74.46	0.10	11.87	0.63	0.06	0.07	0.53	3.41	4.58	0.00	0.00	95.71
ta49_00_11_21_00	74.32	0.07	11.95	0.72	0.00	0.04	0.58	3.43	4.53	0.00	0.09	95.73
ta49_00_11_21_00	73.89	0.18	12.29	0.84	0.01	0.13	0.79	3.48	4.44	0.04	0.00	96.09
ta49_00_11_21_00	74.18	0.09	11.94	0.73	0.04	0.07	0.56	3.29	4.58	0.00	0.00	95.48
ta49_00_11_21_00	73.95	0.19	12.13	0.83	0.02	0.12	0.71	3.43	4.45	0.00	0.20	96.02
ta49_00_11_21_00	74.71	0.14	11.74	0.61	0.06	0.04	0.52	3.32	4.47	0.03	0.15	95.79
ta49_00_11_21_00	74.35	0.07	11.87	0.60	0.03	0.04	0.54	3.38	4.63	0.00	0.10	95.62
ta49_00_11_21_00	73.40	0.29	12.73	0.74	0.02	0.07	0.91	3.60	4.63	0.04	0.12	96.56
ta49_00_11_21_00	74.47	0.08	12.39	0.89	0.04	0.15	0.84	3.57	4.40	0.00	0.00	96.80
ta49_00_11_21_00	74.18	0.08	11.77	0.61	0.08	0.03	0.48	3.55	4.44	0.02	0.00	95.24
ta49_00_11_21_00	72.52	0.12	12.20	0.91	0.03	0.14	0.77	3.39	4.34	0.07	0.05	94.54
ta49_00_11_21_00	74.85	0.09	11.91	0.63	0.06	0.03	0.52	3.50	4.65	0.00	0.00	96.24
ta49_00_11_21_00	73.31	0.21	12.38	0.94	0.01	0.18	0.82	3.39	4.52	0.00	0.00	95.76
ta49_00_11_21_00	74.18	0.08	11.82	0.61	0.03	0.04	0.50	3.33	4.61	0.01	0.06	95.27
ta49_00_11_21_00	72.72	0.18	12.54	0.88	0.05	0.16	0.84	3.55	4.29	0.05	0.08	95.33
ta49_00_11_21_00	73.13	0.18	12.58	0.94	0.05	0.16	0.87	3.48	4.36	0.03	0.00	95.77
ta49_00_11_21_00	72.34	0.15	12.82	0.83	0.06	0.07	1.02	3.51	4.47	0.05	0.24	95.55

continued from page 55

aphyric, with only trace feldspar phenocrysts. Spell (1987) reports that typical Cerro del Medio lavas contain only 1.3% phenocrysts of quartz and feldspar. Additionally, Broxton (unpublished, reported in Reneau and McDonald 1996, Figure 2-10, p. 91) has analyzed aphyric pumices from stratigraphic settings similar to these trench EOC-2 samples and shows their chemistry to be very much like that of the pumices from EOC2/00/11-17-6, -7, and -10. He also indicates these pumices are likely associated with eruptions from the Cerro del Medio dome complex.

C. Electron Microprobe Analyses of Glasses from Reworked Tephros

1. Petrographic descriptions of samples

EOC2/00/11-17-2: unit Qf2a; 8.2H, -2.4V. The sample is from a silty horizon in alluvium. The thin section was made from very fine sand to silt, with most grains angular; sparse larger grains are subangular. Grains are approximately 10% oxidized mafic minerals (subequal amounts of green to brown hornblende and biotite with minor opaque oxides), 10% glass fragments, and 80% felsic com-

continued on page 61

**Table D-2b. Electron Microprobe Analyses of Glasses (wt %) From Selected Tephtras
From Trench EOC-2: Data Normalized on a Volatile-free Basis**

Sample	SiO ₂	TiO ₂	Al ₂ O ₃	FeO	MnO	MgO	CaO	Na ₂ O	K ₂ O	P ₂ O ₅	BaO	Total
EDC2_00-11-17-2	76.696	0.099	12.896	0.864	0.000	0.145	0.807	3.805	4.688	0.000	0.000	100.0
EDC2_00-11-17-2	77.871	0.109	12.457	0.726	0.015	0.092	0.579	3.313	4.718	0.003	0.117	100.0
EDC2_00-11-17-2	77.748	0.121	12.264	0.752	0.078	0.025	0.388	3.795	4.693	0.007	0.129	100.0
EDC2_00-11-17-2	76.790	0.198	12.735	0.859	0.053	0.146	0.802	3.764	4.465	0.046	0.142	100.0
EDC2_00-11-17-2	76.482	0.302	12.962	0.906	0.019	0.170	0.915	3.685	4.522	0.011	0.026	100.0
EDC2_00-11-17-2	77.169	0.199	12.830	0.900	0.049	0.161	0.846	3.566	4.110	0.037	0.134	100.0
EDC2_00-11-17-2	76.391	0.250	13.214	0.981	0.061	0.172	0.950	3.589	4.378	0.015	0.000	100.0
EDC2_00-11-17-2	77.732	0.146	12.023	1.328	0.076	0.000	0.172	3.246	5.277	0.000	0.000	100.0
EDC2_00-11-17-2	77.240	0.149	12.317	1.301	0.087	0.000	0.164	3.835	4.906	0.000	0.000	100.0
EDC2_00-11-17-2	77.274	0.000	12.038	1.425	0.080	0.000	0.030	4.067	4.859	0.046	0.180	100.0
EDC2_00-11-17-2	77.815	0.084	12.483	0.745	0.033	0.078	0.657	3.379	4.591	0.045	0.090	100.0
EDC2_00-11-17-2	75.540	0.267	13.340	1.125	0.062	0.203	1.178	3.812	4.388	0.032	0.053	100.0
EDC2_00-11-17-2	77.338	0.028	12.101	1.520	0.092	0.000	0.191	4.229	4.479	0.021	0.000	100.0
EDC2_00-11-17-2	77.543	0.024	12.209	1.233	0.039	0.000	0.318	3.844	4.696	0.003	0.091	100.0
EDC2_00-11-17-2	77.322	0.116	12.002	1.341	0.060	0.022	0.311	3.945	4.851	0.029	0.000	100.0
EDC2_00-11-17-2	76.494	0.197	12.883	0.878	0.022	0.170	0.886	3.857	4.587	0.025	0.000	100.0
EDC2/00-11-17-3	77.180	0.004	12.141	1.267	0.043	0.011	0.112	3.267	5.959	0.015	0.000	100.0
EDC2/00-11-17-3	77.205	0.072	12.048	1.504	0.062	0.000	0.279	4.533	4.255	0.043	0.000	100.0
EDC2/00-11-17-3	77.156	0.041	12.319	1.209	0.076	0.018	0.273	4.585	4.255	0.003	0.065	100.0
EDC2/00-11-17-3	77.263	0.097	12.207	1.454	0.062	0.001	0.288	4.259	4.369	0.000	0.000	100.0
EDC2/00-11-17-3	76.598	0.122	12.952	0.961	0.064	0.025	0.405	4.096	4.630	0.026	0.121	100.0
EDC2/00-11-17-3	77.051	0.070	12.526	1.025	0.077	0.043	0.361	4.115	4.466	0.000	0.265	100.0
EDC2/00-11-17-3	77.599	0.106	12.247	1.001	0.072	0.022	0.364	4.102	4.484	0.003	0.000	100.0
EDC2/00-11-17-3	78.067	0.057	12.375	0.792	0.029	0.021	0.380	3.768	4.511	0.000	0.000	100.0
EDC2/00-11-17-3	77.170	0.062	12.597	0.855	0.111	0.028	0.369	4.076	4.613	0.000	0.119	100.0
EDC2/00-11-17-3	76.968	0.127	12.722	0.849	0.060	0.052	0.380	4.353	4.488	0.000	0.000	100.0
EDC2/00-11-17-3	77.425	0.052	12.072	1.473	0.108	0.000	0.278	4.311	4.243	0.000	0.039	100.0
EDC2/00-11-17-3	77.015	0.137	12.536	1.046	0.020	0.030	0.260	3.755	5.191	0.011	0.000	100.0
EDC2/00-11-17-3	77.191	0.069	12.112	1.465	0.078	0.000	0.251	3.758	5.061	0.003	0.013	100.0
EDC2/00-11-17-3	77.058	0.103	12.239	1.477	0.107	0.001	0.133	4.352	4.521	0.008	0.000	100.0
EDC2/00-11-17-3	77.027	0.136	11.922	1.555	0.088	0.000	0.090	4.469	4.571	0.000	0.141	100.0
EDC2/00-11-17-3	76.952	0.052	12.216	1.297	0.108	0.002	0.334	4.217	4.783	0.000	0.038	100.0
EOC2_00_11_17_4	77.867	0.124	12.212	0.805	0.046	0.013	0.370	3.913	4.593	0.000	0.058	100.0
EOC2_00_11_17_4	76.989	0.110	12.713	0.865	0.084	0.033	0.414	4.018	4.773	0.000	0.000	100.0
EOC2_00_11_17_4	77.616	0.052	12.009	1.351	0.090	0.000	0.170	4.281	4.431	0.000	0.000	100.0
EOC2_00_11_17_4	77.168	0.118	12.503	0.870	0.081	0.024	0.348	4.303	4.570	0.015	0.000	100.0
EOC2_00_11_17_4	76.911	0.060	12.776	0.907	0.077	0.009	0.361	4.241	4.651	0.008	0.000	100.0
EOC2_00_11_17_4	77.952	0.164	12.234	0.869	0.053	0.040	0.353	3.947	4.348	0.000	0.039	100.0
EOC2_00_11_17_4	77.270	0.077	12.507	0.938	0.033	0.027	0.382	4.097	4.643	0.000	0.026	100.0

Table D-2b Continued. Electron Microprobe Analyses of Glasses (wt %) From Selected Tephras From Trench EOC-2: Data Normalized on a Volatile-free Basis

Sample	SiO ₂	TiO ₂	Al ₂ O ₃	FeO	MnO	MgO	CaO	Na ₂ O	K ₂ O	P ₂ O ₅	BaO	Total
EOC2_00_11_17_4	76.972	0.145	12.638	0.897	0.031	0.026	0.389	4.234	4.510	0.026	0.133	100.0
EOC2_00_11_17_4	76.805	0.118	12.703	0.791	0.085	0.023	0.337	4.285	4.836	0.018	0.000	100.0
EOC2_00_11_17_4	77.453	0.044	12.125	1.185	0.000	0.000	0.278	4.064	4.774	0.000	0.077	100.0
EOC2_00_11_17_4	77.029	0.024	12.486	0.944	0.053	0.023	0.393	4.228	4.764	0.056	0.000	100.0
EOC2_00_11_17_4	77.680	0.089	12.277	0.958	0.055	0.044	0.330	4.124	4.418	0.025	0.000	100.0
EOC2_00_11_17_4	77.786	0.000	12.262	0.950	0.057	0.010	0.350	3.725	4.860	0.000	0.000	100.0
EOC2_00_11_17_4	77.225	0.065	12.560	0.877	0.060	0.114	0.733	3.560	4.622	0.054	0.130	100.0
EOC2_00_11_17_4	76.952	0.137	12.774	0.920	0.039	0.034	0.360	4.055	4.545	0.011	0.173	100.0
EOC2_00_11_17_4	77.810	0.137	12.326	0.613	0.064	0.043	0.541	3.579	4.707	0.025	0.154	100.0
EOC2_00_11_17_4	76.948	0.135	12.815	0.849	0.030	0.055	0.372	4.142	4.644	0.011	0.000	100.0
EOC2_00_11_17_4	77.672	0.144	12.522	0.909	0.035	0.006	0.381	4.105	4.207	0.018	0.000	100.0
EOC2_00_11_17_4	77.137	0.156	12.638	0.870	0.075	0.023	0.375	3.989	4.618	0.000	0.119	100.0
EOC2_00_11_17_4	76.888	0.246	12.679	0.862	0.049	0.026	0.370	4.141	4.655	0.018	0.066	100.0
EOC2_00_11_17_4	77.208	0.203	12.594	0.925	0.071	0.031	0.347	4.076	4.545	0.000	0.000	100.0
EOC2_00_11_17_4	77.010	0.154	12.589	0.858	0.043	0.025	0.358	4.113	4.824	0.025	0.000	100.0
EDC2/00-11-17-5	76.860	0.246	12.123	1.383	0.023	0.019	0.431	3.356	5.542	0.018	0.000	100.0
EDC2/00-11-17-5	77.511	0.169	11.963	1.230	0.066	0.016	0.120	3.499	5.295	0.015	0.116	100.0
EDC2/00-11-17-5	77.434	0.088	12.073	1.353	0.116	0.000	0.175	4.292	4.420	0.010	0.038	100.0
EDC2/00-11-17-5	77.363	0.045	12.051	1.364	0.073	0.000	0.053	4.342	4.682	0.028	0.000	100.0
EDC2/00-11-17-5	77.924	0.008	12.136	0.933	0.087	0.012	0.363	4.139	4.320	0.000	0.077	100.0
EDC2/00-11-17-5	77.155	0.141	12.150	1.226	0.014	0.044	0.340	3.849	4.928	0.000	0.155	100.0
EDC2/00-11-17-5	77.381	0.024	12.050	1.463	0.066	0.000	0.092	4.344	4.451	0.000	0.128	100.0
EDC2/00-11-17-5	77.185	0.042	12.567	0.939	0.044	0.025	0.383	4.331	4.354	0.000	0.132	100.0
EDC2/00-11-17-5	77.455	0.078	12.233	1.250	0.024	0.008	0.310	4.044	4.529	0.003	0.066	100.0
EDC2/00-11-17-5	77.225	0.048	11.925	1.458	0.077	0.009	0.236	4.453	4.508	0.062	0.000	100.0
EOC2/00_11_17_6	77.585	0.090	12.301	0.930	0.035	0.020	0.346	4.125	4.535	0.033	0.000	100.0
EOC2/00_11_17_6	77.761	0.111	12.307	0.991	0.043	0.006	0.344	3.948	4.489	0.000	0.000	100.0
EOC2/00_11_17_6	77.410	0.153	12.300	0.835	0.039	0.010	0.359	3.833	4.903	0.068	0.091	100.0
EOC2/00_11_17_6	77.478	0.105	12.276	0.998	0.020	0.021	0.362	4.198	4.507	0.010	0.026	100.0
EOC2/00_11_17_6	77.636	0.098	12.282	0.974	0.093	0.017	0.366	4.062	4.447	0.025	0.000	100.0
EOC2/00_11_17_6	77.896	0.117	12.110	0.981	0.010	0.011	0.363	4.004	4.429	0.000	0.078	100.0
EOC2/00_11_17_6	78.588	0.110	11.578	0.942	0.016	0.019	0.295	3.500	4.900	0.000	0.052	100.0
EOC2/00_11_17_6	77.827	0.052	12.101	0.965	0.043	0.014	0.360	4.202	4.294	0.000	0.143	100.0
EOC2/00_11_17_6	77.548	0.073	12.178	0.992	0.045	0.030	0.387	4.000	4.459	0.000	0.287	100.0
EOC2/00_11_17_6	77.606	0.089	12.352	0.901	0.020	0.026	0.359	4.066	4.481	0.086	0.013	100.0
EOC2/00_11_17_6	77.750	0.098	12.180	0.847	0.040	0.017	0.390	4.057	4.353	0.007	0.262	100.0
EOC2/00_11_17_6	77.771	0.045	12.315	0.921	0.082	0.019	0.391	4.092	4.363	0.000	0.000	100.0
EOC2/00_11_17_6	77.388	0.130	12.241	1.007	0.060	0.020	0.365	3.985	4.489	0.054	0.261	100.0
EOC2/00_11_17_6	77.628	0.017	12.241	0.911	0.041	0.016	0.370	4.140	4.517	0.003	0.117	100.0

Table D-2b Continued. Electron Microprobe Analyses of Glasses (wt %) From Selected Tephtras From Trench EOC-2: Data Normalized on a Volatile-free Basis

Sample	SiO ₂	TiO ₂	Al ₂ O ₃	FeO	MnO	MgO	CaO	Na ₂ O	K ₂ O	P ₂ O ₅	BaO	Total
EOC2/00_11_17_6	77.938	0.000	12.166	0.952	0.093	0.012	0.330	4.005	4.358	0.003	0.143	100.0
ta49_00_11_21_00	78.118	0.060	12.367	0.540	0.029	0.048	0.578	3.040	5.195	0.025	0.000	100.0
ta49_00_11_21_00	75.902	0.264	13.327	1.021	0.034	0.191	0.941	3.757	4.555	0.007	0.000	100.0
ta49_00_11_21_00	75.810	0.172	13.192	1.093	0.031	0.227	1.014	3.827	4.477	0.003	0.154	100.0
ta49_00_11_21_00	77.850	0.057	12.431	0.697	0.045	0.075	0.593	3.536	4.672	0.043	0.000	100.0
ta49_00_11_21_00	77.414	0.094	12.564	0.653	0.042	0.069	0.611	3.539	4.756	0.011	0.248	100.0
ta49_00_11_21_00	76.210	0.310	13.192	0.840	0.093	0.133	0.750	3.632	4.750	0.000	0.091	100.0
ta49_00_11_21_00	77.880	0.177	12.320	0.679	0.015	0.024	0.506	3.713	4.687	0.000	0.000	100.0
ta49_00_11_21_00	77.629	0.125	12.405	0.738	0.055	0.034	0.531	3.575	4.808	0.035	0.064	100.0
ta49_00_11_21_00	77.793	0.106	12.399	0.661	0.065	0.069	0.554	3.567	4.787	0.000	0.000	100.0
ta49_00_11_21_00	77.639	0.077	12.487	0.752	0.000	0.040	0.604	3.582	4.728	0.000	0.091	100.0
ta49_00_11_21_00	76.895	0.185	12.791	0.878	0.015	0.136	0.817	3.626	4.618	0.039	0.000	100.0
ta49_00_11_21_00	77.693	0.097	12.500	0.759	0.045	0.074	0.587	3.448	4.796	0.000	0.000	100.0
ta49_00_11_21_00	77.020	0.198	12.633	0.864	0.016	0.122	0.737	3.567	4.635	0.000	0.207	100.0
ta49_00_11_21_00	78.000	0.145	12.258	0.638	0.057	0.037	0.542	3.467	4.668	0.032	0.156	100.0
ta49_00_11_21_00	77.760	0.073	12.413	0.628	0.032	0.044	0.565	3.539	4.842	0.000	0.104	100.0
ta49_00_11_21_00	76.014	0.296	13.185	0.769	0.021	0.077	0.938	3.731	4.795	0.046	0.128	100.0
ta49_00_11_21_00	76.923	0.080	12.794	0.915	0.045	0.151	0.863	3.689	4.540	0.000	0.000	100.0
ta49_00_11_21_00	77.891	0.081	12.362	0.639	0.087	0.029	0.500	3.731	4.659	0.021	0.000	100.0
ta49_00_11_21_00	76.707	0.127	12.900	0.963	0.036	0.152	0.815	3.587	4.586	0.075	0.053	100.0
ta49_00_11_21_00	77.775	0.092	12.379	0.658	0.059	0.034	0.537	3.633	4.832	0.000	0.000	100.0
ta49_00_11_21_00	76.561	0.222	12.923	0.980	0.014	0.192	0.851	3.541	4.715	0.000	0.000	100.0
ta49_00_11_21_00	77.865	0.081	12.409	0.638	0.036	0.043	0.520	3.494	4.842	0.007	0.065	100.0
ta49_00_11_21_00	76.277	0.187	13.153	0.926	0.050	0.167	0.881	3.724	4.503	0.053	0.079	100.0
ta49_00_11_21_00	76.359	0.186	13.139	0.978	0.053	0.166	0.909	3.628	4.553	0.028	0.000	100.0
ta49_00_11_21_00	75.705	0.158	13.412	0.871	0.062	0.076	1.065	3.674	4.674	0.057	0.247	100.0

continued from page 58

ponents (quartz plus feldspar). Fresh glass occurs in the form of slightly deformed pumice fragments and discrete acicular shards; the shards could be from disaggregated pumice. Feldspars include plagioclase and sanidine. There are trace amounts of a pale-green pleochroic clinopyroxene.

EOC2/00/11-17-3: unit Qf3a; 31.6H, -4.2V. This sample is from a silty horizon in alluvium. The thin section was made from silt to very fine sand with grains ranging from angular to subangular. Brownish alteration after biotite and/or hornblende

and opaque oxides constitutes approximately 15% of the sample, and most of the mafic grains are oxidized beyond recognition. Glassy components are about 5% of the sample and include pumice fragments, acicular shards, angular fragments of pale-brown glass, and subangular ash of colorless glass. Felsic (quartz and feldspar) components make up 80% of the sample.

EOC2/00/11-17-4: unit Qf3a; 43.6H, -4.4V. This sample is from a silty horizon in alluvium. The thin section was made from silt to very fine sand with

grains ranging from angular to subangular. The felsic component makes up about 80% of sample. The sample has 10% brown alteration after biotite and hornblende in subequal amounts with minor opaque oxides. Glass fragments constitute about 10% of the sample and include flattened pumice, acicular shards, ash-sized fragments of clear, colorless glass, and ash- to fine-sand-sized grains of pale-brown glass.

EOC2/00/11-17-5: unit Qf3a; 54.9H, -4.3V. This sample is from a silty horizon in alluvium. The thin section was made from silt to very fine sand with grains ranging from angular to subangular. The sample is about 70% felsic component, 20% oxidized biotite and hornblende in subequal amounts with minor opaque oxides, and about 10% glass fragments. Forms of the glass include flattened pumice, acicular shards, ash-sized fragments of clear, colorless glass, ash- to fine-sand-sized grains of pale-brown glass, and blocky ash-sized shards.

2. Results

We have only begun to develop compositional data for tephra glasses for use as a correlation tool. Of relevance to this report, data exist for the upper part of the Tshirege Member of the Bandelier Tuff (Gardner et al. 2001), for El Cajete fallout deposits (Gardner and Wolff, unpublished, and this report), and for Cerro del Medio fallout tephras (see below). Thus, except for the El Cajete (and related units; see Wolff and Gardner 1995), which is geochemically distinctive among the post-Valles caldera eruptive products, the correlations we present here should be considered tentative. In the absence of a broader data base, we do not know yet how unique some compositions may be. Two samples in Table D-2 deserve special mention. Sample ta49-00-11-21-00 is a sample of El Cajete ash collected from Frijoles Mesa on the Pajarito Plateau (see Reneau and McDonald 1996, pp. 73–75, for site description) that provides microprobe data that supplement analyses obtained on samples closer to the source (Wolff et al. 1996; Gardner and Wolff, unpublished). Sample EOC2/00/11-17-6, collected from unit Qoal3, is an important sample because it

provides a link between bulk XRF analyses, upon which we base correlation of pumices to the eruption of the Cerro del Medio dome complex (discussed above), and electron microprobe analyses of the pumice glasses. The sample hereby forms the initial basis for correlations of tephra glass composition to Cerro del Medio.

Figure D-2a is a chemical variation diagram of FeO versus CaO that shows good separation of the glass compositions of known units. These data form the basis for the correlation fields in Figure D-2b. The El Cajete analyses are fairly unique in that the glasses form two populations, which is consistent with the petrogenesis of the parent magma (see Wolff and Gardner 1995).

From Figure D-2b we conclude the following:

EOC2/00/11-17-2, collected from unit Qf2a, contains tephras with glass chemistries indicative of components derived from the El Cajete Member (9 analyses), Cerro del Medio (likely, one analysis), and the upper Tshirege Member (5 analyses and, likely, one more analysis). Thus, in the absence of any other stratigraphic evidence, we would infer this portion of Qf2a to be younger than the El Cajete pumice, or less than ca. 50 to 60 ka (age from Toyoda et al. 1995; Reneau et al. 1996a). However, soil-stratigraphic evidence from the trench instead suggests that most or all of Qf2a is older than the El Cajete pumice (Section IV and Appendix C). Because no evidence for an unconformity was observed within Qf2a in this part of the trench (which would be required if the sample site was to post-date the El Cajete pumice), we hypothesize that the sampled layer was close to the ground surface at the time of the El Cajete eruption and that glass from this tephra was either translocated or bioturbated into the underlying soil.

EOC2/00/11-17-3, collected from unit Qf3a, contains tephras with glass chemistries indicative of components derived from Cerro del

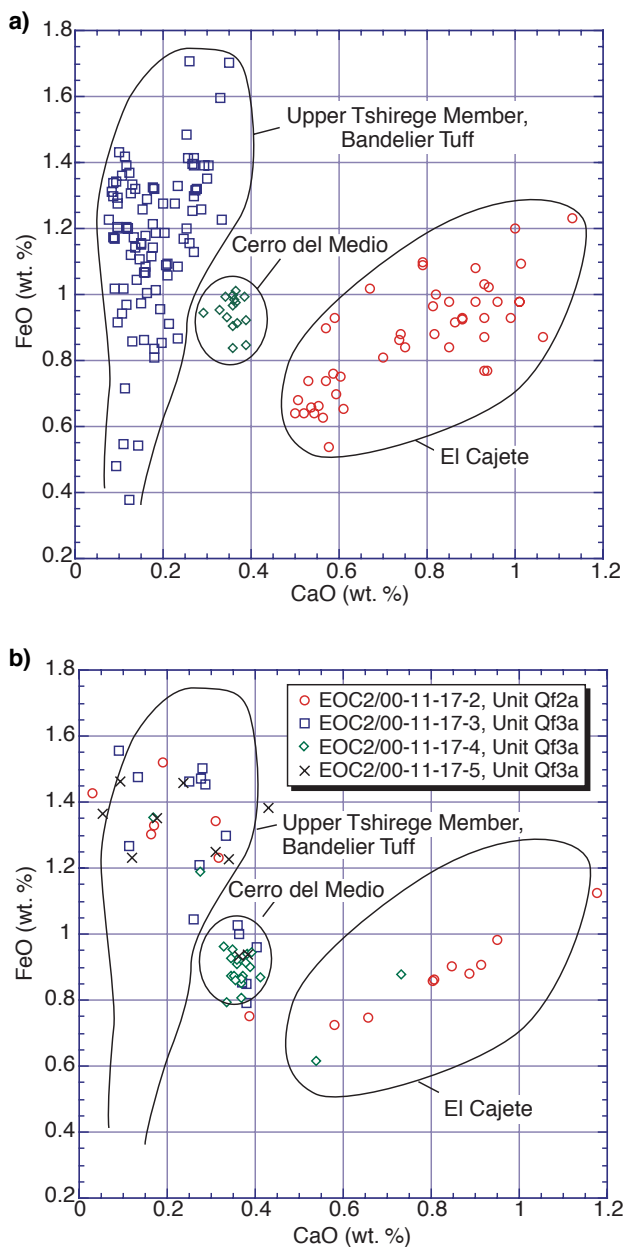


Figure D-2. FeO versus CaO variation diagrams for electron microprobe analyses of glasses. a) definition of correlation fields for the upper Tshirege Member of the Bandelier Tuff glasses (boxes; data from Gardner et al. 2001), Cerro del Medio glasses (diamonds; data from sample EOC2/00/11-17-6, this report), and the El Cajete Member of the Valles Rhyolite (circles; data from Gardner and Wolff, unpublished, and sample ta49-00-11-21-00, this report). b) correlation plot for trench EOC-2 tephra glasses with correlation fields derived from a).

Medio (6 analyses) and the upper Tshirege Member (9 analyses and, likely, one more analysis). Thus, in the absence of any other stratigraphic evidence, we would infer this portion of Qf3a to be younger than some Cerro del Medio eruptions, or less than ca. 1.13 Ma, which is consistent with other evidence from the trench.

EOC2/00/11-17-4, collected from unit Qf3a, contains tephra with glass chemistries indicative of components derived from the El Cajete Member (two analyses), Cerro del Medio (18 analyses), and the upper Tshirege Member (2 analyses). Thus, in the absence of any other stratigraphic evidence, we would infer this portion of Qf3a to be younger than the El Cajete pumice, or less than ca. 50 to 60 ka, which is consistent with other evidence from the trench.

EOC2/00/11-17-5, collected from unit Qf3a, contains tephra with glass chemistries indicative of components derived from Cerro del Medio (2 analyses) and the upper Tshirege Member (6 analyses and, likely, two more analyses). Thus, in the absence of any other stratigraphic evidence, we would infer this portion of Qf3a to be younger than some Cerro del Medio eruptions, or less than ca. 1.13 Ma, which is consistent with other evidence from the trench.

APPENDIX E. BORE HOLE SAMPLES

As part of geotechnical evaluations of foundation conditions for the proposed new EOC, five bore holes were drilled near trench EOC-2 in February 2001 by AMEC Earth & Environmental of Albuquerque, New Mexico (AMEC 2001). The holes were drilled to depths of 7.6 to 15.2 m (25 to 50 ft), and hole locations are shown on Figure 2 (BH-1 through BH-5). All holes were west of the main fault zone. Cores were obtained every 1.5 m (5 ft) in either 5-cm (2-in) diameter, 46-cm (1.5-ft) long split-spoon samplers, or in 7.5-cm (3-in) diameter, 30-cm (1-ft) long sealed tubes. Material from the split spoons and from the base of the larger diameter samples were transferred to plastic bags for transport to a geotechnical laboratory for analysis. In addition to field logging of the holes by AMEC personnel, LANL Seismic Hazard Program personnel also briefly examined the samples in the field. The objective of this latter examination was to provide tentative correlations of the units penetrated in the bore holes with units exposed in the trench to better understand the subsurface stratigraphy and structure at the site. Notes on these samples and inferred unit correlations are presented in Table E-1.

Reliable identification of the exact units penetrated in the bore holes was generally not possible due to differing characteristics of the bore-hole samples and the units exposed in the trench, the poor condition of many samples, the absence of continuous cores, and the inability to analyze samples in the laboratory. However, some conclusions were possible.

The uppermost bore-hole samples consisted of loose material that was texturally similar to the Holocene units exposed in the trench (Qc2 or Qf5). More consolidated and weathered alluvium was encountered in all holes beginning at 3.0 or 4.6 m (10 or 15 ft) and is correlated to unit Qf2a in the trench. Generally fine-grained, commonly clay-rich alluvium, locally containing dacite or tuff clasts, occurred to depths of 4.6 to 7.6 m (15

to 25 ft) in the various holes and may represent older, deeper layers related to Qf2a, although it is also possible that they may represent other unrelated units not exposed in the trench. Less consolidated dacite-bearing alluvium was sampled at a depth of 6.1 m (20 ft) in two holes that could be related to Qf1, although again this correlation is uncertain. Four of the holes yielded samples at depths of 6.1 to 10.7 m (20 to 35 ft) that share characteristics of unit Qoal as exposed in the trench, including relatively well-sorted, sand-rich alluvium and common pumice clasts. The abundance of aphyric pumice in some samples suggests a correlation to Qoal4, whereas one sample (from 10.7 m in BH-4) appeared texturally similar to Qoal1. Two holes (BH-1 and BH-2) yielded samples at depths of 7.6 to 12.2 m (25 to 40 ft) that appeared to be of weathered crystal-rich tuff with crystal-rich pumice, possibly correlative to the nonwelded unit of the Bandelier Tuff exposed in the trench, although the possibility that these samples instead represented alluvium could not be ruled out. A deeper sample of fine- to medium-grained sand from 13.7 m (45 ft) in BH-1 was inferred to possibly represent a weathered surge bed in the Bandelier Tuff. Beneath it, at a depth of 15.2 m (50 ft), was the only sample of more typical Bandelier Tuff recovered from the holes, an ignimbrite with altered pumice that appeared similar to unit Qbt-4 as mapped at TA-3 (Gardner et al. 1999).

Table E-1. Samples From Bore Holes Near Trench EOC-2

Depth (ft)	Depth (m)	Notes
Bore Hole 1		
5	1.5	loose silt and fine sand, with minor gravel (Qc2)
10	3.0	sandy clay-rich alluvium (Qf2a)
15	4.6	Qbt clast-rich alluvium (Qf2a)
20	6.1	aphyric pumice-rich alluvium, with dacite clasts (Qoal4?)
25	7.6	weathered crystal-rich tuff (?) or alluvium, with crystal-rich pumice (Qbt?)
30	9.1	weathered crystal-rich tuff (?) or alluvium, with crystal-rich pumice (Qbt?)
35	10.7	weathered crystal-rich tuff (?) or alluvium, with crystal-rich pumice (Qbt?)
40	12.2	pulverized pumice-rich tuff (?) or alluvium (Qbt?)
45	13.7	medium to fine sand; possible weathered surge bed in tuff (Qbt?)
50	15.2	weathered tuff, with altered pumice; similar to Qbt-4 at TA-3 (Qbt)
Bore Hole 2		
10	3.0	consolidated, weathered, silty fine sand (Qf2a?)
15	4.6	pumice-rich, dacite-bearing, clay-rich alluvium (Qf2a?)
20	6.1	fine-grained, clay-rich alluvium with small pumice clasts (Qf2a?)
25	7.6	weathered crystal-rich tuff (?) or alluvium, with crystal-rich pumice (Qbt?)
30	9.1	pulverized pumice-rich tuff (?) or alluvium (Qbt?)
35	10.7	weathered crystal-rich tuff (?) or alluvium, with crystal-rich pumice (Qbt?)
Bore Hole 3		
5	1.5	loose gravelly sand (Qc2 or Qf5)
10	3.0	silt and very fine sand, with sparse gravel (Qc2?)
15	4.6	clay-rich alluvium, with dacite clasts (Qf2a?)
20	6.1	gravelly alluvium, with dacite clasts and aphyric pumice (Qoal4 or Qf1?)
25	7.6	alluvium, with very coarse sand and granules (Qoal1 or Qoal3?)
Bore Hole 4		
5	1.5	loose silty very fine sand and scattered gravels (Qc2)
10	3.0	fine-grained, clay-rich alluvium, with minor gravel (Qf2a?)
15	4.6	dacite-rich alluvium (Qf2a?)
20	6.1	fine-grained, clay-rich alluvium (Qf2a?)
25	7.6	clay-rich gravelly alluvium (Qf2a?)
30	9.1	medium to coarse sandy alluvium, with pumice (Qoal3?)
35	10.7	pumice-rich alluvium (Qoal1?)
Bore Hole 5		
5	1.5	loose silty very fine sand (Qc2)
10	3.0	fine-grained, clay-rich alluvium (Qf2a)
15	4.6	fine-grained, clay-rich alluvium, with more clay than at 10 ft (Qf2a?)
20	6.1	dacite-rich alluvium, sandier than at 10–15 ft, with scattered small pumice clasts (Qf1?)
25	7.6	aphyric (?) pumice-rich alluvium, with scattered dacite clasts (Qoal4?)

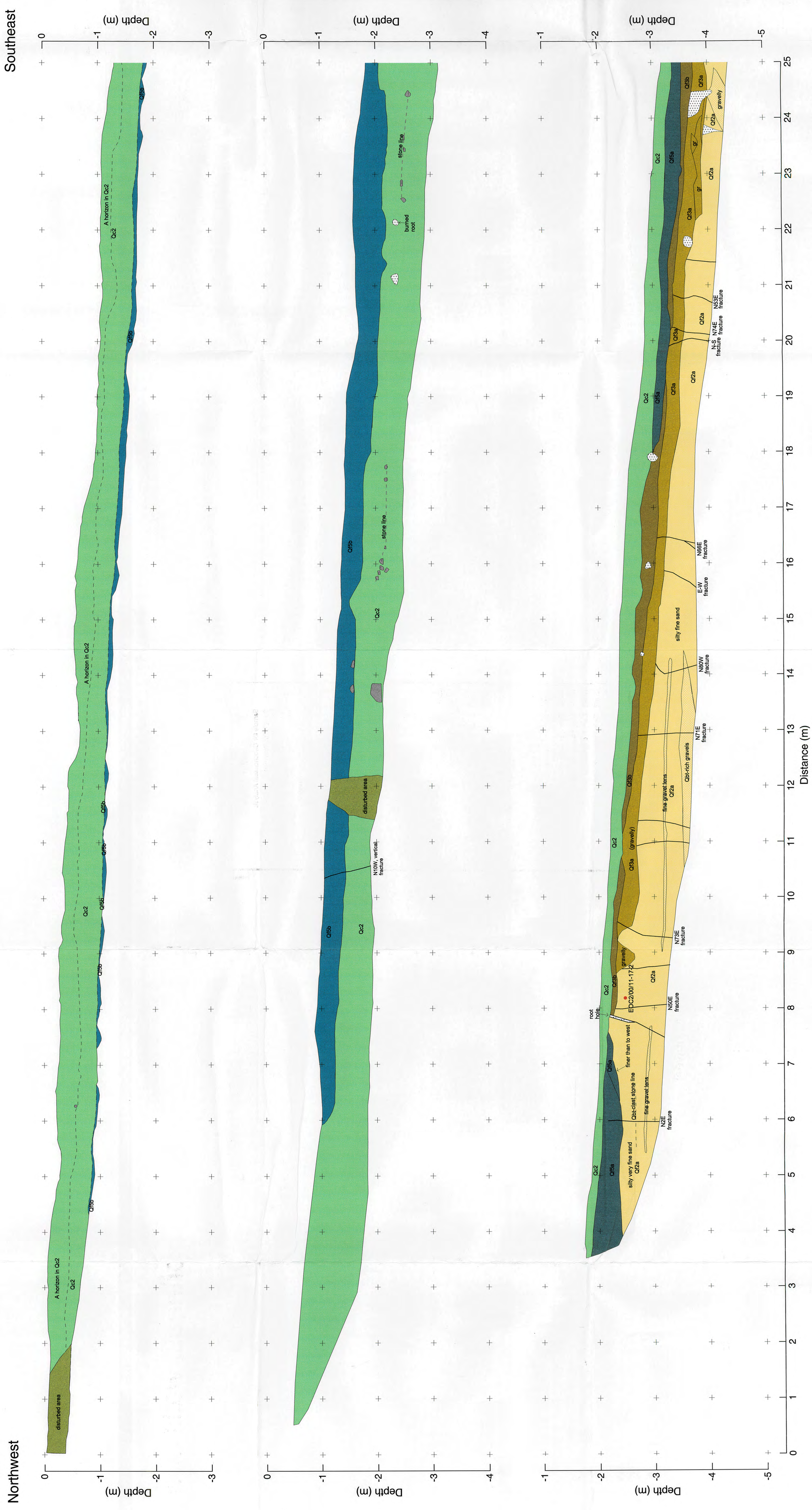


Plate 1. Log of northeast walls of western part of trench EOC-2.

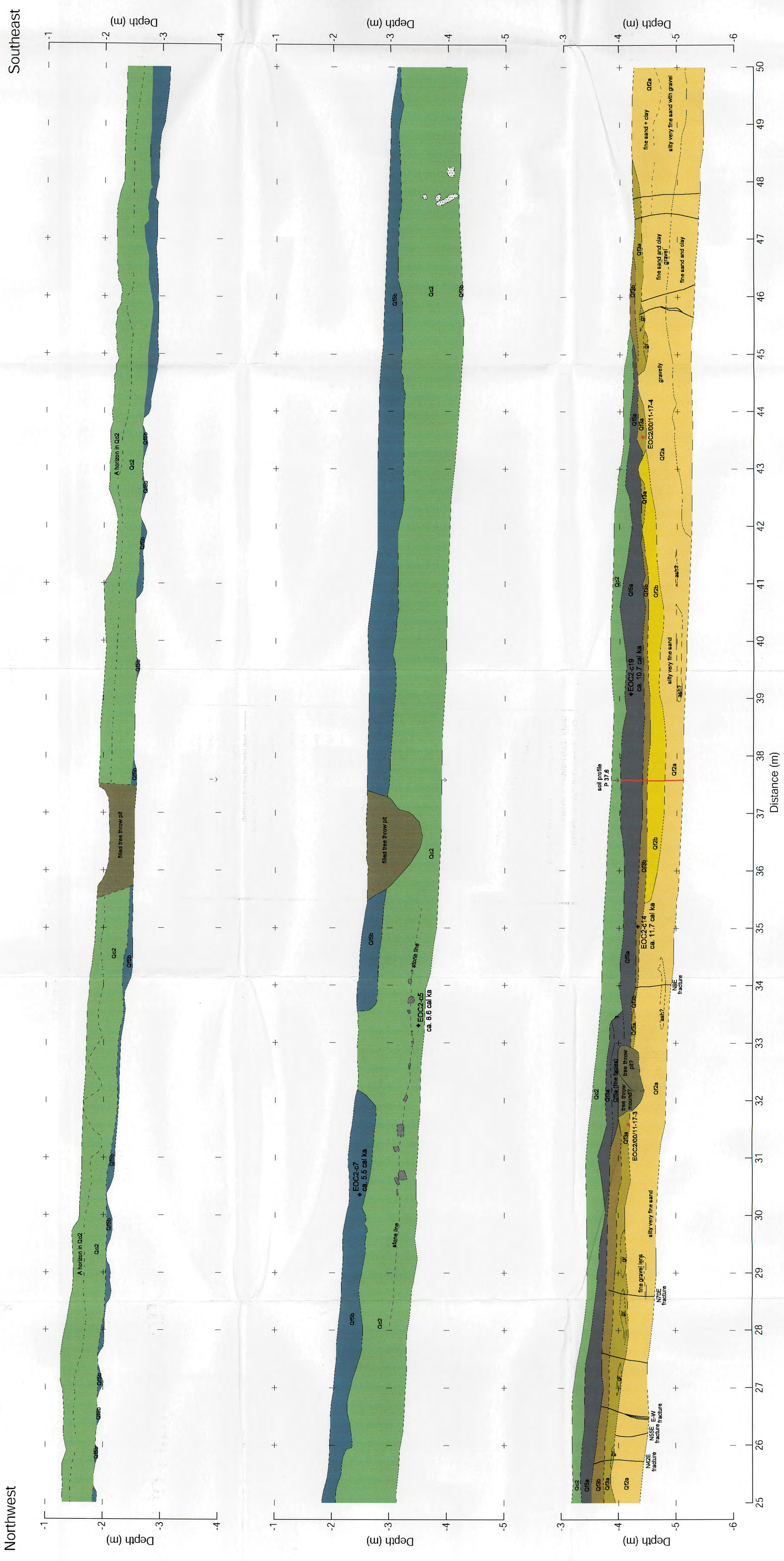
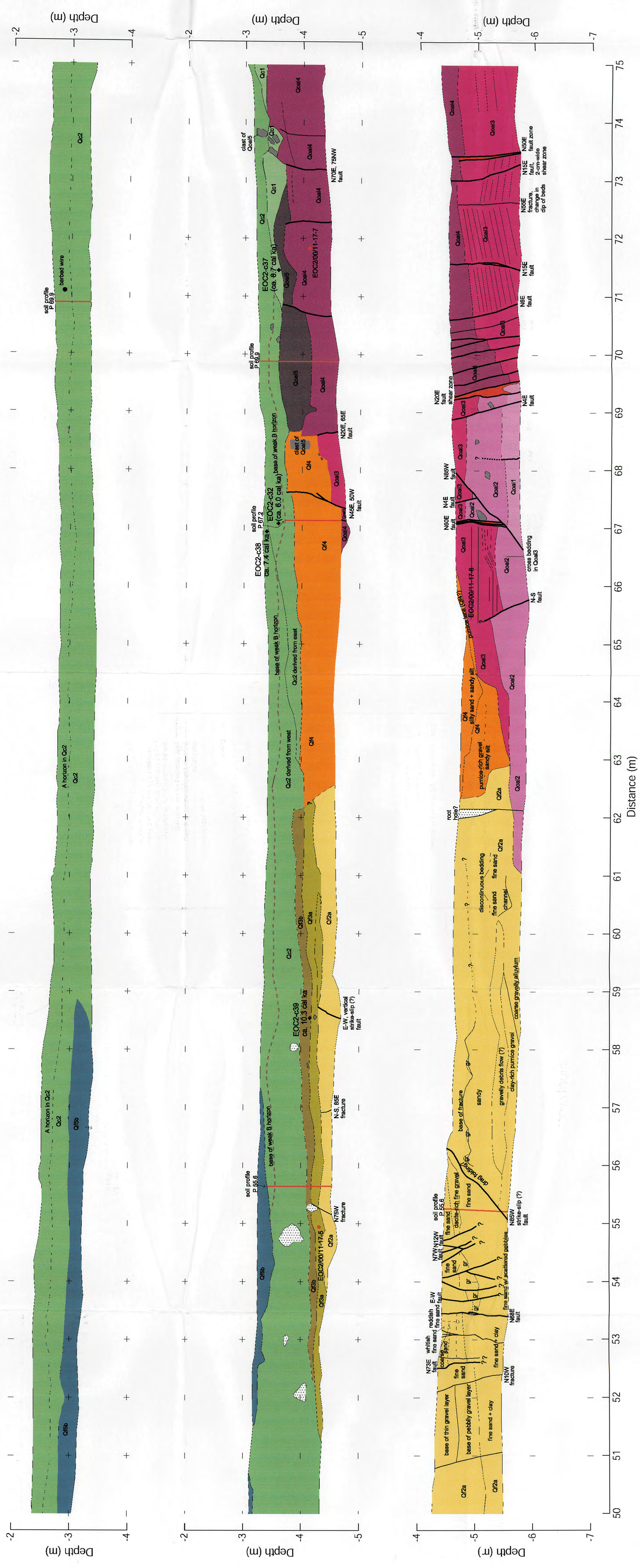


Plate 2. Log of northeast walls of west-central part of trench EOC-2.

Northwest

Southeast



Legend

- Sample for Geochemical Analysis
- Sample for Radiocarbon Analysis (estimated age in calibrated years before present, ages in parentheses are interpreted to be erroneous)
- fracture (dashed where queried)
- soil profile (dashed where queried)
- contact (dashed where approximate)
- bedding
- gravel
- tree throw pit or tree throw mound
- disturbed area on trench wall
- krotovina or root hole
- rock
- fill
- shear zone or cataclaste
- Qc2z
- Qc2y
- Qc2x
- Qc2w
- Qc2v
- Qc2u
- Qc2t
- Qc2s
- Qc2r
- Qc2q
- Qc2p
- Qc2o
- Qc2n
- Qc2m
- Qc2l
- Qc2k
- Qc2j
- Qc2i
- Qc2h
- Qc2g
- Qc2f
- Qc2e
- Qc2d
- Qc2c
- Qc2b
- Qc2a
- Qc1
- Qc0
- Qc-1
- Qc-2
- Qc-3
- Qc-4
- Qc-5
- Qc-6
- Qc-7
- Qc-8
- Qc-9
- Qc-10
- Qc-11
- Qc-12
- Qc-13
- Qc-14
- Qc-15
- Qc-16
- Qc-17
- Qc-18
- Qc-19
- Qc-20
- Qc-21
- Qc-22
- Qc-23
- Qc-24
- Qc-25
- Qc-26
- Qc-27
- Qc-28
- Qc-29
- Qc-30
- Qc-31
- Qc-32
- Qc-33
- Qc-34
- Qc-35
- Qc-36
- Qc-37
- Qc-38
- Qc-39
- Qc-40
- Qc-41
- Qc-42
- Qc-43
- Qc-44
- Qc-45
- Qc-46
- Qc-47
- Qc-48
- Qc-49
- Qc-50
- Qc-51
- Qc-52
- Qc-53
- Qc-54
- Qc-55
- Qc-56
- Qc-57
- Qc-58
- Qc-59
- Qc-60
- Qc-61
- Qc-62
- Qc-63
- Qc-64
- Qc-65
- Qc-66
- Qc-67
- Qc-68
- Qc-69
- Qc-70
- Qc-71
- Qc-72
- Qc-73
- Qc-74
- Qc-75
- Qc-76
- Qc-77
- Qc-78
- Qc-79
- Qc-80
- Qc-81
- Qc-82
- Qc-83
- Qc-84
- Qc-85
- Qc-86
- Qc-87
- Qc-88
- Qc-89
- Qc-90
- Qc-91
- Qc-92
- Qc-93
- Qc-94
- Qc-95
- Qc-96
- Qc-97
- Qc-98
- Qc-99
- Qc-100

Plate 3. Log of northeast walls of east-central part of trench EOC-2.

This report has been reproduced directly from the best available copy. It is available electronically on the Web (<http://www.doe.gov/bridge>).

Copies are available for sale to U.S. Department of Energy employees and contractors from—

Office of Scientific and Technical Information
P.O. Box 62
Oak Ridge, TN 37831
(865) 576-8401

Copies are available for sale to the public from—

National Technical Information Service
U.S. Department of Commerce
5285 Port Royal Road
Springfield, VA 22161
(800) 553-6847



Los Alamos NM 87545